박사 학위논문

Ph. D. Dissertation

삼중항 P-상태의 광펌핑을 통한 이터븀 원자의 자기광포획 효율 증가

Enhancement of Magneto-Optical Trap of Ytterbium Atom via Optical Repumping of Triplet P-states

조 준 우 (曺 準 佑 Cho, Jun Woo)

물리학과

Department of Physics

KAIST

2012

삼중항 P-상태의 광펌핑을 통한 이터븀 원자의 자기광포획 효율 증가

Enhancement of Magneto-Optical Trap of Ytterbium Atom via Optical Repumping of Triplet P-states

Enhancement of Magneto-Optical Trap of Ytterbium Atom via Optical Repumping of Triplet P-states

Advisor : Professor Jaewook Ahn

by
Cho, Jun Woo
Department of Physics
KAIST

A thesis submitted to the faculty of KAIST in partial fulfillment of the requirements for the degree of Doctor of Philosophy in the Department of Physics . The study was conducted in accordance with Code of Research Ethics[1].

2011. 11. 25.

Approved by

Professor Jaewook Ahn

[Advisor]

---

[1]Declaration of Ethical Conduct in Research: I, as a graduate student of KAIST, hereby declare that I have not committed any acts that may damage the credibility of my research. These include, but are not limited to: falsification, thesis written by someone else, distortion of research findings or plagiarism. I affirm that my thesis contains honest

삼중항 P-상태의 광펌핑을 통한 이터븀 원자의 자기광포획 효율 증가

조 준 우

위 논문은 한국과학기술원 박사학위논문으로
학위논문심사위원회에서 심사 통과하였음.

20011년 11월 25일

심사위원장 안 재 욱 (인)

심사위원 남 창 희 (인)

심사위원 이 해 웅 (인)

심사위원 이 원 규 (인)

심사위원 박 창 용 (인)

conclusions based on my own careful research under the guidance of my thesis advisor.

DPH
20055144

조 준 우. Cho, Jun Woo. Enhancement of Magneto-Optical Trap of Ytterbium Atom via Optical Repumping of Triplet P-states. 삼중항 P-상태의 광펌핑을 통한 이터븀 원자의 자기광포획 효율 증가. Department of Physics . 2012. 70p. Advisor Prof. Jaewook Ahn. Text in English.

ABSTRACT

Cold atomic ytterbium (Yb, Z=70) densely captured in a magneto-optical trap (MOT) has opened many possibilities for fundamental studies and applications, including optical frequency standards, parity non-conservation tests, and cold collisional properties. Ytterbium atoms can be cooled and trapped by two types of magneto-optical trapping: the strongly interacting $(6s^2)^1S_0$-$(6s6p)^1P_1$ transition with a laser wavelength of 398.9 nm and the weakly interacting $(6s^2)^1S_0$-$(6s6p)^3P_1$ transition with a laser wavelength of 555.8 nm. In this dissertation, we summarize how an ytterbium MOT has been constructed, what are the characteristics of trapped cold Yb gas, and how the performance of Yb MOT has been improved, after a brief review of the principles of Doppler cooling, Zeeman slowing, and magneto-optical trapping.

Radiative decay from the $^1P_1$ state to metastable ^3P states limits the number of trapped atoms, as well as the $(6s^2)^1S_0$-$(6s6p)^1P_1$ transition MOT lifetime. Therefore, researchers have attempted to improve the Yb MOT by eliminating the shelving loss characteristics. In this thesis, we report that the atoms associated with the metastable states $(6s6p)^3P_{0,2}$ are optically repumped, and that the loss rate of the $^1S_0$-$^1P_1$ transition is extracted using trapping laser power-dependent fluorescence measurements. Experiment were performed with and without each repump laser, i.e., a 650-nm laser ($^3P_0$-$^3S_1$) and a 770-nm laser ($^3P_2$-$^3S_1$). The loss rates associated with radiative decay to the metastable states were then analyzed. The experimental results indicate that the number of trapped atoms increases compared to the no-repumping case, by up to 30%. The repumping has also more than doubled the lifetime of the trapped atoms. The loss rate term was affected by three major physical properties: the background gas collisions, the Yb-Yb collisions, and the loss to the metastable states. By considering all of these contributions to this particular loss, we experimentally measured the rate of decay from $^1P_1$ state to metastable states. The measurement results show a good agreement with the theoretical predictions.

Contents

List of Tables

List of Figures

Chapter 1. Introduction

1.1 Research with cold ytterbium atoms and its application

Optical trapping of neutral atoms has been a powerful tool for generating cold and ultracold of gases [1]. Much work has been done with alkali metals such as rubidium [2], sodium [3], and so on. Recently, like alkaline earth atoms, two-electron atoms have become an attractive subject for the cooling and trapping research. Ytterbium atom has a closed valence-shell electronic structure which is similar to alkaline-earth atoms, such as calcium (Ca) [4], strontium (Sr) [5] and magnesium (Mg) [6]. There are some interesting trapping properties in an ytterbium atom due to the spin zero electronic ground state, which are different from those in alkali metal atoms. And ytterbium atom has many naturally stable isotopes: seven isotopes, five bosonic atoms and two fermionic atoms. The isotopes have similar abundance in nature. The bosonic isotopes have no angular momentum in the ground state, and the fermionic isotopes, however, have nuclear spin, allowing us to utilize the effects of hyperfine structures.

1.1.1 Optical frequency standards

Ytterbium atoms in the ground have a closed S-shell, and they have a weak intercombination transition between the ground state and the triplet state. This transition has an extremely narrow linewidth and, therefore, used for optical frequency standards. The uncertainty of a frequency standard is defined as $\sigma(\tau) = \frac{\Delta f}{f_o}\frac{1}{\sqrt{N\tau}}$, where f_0 is a exact reference frequency, Δf is the error of from the reference frequency, N is the number of oscillators measured in unit time, and τ is the total interrogation time. As the number of the atoms and the interrogation time are increased, the frequency uncertainty is lowered. So the neutral atoms often are trapped at Lamb-Dicke regime in an optical dipole-induced lattice for Doppler-free spectroscopy. This concept has been a new candidate for an optical frequency standard [7].

But the optical lattice field perturbs the atomic internal state, and cold ytterbium would appear to be unsuited for a clock. To overcome this defect, a concept of magic-wavelength has been proposed: the AC Stark shifts of the ground and the excited state energy can be canceled by the proper choice of wavelength (magic wavelength) of the

lattice laser. Katori proposed that such a clock based on the polarization insensitive $^1S_0$-$^3P_0$ transition in ^{87}Sr [8] could have extremely small, quantum projection-noise limited instability of less than 10^{-17} in one second. However, there are still many sources that give uncertainty in frequency standards [9] such as Zeeman shift, collision shift [10], blackbody radiation shift [11], etc.

For ytterbium atomic lattice clock, ^{171}Yb isotope, which has a nuclear spin I=1/2 and simple hyperfine structure [12], has been researched. There are several advantages of ytterbium atomic clock. The lattice electric field induced frequency shift is removed in spin-1/2 system. And ^{171}Yb reduces the collisional shift because fermionic isotope atoms does not interact with each other due to Pauli exclusion principle.

1.1.2 Cold collision properties

The interaction between atoms can be described by collisional parameters. Cold collision research is related to a variety of different research areas including optical manipulation of chemical processes, quantum degenerate gases, precision measurements, and spectroscopy. When the inter-atomic distance is the order of de Broglie length, their interaction can be no more treated as of classical nuclear point-particles with atom's electron distribution. There are two kinds of low temperature collisions: cold and ultracold collisions.

Cold collisions occur when the de Broglie length is on the order of a chemical bond distance. For example, when two atoms move to each other, they can absorb photons, which are resonant with their molecular states, and form a bound excited molecule; quasi-molecule. This molecule decays and emits photons at different internuclear separation from the one at which they were made. The difference in binding energy the molecules results in the kinetic energy of atoms and therefore they escape from the trap region [13], [14], [15], [16], [17].

Ultracold collisions occur when the de Broglie length is on the order of the mean distance between atoms. There are no photon-related processes in this case. They are described in terms of a phase shift or scattering length, a, of the ground state wave functions. The sign of a determines the stability of condensation: $a > 0$ results in stable condensate, $a < 0$ results in unstable BECs, where they have an attractive interaction, and the BECs collapse [18], [19], [20], [21], [22], [23].

1.2 Outlines

In chapter 2, we introduce the general properties and the optical properties of ytterbium. In chapter 3, we explain the qualitative descriptions and quantitative mathematical expressions for atomic cooling process with laser. In chapter 4, we introduce the experimental setups for ytterbium MOT: the ultra high vacuum chamber system, the laser systems. In chapter 5, we explain how the ytterbium MOT was constructed and the characteristics of MOT, such as the temperature, the number of trapped atoms. And we measured the loss terms of the blue Yb MOT.

Chapter 2. Properties of ytterbium

Ytterbium atom is a rare earth element of the lanthanide series, represented by the symbol Yb and its atomic number is 70. The ground state electronic configuration of Yb is [Xe]$4f^{14}6s^2$, where [Xe] is the closed shell electronic configuration of a Xenon atom. Yb has two electrons in its valence shell (6s). The melting and boiling temperatures are 1097 K and 1469 K, respectively, and is fairly stable in air but will slowly react with moisture in the air. Ytterbium has seven isotopes, five even isotopes with I=0 (^{168,170,172,174,176}Yb) and two odd isotopes, ^{171}Yb (I=1/2) and ^{173}Yb (I=5/2). The even isotopes are bosons, and the odd isotope are fermions.

2.1 Optical transitions of ytterbium

For the cooling and trapping of Yb, there are two optical transitions available: the blue ^{1}S$_0$-^{1}P$_1$ transition at 398.9 nm and the narrow green inter-combination transition ^{1}S$_0$-^{3}P$_1$ at 555.6 nm [24]. The low energy levels of ytterbium (^{174}Yb) are shown in Fig 2.1. The blue transition is an allowed dipole transition, and it has a short lifetime of the state ^{1}P$_1$ of 5.5 ns, with a broad linewidth of 28 MHz. The green transition is an intercombination transition ($\Delta S = 1$), and has a relatively long lifetime of 850 ns, with a linewidth of 187 kHz. Both of these transitions are approximately two-level optical transitions, but the blue transition is not completely closed. Atoms in the ^{1}P$_1$ state have non-zero decay probability into either one of the ^{3}D$_2$ or ^{3}D$_1$ states with a branching ratio that has a lower limit of 1.2×10^{-7} [25]. The atoms in ^{3}D$_2$ or ^{3}D$_1$ states can then decay into one of the ^{3}P$_2$,^{3} P$_1$,^{3} P$_0$ states, where ^{3}P$_2$ and ^{3}P$_0$ are metastable [26]. The lifetimes of these states, ^{3}P$_2$ and ^{3}P$_0$, are extremely long (12 s for ^{3}P$_2$, 21 s for ^{3}P$_0$). Table 2.2 and Figure 2.2 show the relative strength, the isotope shifts, and the hyperfine splitting for the blue (^{1}S$_0$-^{1}P$_1$) transition. Table 2.3 and Figure 2.3 show the same physical parameters for the green (^{1}S$_0$-^{3}P$_1$) transition.

Table 2.1: Natural abundance and nuclear spin of stable isotope of Yb

Isotope	Natural abundance(%)	Nuclear spin
^{168}Yb	0.13	0
^{170}Yb	3.04	0
^{171}Yb	14.28	1/2
^{172}Yb	21.83	0
^{173}Yb	16.13	5/2
^{174}Yb	31.83	0
^{176}Yb	12.76	0

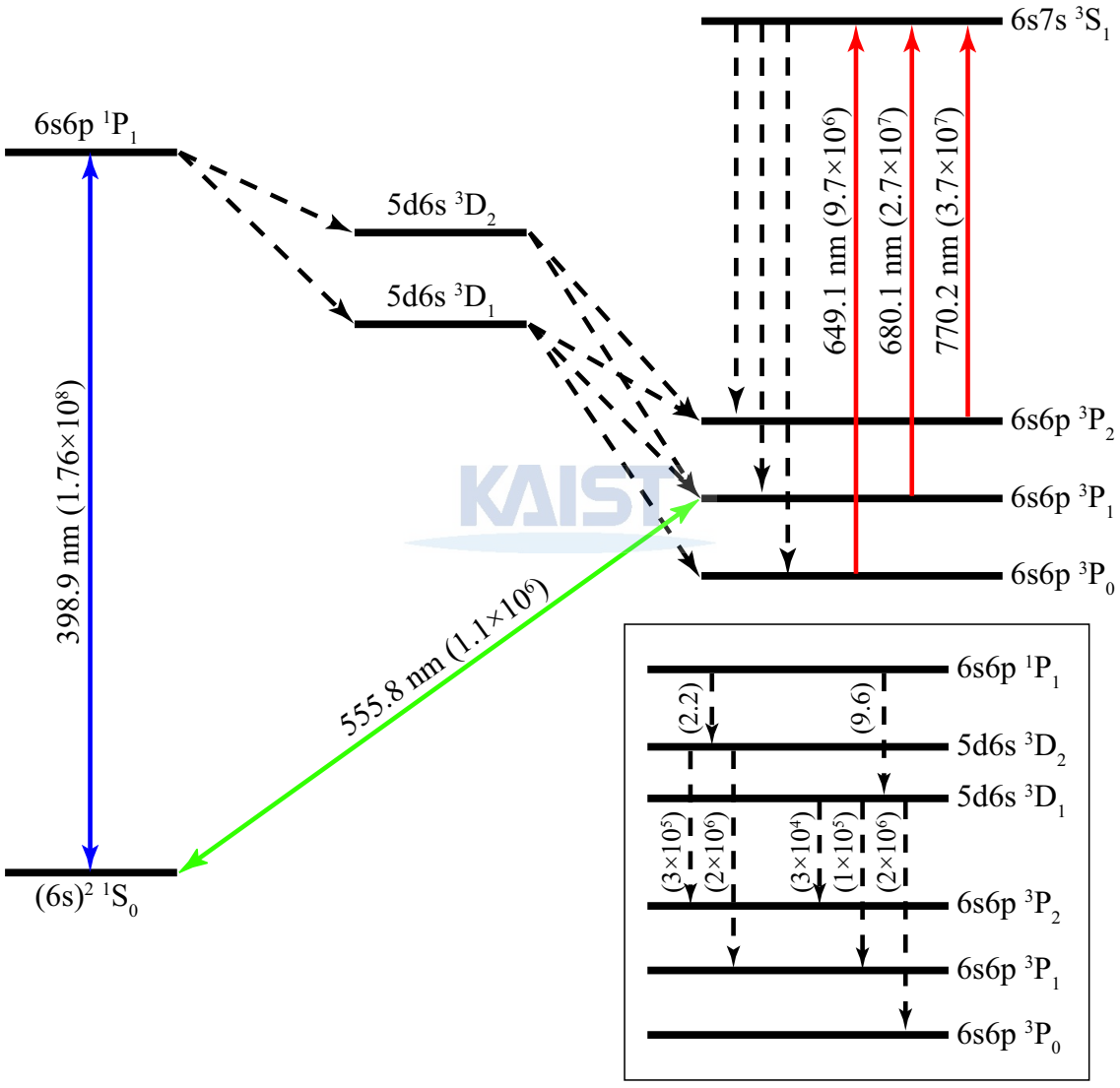

Figure 2.1: The lowest energy levels of ytterbium

Table 2.2: Hyperfine levels, relative strength, isotope shifts and hyperfine splitting of the $^1S_0$-$^1P_1$ transition [27].

Isotope/hyperfine	Relative Strengths	Shift(MHz)
176	0.1273	0
173 (5/2 - 5/2)	0.0498	272.1
174	0.3184	509.4
173 (5/2 - 3/2)	0.0225	1008.86
172	0.2182	1039.3
173 (5/2 - 7/2)	0.0884	1092.8
171 (1/2 - 3/2)	0.1140	1352.7
171 (1/2 - 1/2)	0.0285	1654.5
170	0.0303	1690.8
168	0.00135	2388.5

Table 2.3: Hyperfine levels, relative strength, isotope shifts and hyperfine splitting of the $^1S_0$-$^3P_1$ transition [28].

Isotope/hyperfine	Relative Strength	Shift(MHz)
173 (5/2 - 7/2)	0.0715	0
171 (1/2 - 1/2)	0.0476	255
176	0.1274	1432
174	0.3187	2386
172	0.2184	3387
170	0.0303	4673
173 (5/2 - 5/2)	0.0537	4698
168	0.0014	6044
171 (1/2 - 3/2)	0.0952	6192
173 (5/2 - 3/2)	0.0358	6193

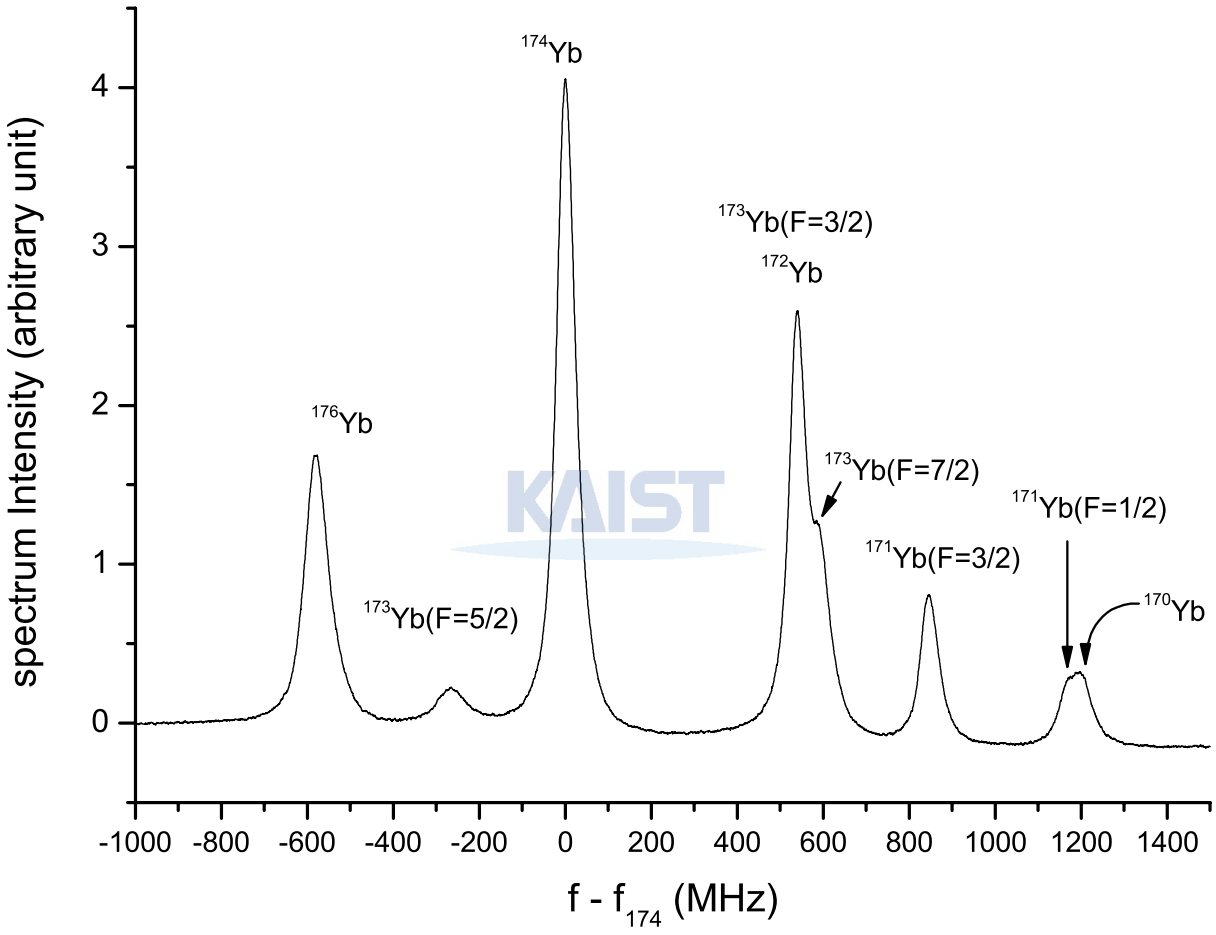

Figure 2.2: The isotope shift of ytterbium atom in $^1S_0$-$^1P_1$ (398.9 nm) transition fluorescence signal

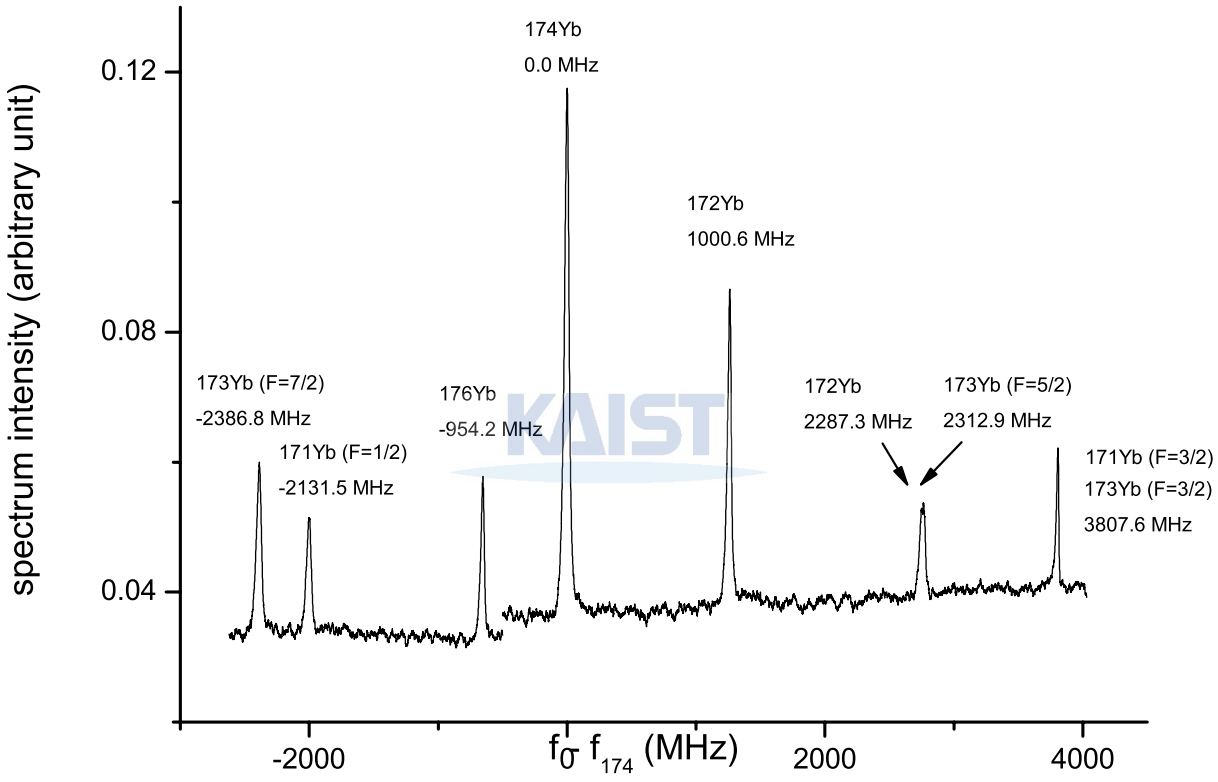

Figure 2.3: The isotope shift of ytterbium atom in $^1S_0$-$^3P_1$ (555.8 nm) transition fluorescence signal

2.2 Physical parameters for the cooling and trapping of ytterbium atoms (Yb^{174})

The physical parameters of ytterbium atom (Yb^{174}) useful for the cooling and trapping experiments are listed in Table 2.4 [29]. For example, the main optical two-level transition is at 398.9 nm and the saturation intensity for this transition is 59.6 mW/cm^2. The Doppler limit temperature is $T_D = 694$ μK which corresponds to the Doppler limit velocity of $v_D = 18$ cm/s. The capture velocity for the experiment has been designed as $v_c = 1154$ cm/s.

Table 2.4: Calculation of ytterbium parameters for cooling and trapping

Parameters	$^1S_0 - ^1P_1$	$^1S_0 - ^3P_1$	Description
g_J	1.035	1.493	Landé g-factor
τ (ns)	5.5	850	Life time of excited state
$\gamma/2\pi$ (MHz)	28.9373	0.1872	Spontaneous decay frequency
I_s (mW/cm^2)	59.5817	0.1425	Saturation intensity
T_D (μK)	694.3839	4.4931	Doppler limit temperature
v_D (cm/s)	18.2660	1.4693	Doppler limit velocity
v_c (cm/s)	1154.34	10.4069	Capture velocity
Ω (Hz/$\sqrt{W/m^2}$)	5.2670E+06	6.9679E+05	Rabi frequency per unit power

Chapter 3. Laser cooling and trapping

3.1 Doppler cooling

Doppler cooling is atomic cooling technique with laser. When an atom moves with velocity of $\vec{v}$ and laser field is counter-propagating to the atom with the frequency ω_L, which is lower than the atomic resonance frequency, in the atom's reference frame, the laser frequency is shifted by Doppler effect. The laser frequency ω'_{L} is similar to the atomic resonance frequency ω_{o} in atom's reference frame. The schematic description is shown in Fig. 3.1 a). The laser frequency in atom's reference frame is given by

$$\omega'_{\mathrm{L}} = \omega_{\mathrm{L}} - \Delta\omega_{\mathrm{D}}, \tag{3.1}$$

where $\Delta\omega_{\mathrm{D}}$ is the Doppler frequency shift. We consider only the first-order Doppler shift, then $\Delta\omega_{\mathrm{D}}$ is given by

$$\Delta\omega_{\mathrm{D}} = \vec{\mathrm{k}} \cdot \vec{v}, \tag{3.2}$$

where $\vec{\mathrm{k}}$ is the wavevector of laser field. When an atom absorbs a photon from the laser field, the atom loses the momentum $\hbar\vec{\mathrm{k}}$ and the atomic internal state changes from the ground state to the excited state. After the time τ (lifetime of the excited state), the excited atom releases a photon through spontaneous emission process. Then the atom receives momentum kicking of $-\hbar\vec{\mathrm{k}}'$, where $\vec{\mathrm{k}}'$ is the wavevector of the spontaneously emitted photon. Figure 3.1 b) shows the schematic description of the whole process. After N times of absorption and emission process, the sum of momentum changes in the spontaneous emission process is almost zero, because the emitted photon is released to random direction. The net change of atomic momentum is decreased by the amount of $N\hbar\mathrm{k}$. And the translational kinetic energy $\mathrm{E_K} = P^2/2m$, where P is the atomic momentum and m is the atomic mass, decreases and the atom slows down. We describe this process with mathematical formula: In steady-state, the total force exerted by laser is equal to the momentum change by single photon times the mean number of photons absorbed from the laser field per unit time.

$$\vec{\mathrm{F}} = \left[\frac{dN}{dt}\right]_{ss} \hbar\vec{\mathrm{k}}, \tag{3.3}$$

where $\left[\frac{dN}{dt}\right]_{ss}$ is the scattering rate, and N is the mean number of photons absorbed from the laser field per unit time.

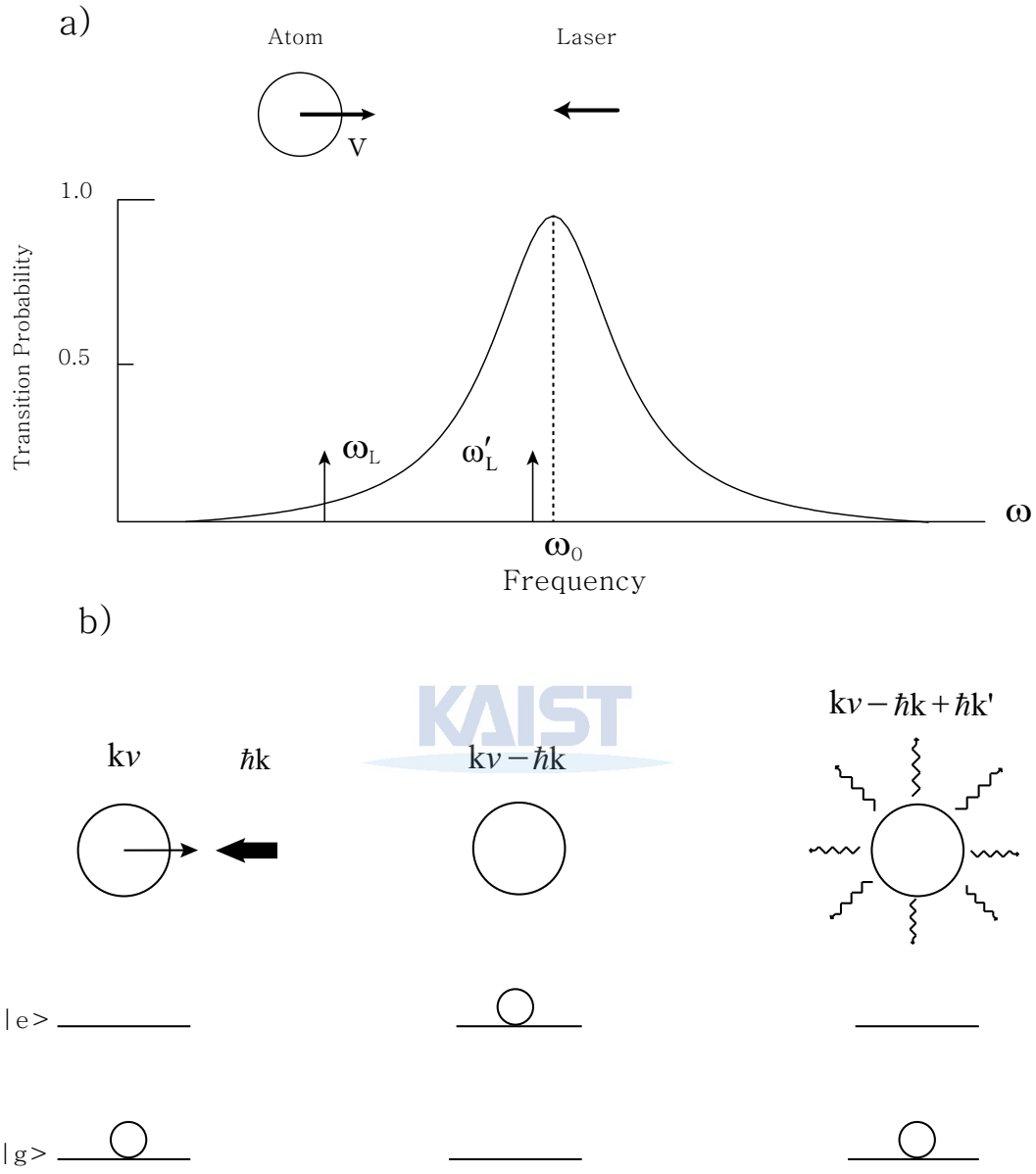

Figure 3.1: Schematic description of the Doppler cooling. a) An atom moves toward laser incoming direction. In atom's reference frame, the laser frequency ω_L is up-shifted to ω'_L near ω_o, which is the atomic resonant frequency in the atom's reference frame. b) When an atom absorbs a photon, the atom in the ground state transits to the excited state. After the lifetime of the excited state, the atom in the excited state decays to the ground state and releases a photon.

In steady state, the number of photons absorbed per unit time equals the number of photons emitted spontaneously per unit time. Then, scattering rate is expressed by

$$\left[\frac{dN}{dt}\right]_{ss} = \Gamma\rho_{ee}, \tag{3.4}$$

where ρ_{ee} is the excited-state population in the steady state. When the atoms in a two-level energy system are excited by the laser field, it is described by the optical Bloch equations [30]. From the result of optical Bloch equation, the value ρ_{ee} is given by

$$\rho_{ee} = \left(\frac{\Omega^2}{4\Delta^2 + \Gamma^2 + 2\Omega^2}\right). \tag{3.5}$$

Then the force is

$$\vec{\mathrm{F}} = \hbar\vec{\mathrm{k}}\left(\frac{\Gamma\Omega^2}{4\Delta^2 + \Gamma^2 + 2\Omega^2}\right). \tag{3.6}$$

We can express equation (3.6) in more useful form by using the saturation parameter s, which is related to the Rabi frequency of transition, are given

$$s = \frac{I}{I_s} = \frac{2\Omega^2}{\Gamma^2}, \tag{3.7}$$

where I is the laser intensity and I_S is the saturation intensity of transition Then the force equation for an atom is

$$\vec{\mathrm{F}}(s,\Delta) = \frac{\hbar\vec{\mathrm{k}}\Gamma}{2}\left(\frac{s}{1 + s + \frac{4(\Delta - \vec{\mathrm{k}}\cdot\vec{v})^2}{\Gamma^2}}\right) = m\vec{a}, \tag{3.8}$$

where m is the atomic mass and $\vec{a}$ is the acceleration. For $s \gg 1$, the acceleration, $|\vec{a}|$, approaches to a maximum value :

$$a_{max} = \frac{\hbar\mathrm{k}\Gamma}{2m}. \tag{3.9}$$

Next, when an atom is between two counter-propagating lasers, known as the optical molasses [31], the total force experienced by the atom is the sum of each laser force. The total force is given by

$$\begin{aligned}
\mathrm{F}(s,\Delta) &= \frac{\hbar\mathrm{k}\Gamma}{2}\left(\frac{s}{1 + s + \frac{4(\Delta - \mathrm{k}v)^2}{\Gamma}} - \frac{s}{1 + s + \frac{4(\Delta + \mathrm{k}v)^2}{\Gamma}}\right) \\
&\approx \frac{\hbar\mathrm{k}\Gamma}{2}\left(\frac{s}{1 + \frac{4(\Delta - \mathrm{k}v)^2}{\Gamma}} - \frac{s}{1 + \frac{4(\Delta + \mathrm{k}v)^2}{\Gamma}}\right) \qquad (\text{for } \; s \ll 1) \\
&= \frac{\hbar\mathrm{k}\Gamma}{2}\frac{\mathrm{k}v}{\Gamma}\left(\frac{16\Delta s/\Gamma}{1 + \frac{8}{\Gamma^2}(\Delta^2 + \mathrm{k}^2v^2) + \frac{16}{\Gamma^2}(\Delta^2 - \mathrm{k}^2v^2)^2}\right).
\end{aligned} \tag{3.10}$$

The force is maximum value at $|2\mathrm{k}v/\Gamma| \sim 1$. For $\Delta < 0$, the force damps the atomic velocity. And for $\Delta > 0$, the force accelerates the atoms. For $|\mathrm{k}v| \ll \Gamma$ and $|\mathrm{k}v| \ll |\Delta|$, Equation (3.10) can be expressed by the velocity dependent form

$$F = 4\hbar \mathrm{k} s \frac{\mathrm{k}v(2\Delta/\Gamma)}{(1+(2\Delta/\Gamma)^2)^2} = \alpha v, \tag{3.11}$$

where the damping coefficient α is

$$\alpha = 4\hbar \mathrm{k}^2 s \frac{2\Delta/\Gamma}{(1+(2\Delta/\Gamma)^2)^2}. \tag{3.12}$$

And velocity damping occurs when $\alpha < 0$.

3.2 Zeeman slowing

To decelerate the atomic velocity continuously along the atomic propagating direction, Zeeman shift cooling is used. In Zeeman shift cooling, atomic resonance phenomenon is maintained between the laser frequency change with Doppler effect and atomic transition frequency change with Zeeman shift due to the external magnetic field. Zeeman shift cooling is schematically described in Fig. 3.2. In the presence of external magnetic field, the Zeeman energy shift energy is given by

$$\Delta E = \pm \mu B, \tag{3.13}$$

where μ is the magnetic moment and B is the magnetic field amplitude. Then the $m_J = \pm 1$ excited state energy is changed by Zeeman effect from the $m_J = 0$ state energy. σ^+ polarized light drives transition between the J = 0 and the J = 1 ($m_J = 1$), σ^- polarized light drives transition between the J = 0 and the J = 1 ($m_J = -1$). Then we have two possible Zeeman slowing configurations; σ^- cooling (Fig. 3.2 a) and σ^+ cooling (Fig. 3.2 b). For σ^- cooling, the σ^- polarized cooling laser is resonant frequency with atomic transition by Doppler effect. The magnetic field magnitude is small at the entrance of the slowing region and is large at the exit of the slowing region. Here, the laser frequency changes by the Doppler shift due to the slowing atom is matched the Zeeman shift of the J = 0 $\rightarrow$ J = 1 ($m_J = -1$) transition frequency. As the atomic velocity is slowed down, the Zeeman shift increases. For σ^+ cooling, the σ^+ polarized cooling laser is resonant with atomic transition J = 0 $\rightarrow$ J = 1 ($m_J = 0$). The magnetic field magnitude is large at the entrance of the slowing region and the magnetic field magnitude is small at the exit of the slowing region. As atoms enter the slowing region, the J = 0 $\rightarrow$ J = 1 ($m_J = 1$) transition energy is shifted by the magnetic field and matched the laser frequency shift by Doppler effect. As the atomic velocity is slowed down, the Zeeman shift also decreases.

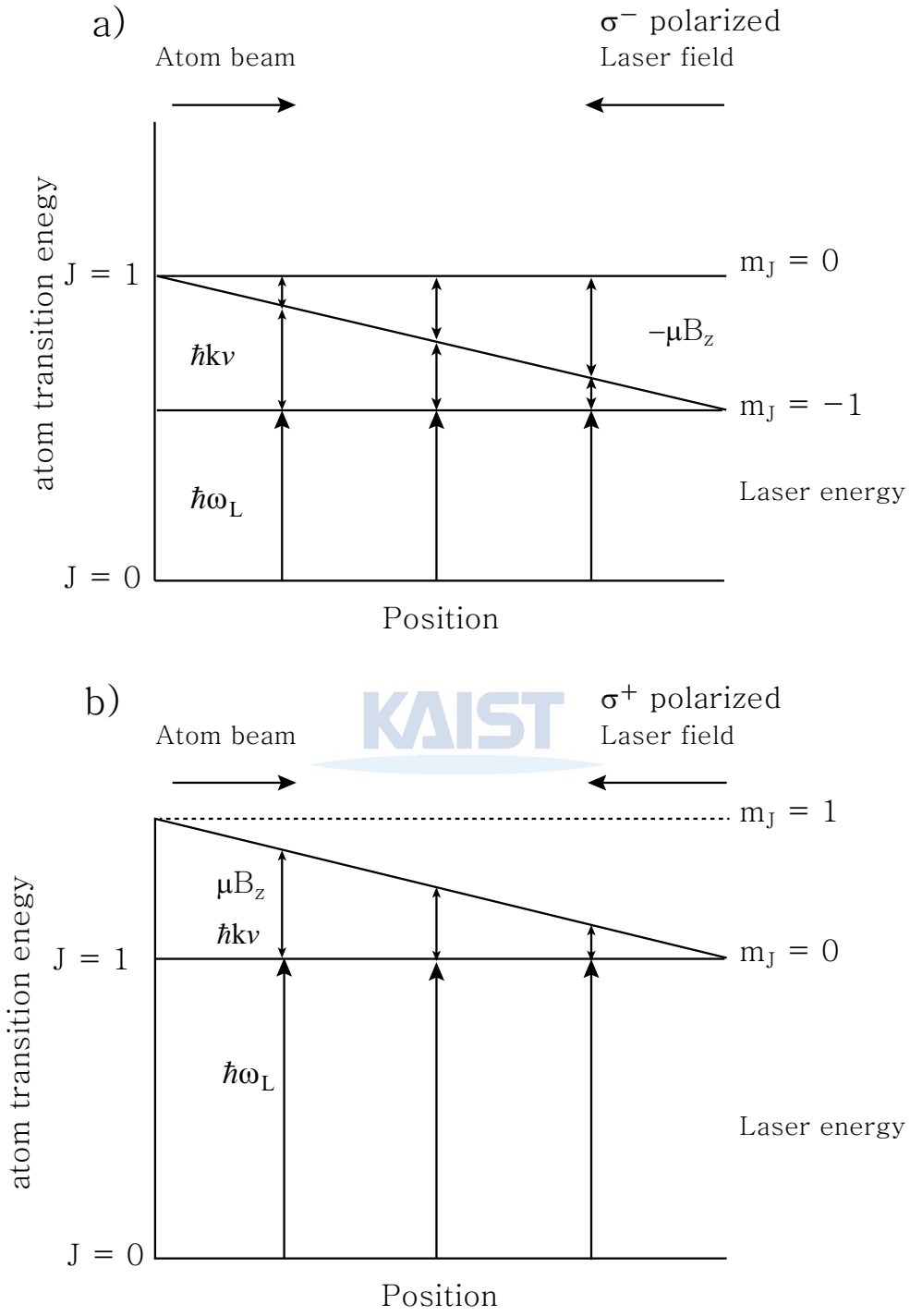

Figure 3.2: Schematic descriptions of (a) σ^- and (b) σ^+ polarized Zeeman shift cooling configurations.

3.3 Magneto-optical trap

To trap an atom at specific position, the position-dependent force is required. The magneto-optical trap uses optical molasses and position-dependent force. Figure 3.3 describes the magneto-optical trapping of atom in one dimension. An atom located at $z = 0$ is illuminated by two counter-propagating light fields having opposite polarization and the frequency, ω_L, slightly below the unperturbed atomic resonance frequency ω_o. The magnetic field $\vec{B}_z$ that increases linearly with distance from $z = 0$, where magnetic is. For $z < 0$, the magnetic field vector is in the opposite direction.

As shown in Fig. 3.3, for $z > 0$ the magnetic field up-shifts for the J = 0 → J = 1 ($m_J = 1$) transition frequency and down-shifts for the J = 0 → J = 1 ($m_J = -1$) transition frequency. While for $z < 0$, the magnetic field up-shifts for the J = 0 → J = 1 ($m_J = -1$) transition frequency and down-shifts for the J = 0 → J = 1 ($m_J = 1$) transition frequency. When an atom with near zero velocity that is moved to $z < 0$. Here, the σ^+ cooling laser propagating to the $+\hat{z}$ direction is nearly resonant with the J = 0 → J = 1($m_J = 1$). So, the atom will absorb photons from σ^+ light, time averaged force toward $z = 0$ where the absorption rates for the two cooling lasers are equal. Then force equation is modified from Eq. (3.10) with magnetic field effect to

$$\begin{aligned} F &= \frac{\hbar \mathrm{k}\Gamma}{2}\left(\frac{s}{1+s+\frac{4(\Delta-\mathrm{k}\upsilon-\mu\mathrm{bz}/\hbar)}{\Gamma}^2}-\frac{s}{1+s+\frac{4(\Delta+\mathrm{k}\upsilon+\mu\mathrm{bz}/\hbar)^2}{\Gamma}}\right) \\ &\approx \frac{\hbar \mathrm{k}\Gamma}{2}\left(\frac{s}{1+\frac{4(\Delta-\mathrm{k}\upsilon-\mu\mathrm{bz}/\hbar)}{\Gamma}^2}-\frac{s}{1+\frac{4(\Delta+\mathrm{k}\upsilon+\mu\mathrm{bz}/\hbar)^2}{\Gamma}}\right) \qquad (\text{for } \; s \ll 1) \\ &= \frac{\hbar \mathrm{k}\Gamma}{2}\left(\frac{(16\Delta s/\Gamma^2)(\mathrm{k}v+\mu bz/\hbar)}{1+\frac{8}{\Gamma^2}\left(\Delta^2+\mathrm{k}^2v^2+\left(\frac{\mu bz}{\hbar}\right)^2\right)+\frac{16}{\Gamma^4}\left(\Delta^2-\mathrm{k}^2v^2-\left(\frac{\mu bz}{\hbar}\right)^2\right)^2}\right). \end{aligned} \tag{3.14}$$

Zeeman shift is linear with respect to the position and the Doppler shift is also linear with respect to the velocity at near the trap center, satisfying the condition $|\mathrm{k}v|$, $\mu bz/\hbar\Gamma < \Gamma$, Δ, the force equation of MOT becomes

$$F = 4\hbar \mathrm{ks}\frac{2\Delta/\Gamma}{(1+(2\Delta/\Gamma)^2)^2}\left(\mathrm{kv}+\frac{\mu \mathrm{bz}}{\hbar}\right) = \alpha \mathrm{v} + \kappa \mathrm{z}, \tag{3.15}$$

where the damping coefficient α is given by Eq. (3.12) and the spring constant κ is

$$\kappa = 4\hbar \mathrm{k}s\frac{2\Delta/\Gamma}{(1+(2\Delta/\Gamma)^2)^2}\frac{\mu \mathrm{b}}{\hbar}. \tag{3.16}$$

Thus, for $\Delta < 0$, atoms move toward the trap center and the velocity of is near zero.

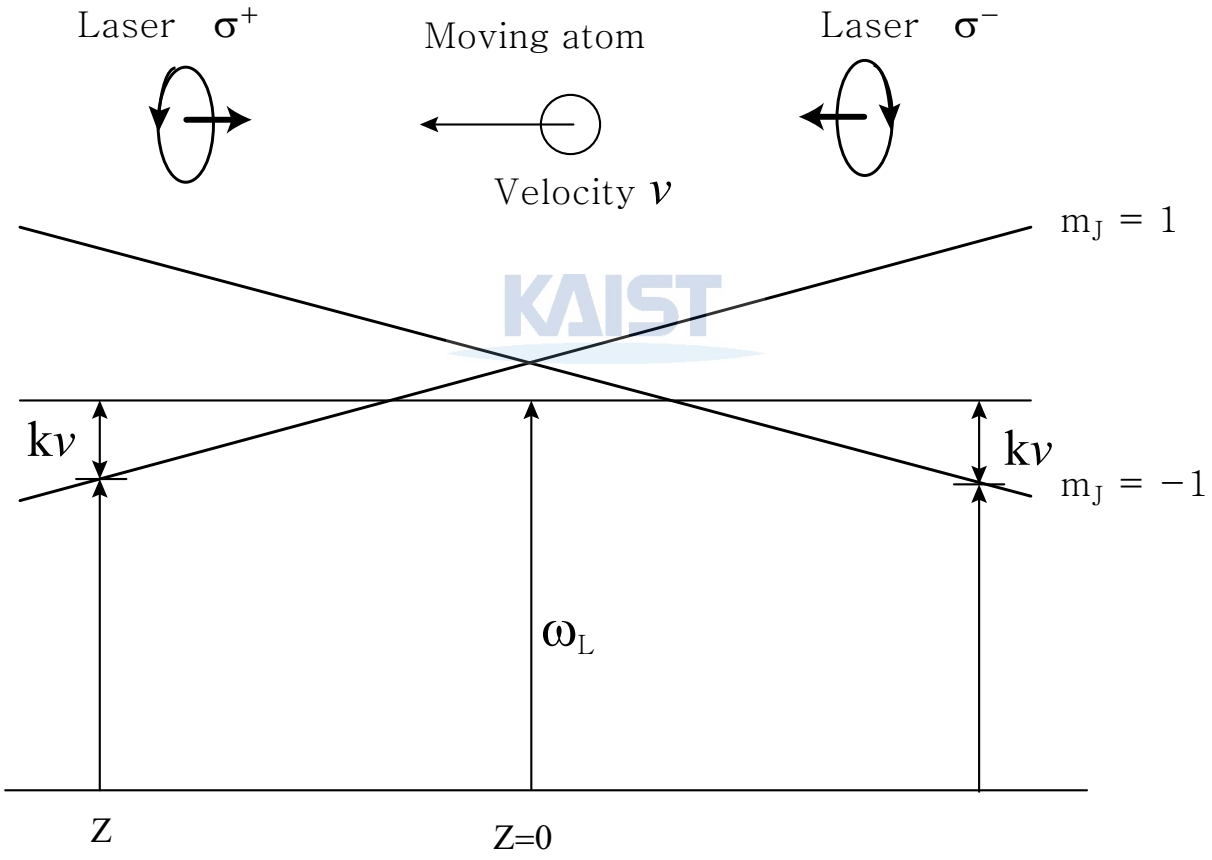

Figure 3.3: Schematic description of the magneto-optical trap in one dimension. At the position z, the Zeeman shift of transition frequency and Doppler shift are equal, and atom slows down and moves toward the center of MOT.

Chapter 4. Experimental setup

4.1 Vacuum system

There are two methods for generating atomic sources: atomic beam, which is densely accumulated and collimated; and vapor gases, which is relatively freely moving gases in the chamber. Alkali metals have room-temperature vapor pressure on the order of 10^{-7} Torr, which is sufficient for atomic source density. However, ytterbium atom should be heated to 200°C to obtain the given atomic source density. To trap ytterbium atoms in a magneto-optic trap for a long time, the ambient gas pressure should be maintained below the $10^{-8\sim9}$ Torr. There is a problem that the ambient gas pressure rises as the temperature of chamber is increased.

For this situation, a differential pumping is required. Differential pumping scheme is illustrated in Fig. 4.1. A main idea of differential pumping is that the oven region for the atomic source is separated from the trapping atom region. The atomic oven region and the main trap region are connected with very low-conductance vacuum component, which has a diameter of 16 mm, a length of 400 mm, and is used for the Zeeman slower coil mount in this system.

Then the main trap region has a lower vacuum pressure than the oven region on the order of 10^{-2} Torr. As the pressure of the oven region is lowered, the pressure of main trap part is lowered in the differential pumping scheme. To maintain the pressure of oven region low enough, we have installed an ion pump (40 l/s). We have also connected an ion pump (50 l/s) to the main chamber for maintaining the pressure of the chamber. Then we have achieved the vacuum pressure of the main chamber on the order 10^{-10} Torr.

4.1.1 Atom beam system

As mentioned before, a metal atomic sample is placed inside an oven and is heated to obtain the atomic source. The heated atoms effuse from the oven through a collimator, which is placed at the oven exit, and they form atomic beam. In this section, we review a theoretical explanation of atomic beam, and discuss the atomic beam's longitudinal velocity distribution and the total flux. When atoms in the oven are in thermal equilibrium with the oven wall, the velocity distribution for atoms follows Maxwell-Boltzmann

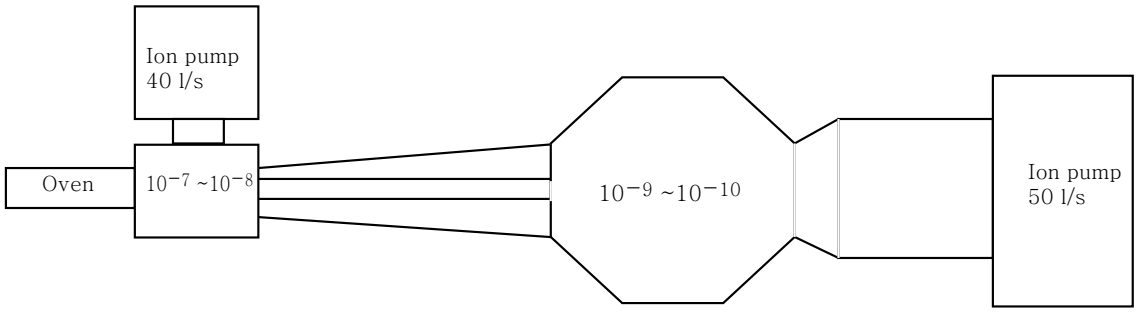

Figure 4.1: A schematic description for differential pumping system. The pressure of atomic oven region is below 10^{-7} Torr, and the pressure of main trap chamber region is below 10^{-9} Torr. They are connected with very narrow and long(low conductance) component.

velocity distribution function

$$f(v) = 4\pi \left(\frac{m}{2\pi \mathrm{k_B T}}\right)^{3/2} v^2 \exp\left(-\frac{mv^2}{2\mathrm{k_B T}}\right), \tag{4.1}$$

where m is the atomic mass, v is the speed of atoms, T is the absolute temperature of the oven, and $\mathrm{k_B}$ is Boltzmann constant. In this velocity distribution, the most probable velocity and the mean velocity are given by

$$\begin{aligned} v_{\mathrm{mp}} &= \sqrt{\frac{2k_B T}{m}}, \\ \bar{v} &= \int_0^\infty v f(v)\mathrm{dv} = \sqrt{\frac{8\mathrm{k_B T}}{\pi \mathrm{m}}}. \end{aligned} \tag{4.2}$$

When atoms escape from the oven, the mean velocity of atom is increased. Because the escaping probability increases as the velocity of atom increases. Consequently the velocity distribution for atoms exiting the atomic oven is modified and is shifted to higher velocity. This is known as a modified Maxwell-Boltzmann distribution [32] :

$$g(v) = 2\left(\frac{m}{2\mathrm{k_B T}}\right)^2 v^3 \exp\left(-\frac{mv^2}{2\mathrm{k_B T}}\right). \tag{4.3}$$

In this velocity distribution, the most probable velocity and the mean velocity are given by

$$\begin{aligned} v_{\mathrm{mp}} &= \sqrt{\frac{3k_B T}{m}}, \\ \bar{v} &= \sqrt{\frac{9\pi \mathrm{k_B T}}{8m}}. \end{aligned} \tag{4.4}$$

In Fig. 4.2, the solid line is Maxwell-Boltzmann distribution function ($f(v)$) and the

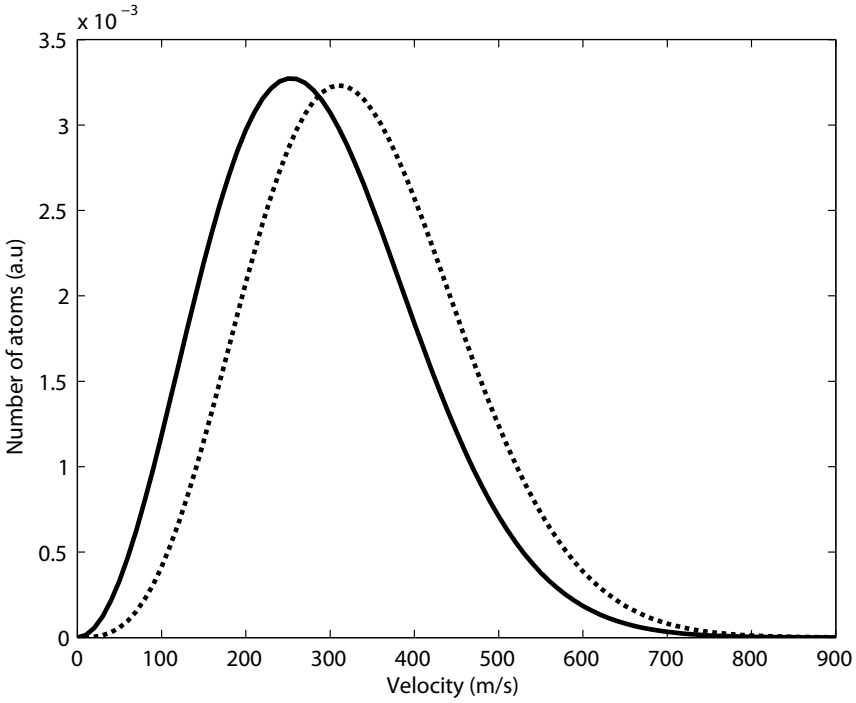

Figure 4.2: Solid line shows the Maxwell-Boltzmann velocity distribution and the dotted line shows the modified Maxwell-Boltzmann velocity distribution for the temperature 400°C.

dotted line is the modified Maxwell-Boltzmann distribution ($g(v)$) for the temperature of 400 °C in the atomic oven. The most probable velocity is up-shifted from 250 m/s (Maxwell-Boltzmann distribution) to 300 m/s (modified Maxwell-Boltzmann distribution).

The atomic flux through a circular hole(thin hole) with an area of A is given by

$$Q_0 = \frac{1}{4} n \bar{v} A, \tag{4.5}$$

where n is the atomic density inside atomic oven and $\bar{v}$ is the atomic mean velocity in the oven. For a channel with area A, radius r, and length l, the atomic flux is modified from Eq. (4.5) :

$$Q = \frac{1}{\kappa} \frac{1}{4} n \bar{v} A, \tag{4.6}$$

where $\frac{1}{\kappa} = \frac{8}{3}\left(\frac{r}{l}\right)$ for a channel with $l \gg r$.

Figure 4.3 shows a collimator used for atomic oven. The collimator is made by a plasma drilling machine. It has 25 holes with a 0.5-mm diameter and 4-cm length. There are two advantages in this feature: 1) Each hole acts as a good collimator which reduces the transverse velocity; 2) For making a high vacuum system, the holes act as parallel conductance of holes; it saves the time for the pumping. Atomic flux of one channel in the

Figure 4.3: A picture for the atom beam collimator. It is made by drilling holes into a stainless steel bolt and has 25 holes of a diameter of 0.5 mm and length of 40 mm.

collimator is $\frac{1}{\kappa} = \frac{8}{3}\left(\frac{0.35}{40}\right) \approx 0.0167$ for our collimator, and the total flux is a summation over all channels.

4.1.2 Zeeman slower

To effectively slow down the velocity of atoms in the Zeeman slower, the relation between the atomic velocity and the magnetic field profile satisfies the following equation:

$$\Delta = \frac{\mu B(z)}{\hbar} + \mathrm{k}v, \tag{4.7}$$

where Δ is the detuning from the resonance frequency of atom, k is the wavevector of laser field, and μ is the magnetic moment.

To characterize the Zeeman slower, we introduce several terms related to the velocity of atom shown in Fig. 4.4. At the entrance of Zeeman slower, the cut-off velocity, which is the maximum velocity to slow down, is given by

$$v_{cov} = \frac{\Delta}{\mathrm{k}}. \tag{4.8}$$

At the end of the Zeeman slower, the terminal velocity, which is the final velocity at the exit of Zeeman slower, is obtained from the Eq. (4.7) as

$$v_{terminal} = \frac{\Delta}{k} - \frac{\mu B_{exit}}{\hbar k}. \tag{4.9}$$

And the magnetic field profiles for σ^- Zeeman slower is given by,

$$B(z) \propto \ 1 - \sqrt{1 - \frac{z}{z_0}}, \tag{4.10}$$

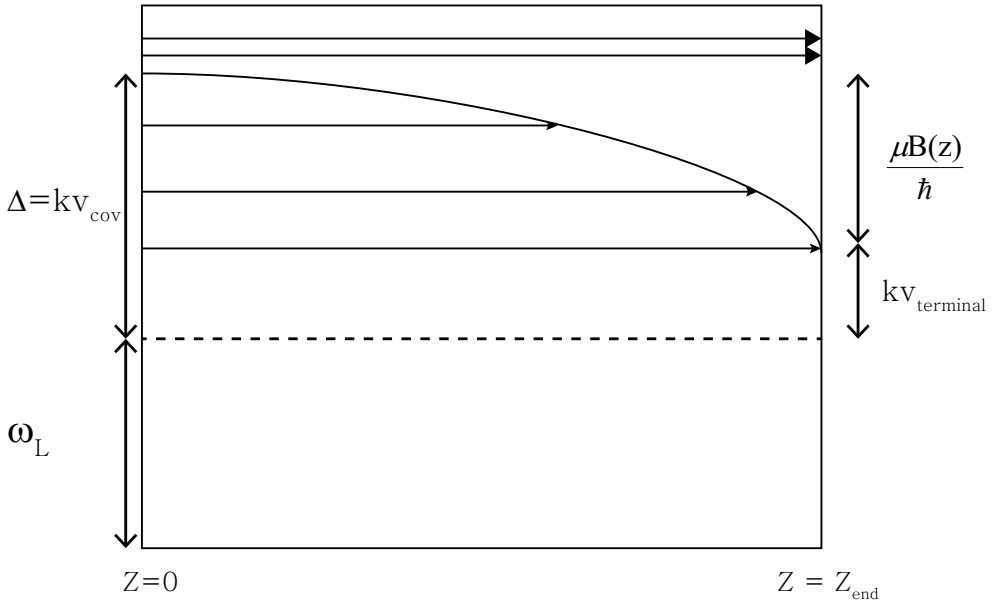

Figure 4.4: Zeeman slower configuration. Atoms with the velocity below the cut-off velocity are slowed down the terminal velocity.

where z_0 is the total length of the Zeeman slower.

We have constructed the σ^- cooling configuration. The coils are wounded on the coil mount (Fig. 4.5). At the starting point of Zeeman slower, the number of turns is less than the rest. And the number of turns increases toward the end. For σ^- slowing laser condition, the magnetic field tail of Zeeman solenoid coil could affect the magnetic field distribution at the trap center. So we have added the compensation coil to cancel out the magnetic field effect. The total length of Zeeman slower component is 400 mm. And the length of coil mount region is 290 mm. For satisfying the magnetic field distribution, the radius of coil mount varies like a step. The copper cooling water pipe was installed after the wire was wounded on the coil mount. The copper pipe is wrapped with aluminum foil for efficient cooling.

To obtain the velocity distribution change in the Zeeman slower, we have measured the fluorescence signal with a probe-laser. The probe-laser input direction is aligned 135° from the propagating direction of the atom beam. The reference-laser input direction is aligned 90° from the propagating direction of the atom beam without Doppler effect. Then the atomic velocity is calculated from the difference in fluorescence signal depending on the velocity.

Figure 4.6 shows the magnetic field distribution along the axial direction of the solenoid coil. The solid line is the measured magnetic field profile with a given geometric configuration in Fig. 4.5. We have measured the magnetic field with using the gauss meter along the Zeeman slower coil axis with the coil current of 2.5 A. And the dotted

line shows the theoretical line from Eq. (4.10). The theoretical line is calculated with conditions, the Zeeman slowing laser power is about 10 mW ($I = 0.4\ I_s$) and the cut-off velocity is 340 m/s. The difference between the theoretical line and the measured line is matched by adjusting the current and biased field. Figure 4.7 shows the velocity of atom and acceleration of Zeeman slower. Atoms with the cut-off velocity of 340 m/s are slowed down to the terminal velocity with constant deceleration.

Figure 4.8 shows the velocity distributions versus various slow laser detunings. The result shows the high fluorescence signal near the zero velocity due to the scattering from slowed atoms. The velocity is slowed down to zero velocity, and then the atomic beam is diffusing from the axis of atom beam line. If the velocity of atoms is not sufficiently cooled down, then the atoms pass thorough the trap region. So we need to tweak the detuning of Zeeman laser for maximizing the Zeeman slower performance. Ideally, all atoms with the velocity below the cut-off velocity at starting position are slowed down. Figure 4.9 shows the result of cut-off and terminal velocity depending on the slow laser detuning. As the detuning is large, the terminal velocity and cut-off velocity is large. Figure 4.10 shows cut-off velocity is 260 m/s for the current of Zeeman slower of 1.6 A and laser detuning of 580 MHz. Then the terminal velocity of atom beam is 13 m/s.

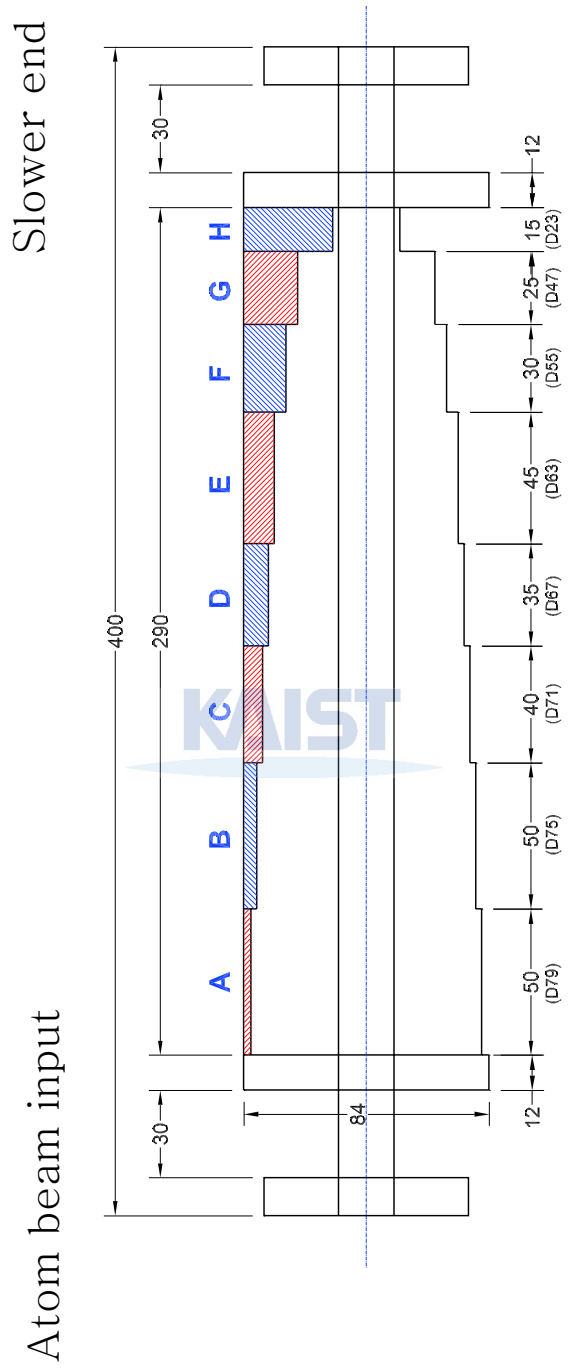

Figure 4.5: Zeeman Slower coil mount design. To make magnetic field gradient, the copper wire is wounded like a step.

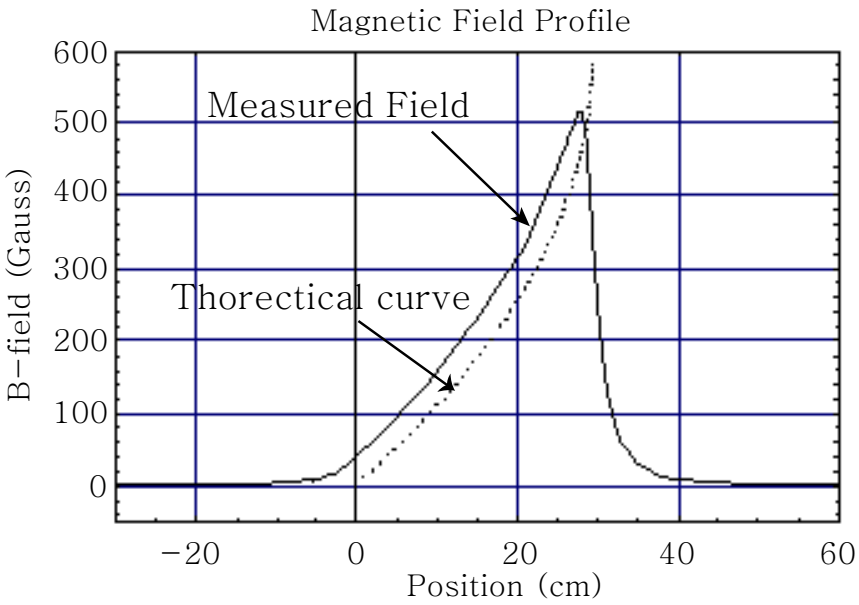

Figure 4.6: The solid line is the measured magnetic field profile for a current of 2.5 A and the dotted line is a numerical simulation for a given cut-off velocity and laser intensity.

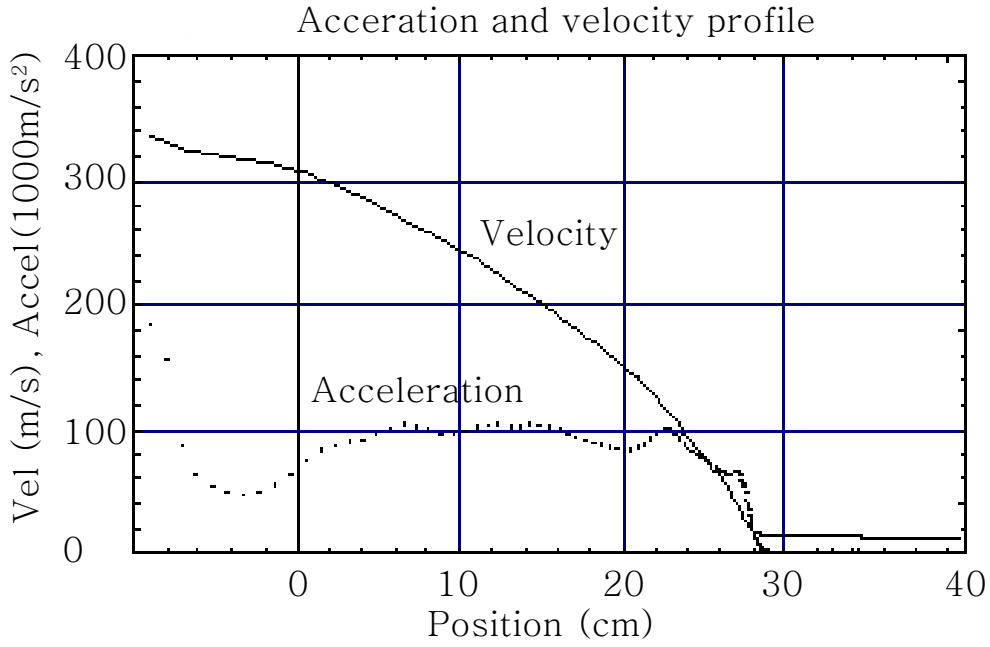

Figure 4.7: The deceleration (dotted line) and the velocity profile along the Zeeman slower (solid line), when the velocity of atom is 340 m/s.

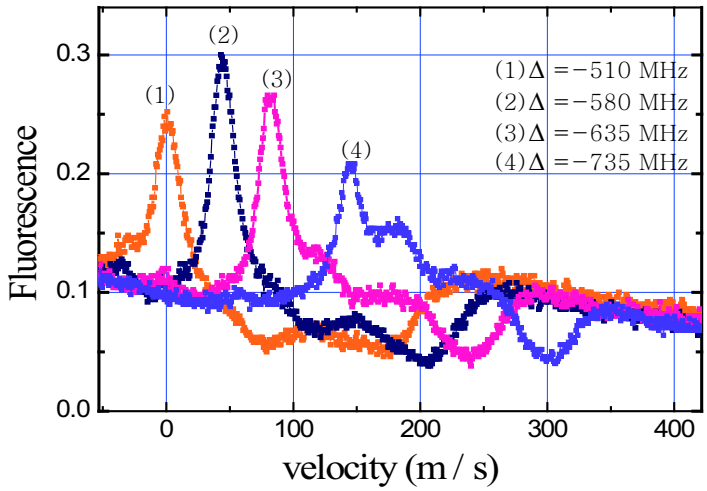

Figure 4.8: The Zeeman slowed velocity distributions for ^{174}Yb as a function of the detuning of slowing laser. (1) Δ = -510 MHz, $v_{terminal}$ =1.4 m/s, (2) Δ = -580 MHz, $v_{terminal}$ = 44 m/s, (3) Δ = -635 MHz, $v_{terminal}$ = 80 m/s, (4) Δ = -735 MHz, $v_{terminal}$ = 145 m/s.

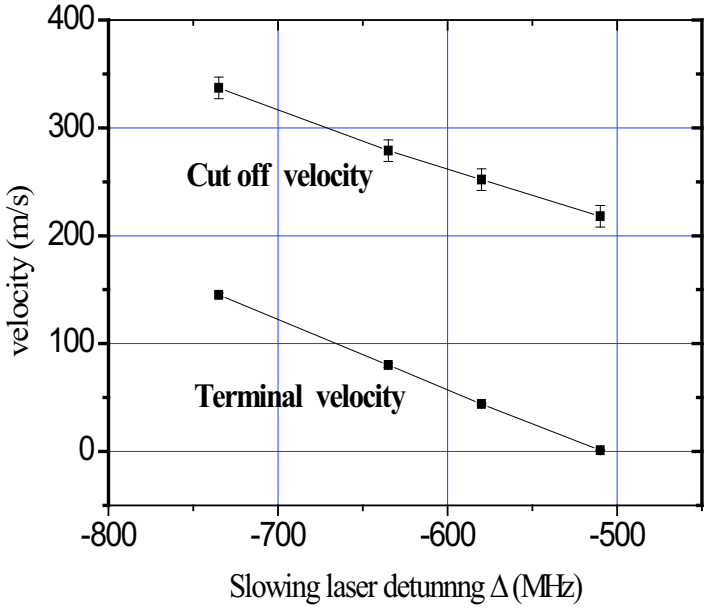

Figure 4.9: The cut-off velocity and the terminal velocity of Zeeman slower versus the slow laser detuning.

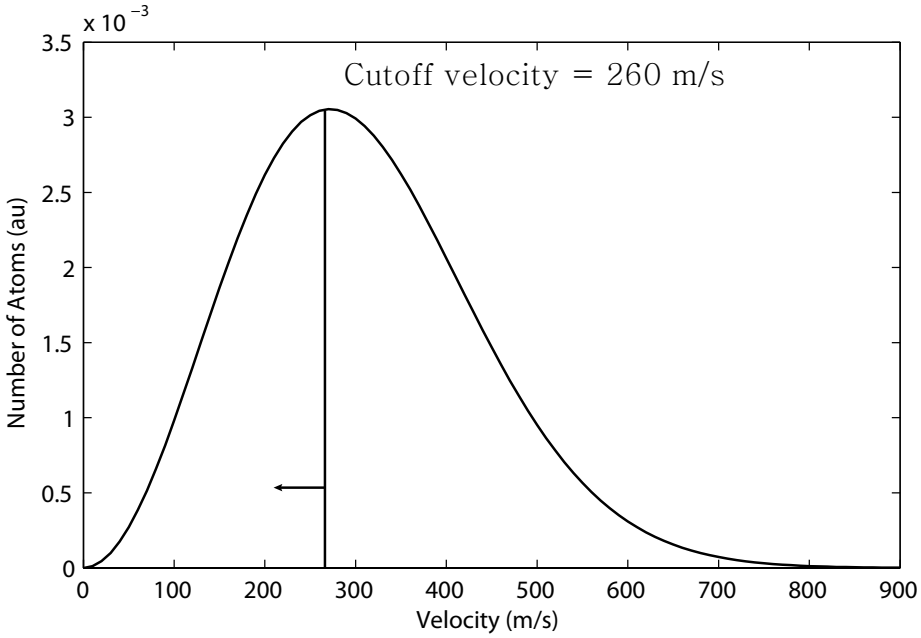

Figure 4.10: When a current of a Zeeman slower is 1.6 A, the cut-off velocity is 260 m/s.

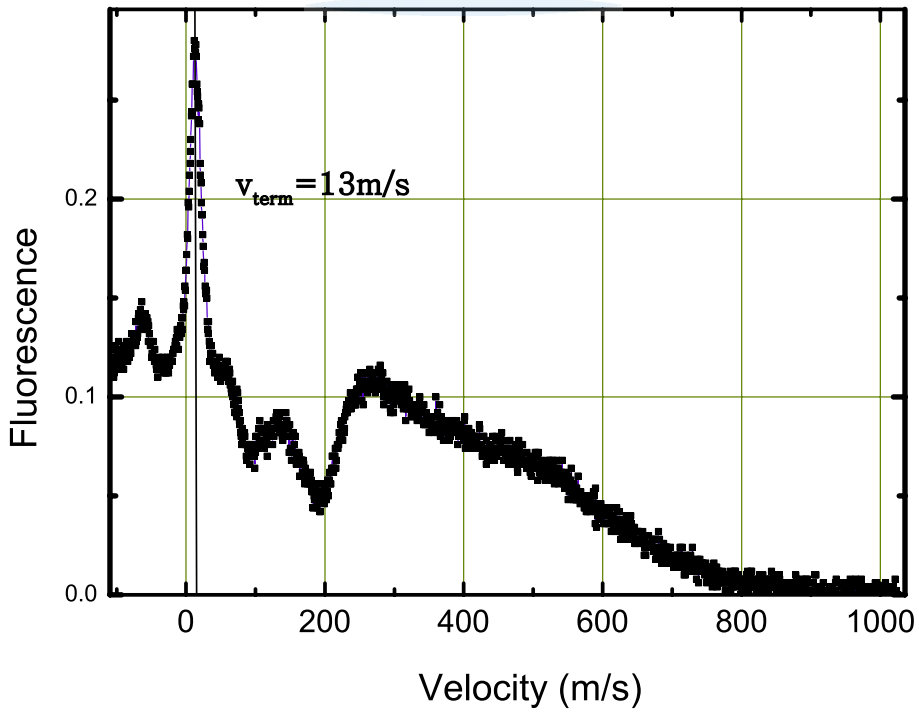

Figure 4.11: A terminal velocity of Zeeman slower. Most of atoms with velocity below the cut-off velocity are slowed down to the terminal velocity 13 m/s.

4.1.3 Trap chamber

The main chamber, where the ytterbium atoms are trapped, has 18 faces. It consist of 16 windows, 1 atom beam source input port, and 1 pumping port. To construct magneto-optical trapping of ytterbium atoms, the quadrupole magnetic field configuration has been used. Figure 4.12 shows the pair of coils have been mounted on the main trap chamber surface. As the radius of the coil is smaller, the magnetic field gradient is larger with the same current of coils in the trap chamber center. Therefore, we have made grooves on the surface, which is used for coil mount with a depth of 4 cm and a width of 2 cm. Total number of turns of the wounded wire was 170 on the groove and we have wounded an additional wire more than 200 turns. For sufficient magnetic field gradient for MOT, we had to send a bigger current through the winding wire of 170 turns. Then, the pressure of the main chamber was increased due to the heat of the coils.

The magnetic field gradient was measured in the axial and the radial direction for the anti-Helmholtz coil in Fig. 4.13. The axial directional magnetic field gradient is 20 G/cm and the radial directional gradient is 10 G/cm with 3-A current. The magnetic field gradient for the axial direction is 2 times larger than the radial direction.

The center position of the main chamber, which is also the MOT center, is not the zero magnetic field point, because many external sources affect the magnetic field such as geomagnetic field, the ion pump magnet, the Zeeman slower coil, etc. To make zero magnetic field at the chamber, we have installed shimming coil (Helmholtz coil) for x-, y-, and z-direction. The additional coils, which are shown in Fig. 4.12, are wounded on the surface of the trap chamber.

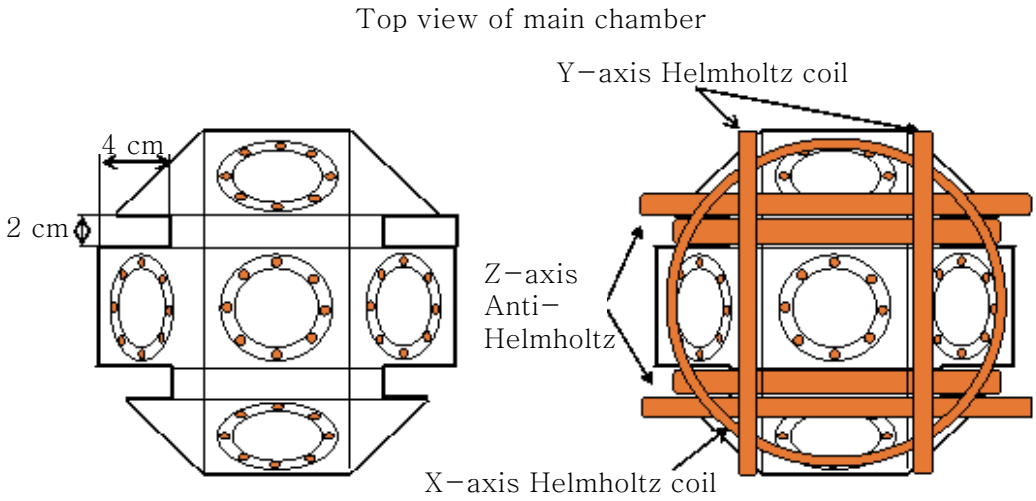

Figure 4.12: Geometrical distribution of anti-Helmholtz coil and shimming coil (Helmholtz coil).

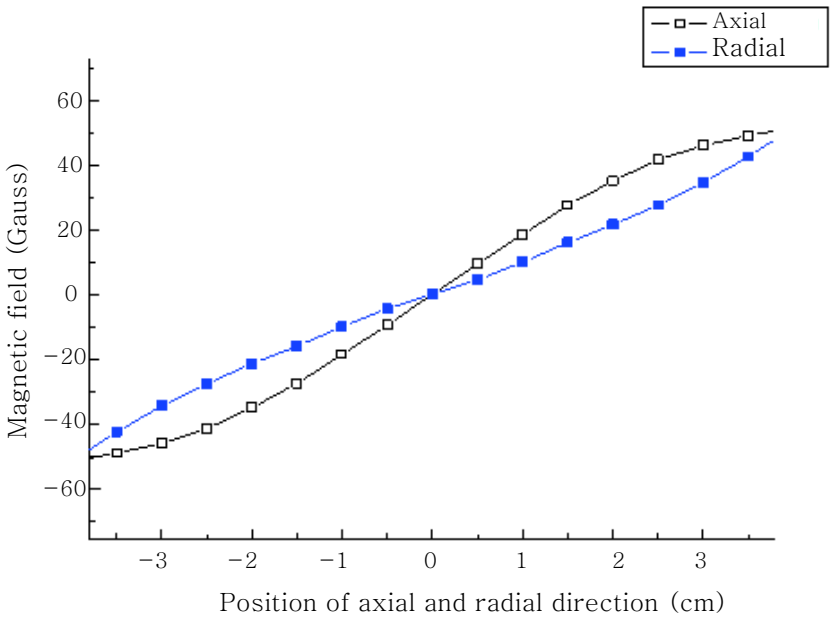

Figure 4.13: The magnetic field magnitude along the axial and radial directions generated by the anti-Helmholtz coil.

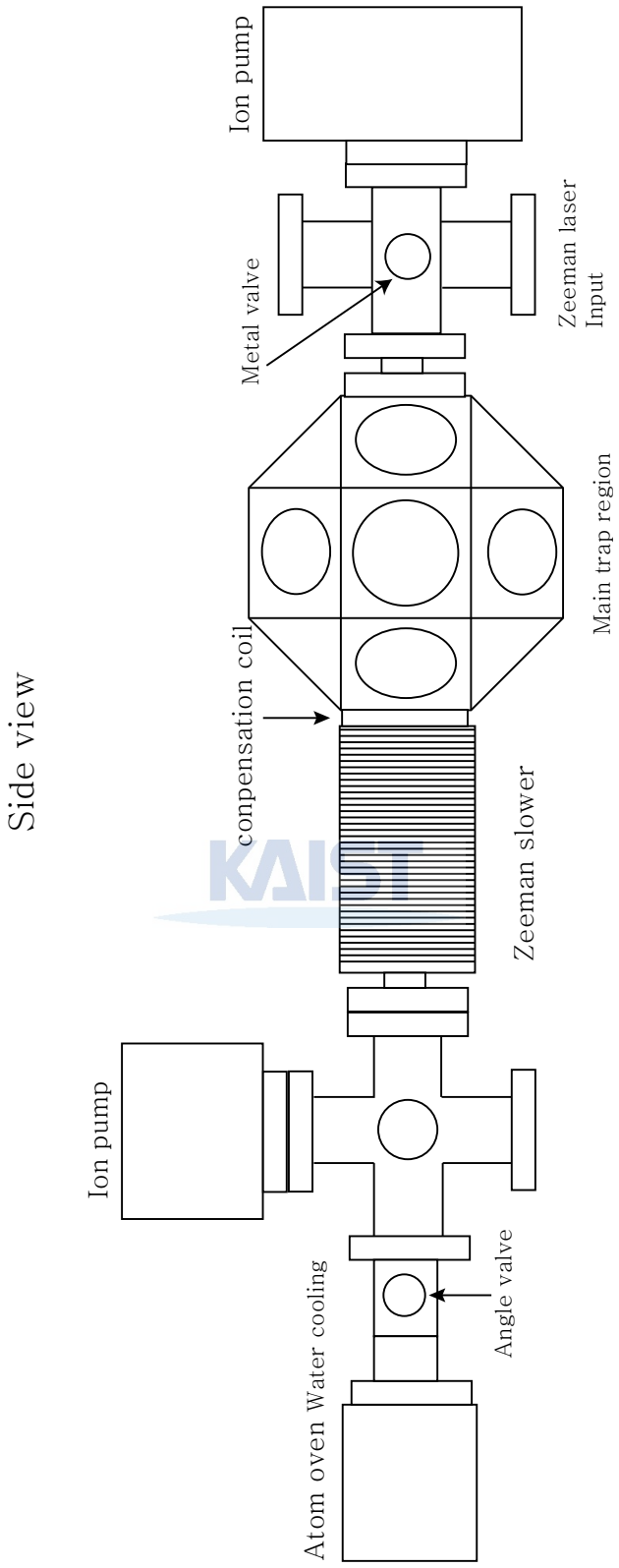

Figure 4.14: Schematic description for the whole vacuum chamber system.

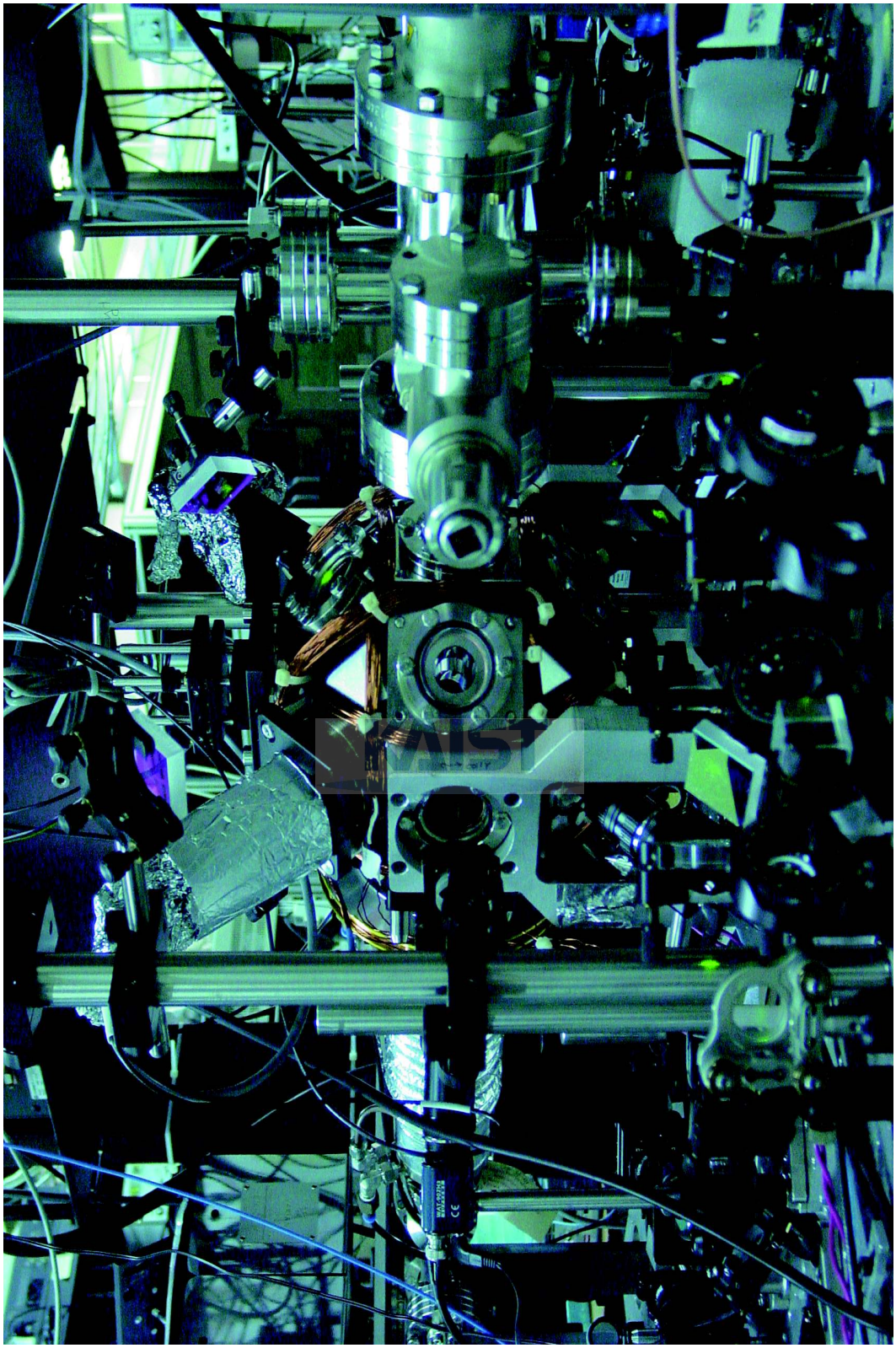

Figure 4.15: A picture of trap chamber.

4.2 Laser system

4.2.1 398.9 nm blue laser

There are many different laser systems with a wavelength of 398.9 nm. Examples include, dye lasers, frequency-doubling lasers, and diode lasers. In this dissertation, we have made a laser system using a commercial diode laser, which is easy to obtain and which is tunable along the wavelength by adjusting the current and the temperature of the diode laser. Commercial GaN diode lasers (Nichia NDV4313) with a wavelength ranging from 400 nm to 410 nm at room temperature (25°C) can be used. Because these lengths are slightly longer than 398.9 nm, we cooled the temperature of the diode laser below room temperature in this case. With this laser with the wavelength range of 400 nm to 401 nm, we obtained a wavelength of 398.9 nm cooling the diode laser until it was slightly below room temperature. We used a diode laser controller to control the current and temperature of the diode laser (SRS LDC500), and thus obtained the wavelength of 398.9 nm by cooling the temperature of the laser diode mount to 13 °C. The temperature of the diode laser was measured by a thermistor which was placed on the diode laser mount. The temperature of the diode laser was maintained to an accuracy of 1 mK. If the diode laser temperature falls below the dew point in summer, dewdrops can develop, which poses a problem. We therefore created an outer laser box with air-tight seal to maintain dry-air condition.

To investigate the atomic spectrum, the linewidth of the laser should be narrower than the linewidth of the atomic transition. The wavelength of the laser should also be tunable. A well-known method of atomic spectroscopy with a diode laser is to construct an external cavity diode laser (ECDL) system. The diode laser output beam propagates to the diffraction grating and the first diffracted laser beam provides feedback regarding the diode laser. The wavelength of the diode laser is determined according to the angle between the grating and the diode laser, and the length between the surface of the grating and the gain medium inside the diode laser. Therefore, a piezo translator, placed behind the grating, is used to tune the frequency of the diode laser (Littrow configuration).

We have made an injection locking system for cooling and trapping lasers. It consists of one master laser with, a narrow linewidth and a tunable the wavelength, and two slave lasers, controlled by the master laser that are used for cooling and trapping. The master laser was constructed with the ECDL system. By controlling the current and the temperature of the slave diode lasers, the spectrum of slave lasers follow the spectrum of the master laser.

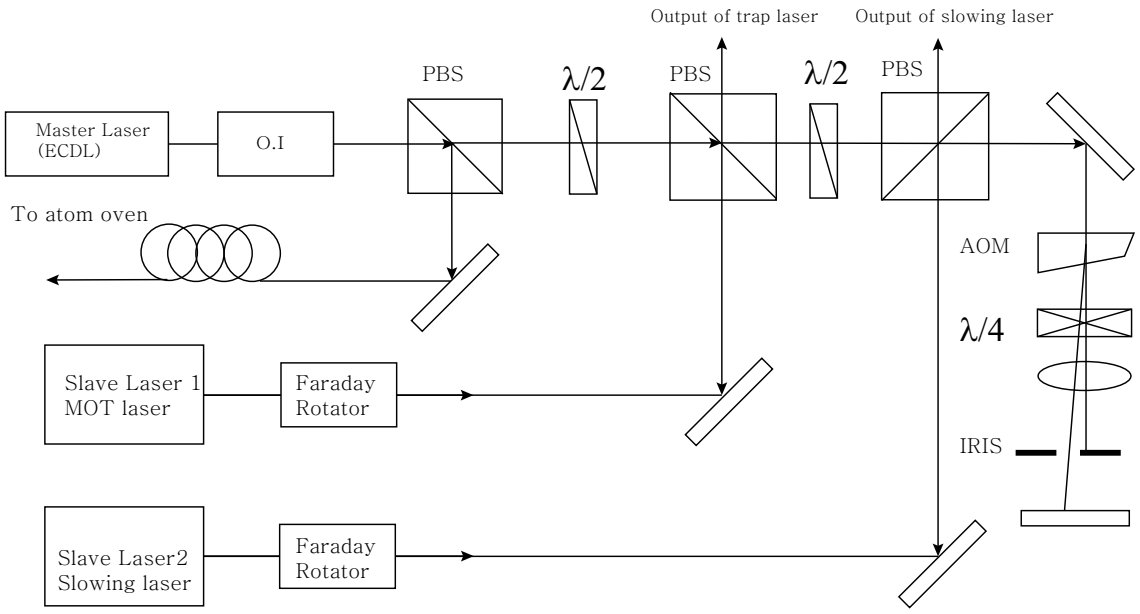

Figure 4.16: Injection laser system for 398.9 nm, O.I: Optical isolator, PBS: Polarizing beam splitter, $\lambda/4$: Quarter-wave plate, $\lambda/2$: Half-wave plate, AOM: Acousto-optic modulator.

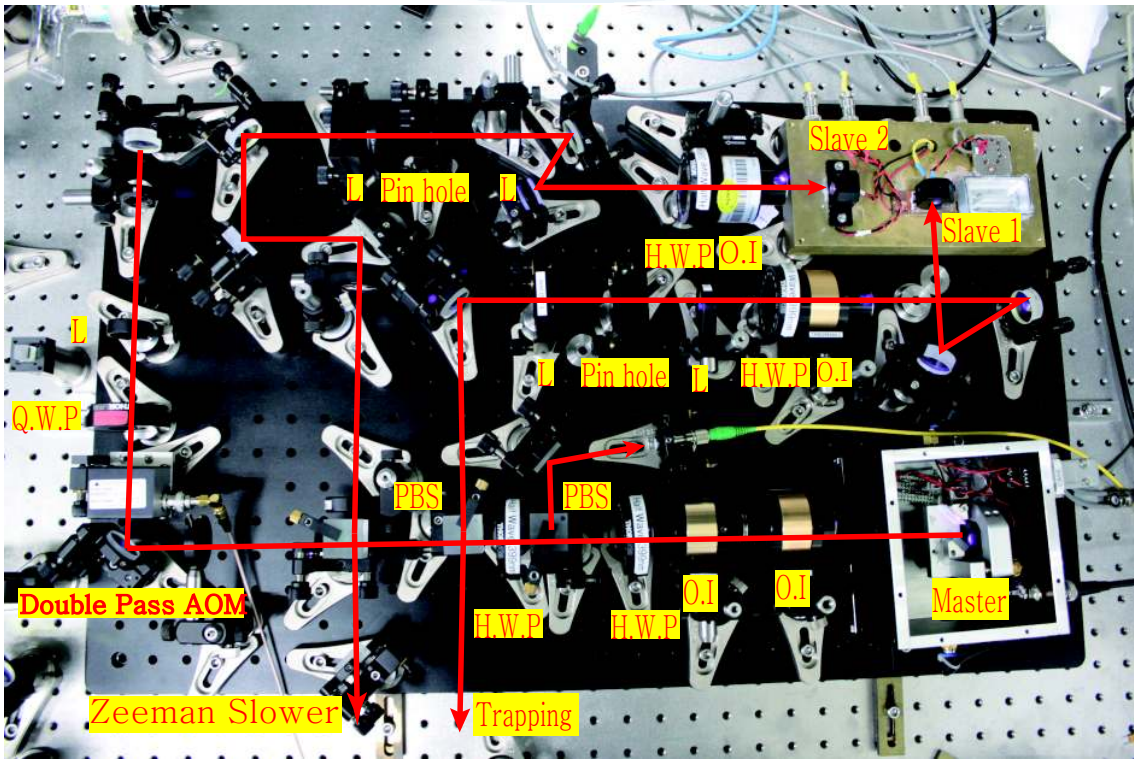

Figure 4.17: A picture of 398.9 nm injection locking laser setup.

There are several advantages of the master and slave laser system compared to the use of two independent ECDL lasers. First, we can gain more output power from the slave lasers. In the ECDL system, some of the laser output is used to stabilize the wavelength. Second, merely by stabilizing the frequency of the master laser, the frequencies of several slave lasers are stabilized simultaneously. Figure 4.16 shows a schematic diagram of the injection locking system. The output beam of the master laser is divided into two parts: One part is for frequency stabilization of the master laser, and the other part is for seed beams for the slave lasers. We used two optical isolators operating with 60 dB at the front of the master laser exit. It was installed to block laser feedback into the master from external sources. We also used Faraday rotators of the optical isolator for polarization matching of the seed laser and the slave lasers at the exit of the slave lasers. Figure 4.17 shows the overall optical layout of the injection locking laser system.

The master laser was constructed with the ECDL system. We used a holographic diffraction grating with 3600 groove/mm (Edmund optics). The diffraction efficiency is 10% for p-polarization and 50% for s-polarization. We have used the s-polarization in this case. The output beam of the diode laser is collimated with an aspheric lens (Thorlabs A230TM-A) propagating to the diffraction grating. The master laser output is separated into three parts with a total power of 20 mW. One line of the output power was sent to the frequency locking system. The other two laser beams act as seed beams for the slave lasers. The laser frequency of the master laser is locked to the fluorescence signal of the ytterbium transition. An atom beam machine system can be used for Doppler-free spectroscopy. In a well-collimated atom beam, transverse velocity component of the atom beam is suppressed. The fluorescence signal was detected by a PMT(photomultiplier tube) on the atom beam apparatus. The measured mod-hop free range was 3.6 GHz in the florescence spectrum. The laser frequency was stabilized by side-lock to the fluorescence signal using a PI-servo system. The PI-servo system sends the feedback signal to the piezo translator, and the frequency is locked at one side of the resonance line. The laser frequency is red-detuned from the transition resonance. For optimal cooling and trapping, the detuning is controlled at $\Delta = \Gamma/2$.

Slave laser-1 is used for the trap laser. In the injection locking system, the wavelength of the slave lasers is determined by the injection seed beam. The temperature of the diode laser is adjusted to maximize the single-mode operation. The output power of slave laser-1 was determined to be 80 mW. Slave laser-2 is used as a Zeeman slowing laser. The master laser output is fed back into the slave laser after passing the double pass AOM system. The AOM crystal is tunable in the range from 220 MHz to 260 MHz. There are two advantages of using double pass AOM system. First, we can ignore beam path

steering due to the frequency tuning process. The angle of the first-order diffracted beam in the AOM depends on the modulation frequency of the AOM. Accordingly, the laser path is steered when the AOM frequency is tuned. However, the laser beam path does not change during the frequency tuning of the AOM. Second, the tunable frequency range is broader than it is in one pass AOM, because the frequency is twice that of the one pass AOM case. To slow the atoms effectively, the frequency of slave laser-2 is detuned by -500 MHz from the master laser frequency. The output power of slave laser-2 was 60 mW in this case.

To check the wavelength of the slave laser, we measured the absorption signal by means of ytterbium hollow cathode lamp. Figure 4.18 a) shows the properties of the slave laser, which is dependent on the seed laser power. When the seed laser power is low (0.1$\sim$ 0.3 mW) the injection effect was increased. With a seed beam power 0.3 mW, the Doppler absorption signal was very similar to the master signal, as shown in Fig. 4.18 b). When the seed laser power is more than 0.3 mW, the slave laser operates at a multi-mode frequency. Figure 4.18 c) shows the seed-laser power-dependent property of slave laser-2. At a seed beam power of 1.3 mW, the Doppler absorption signal was very similar to the signal of the master laser, as shown in Fig. 4.18 b).

a) Slave laser 1

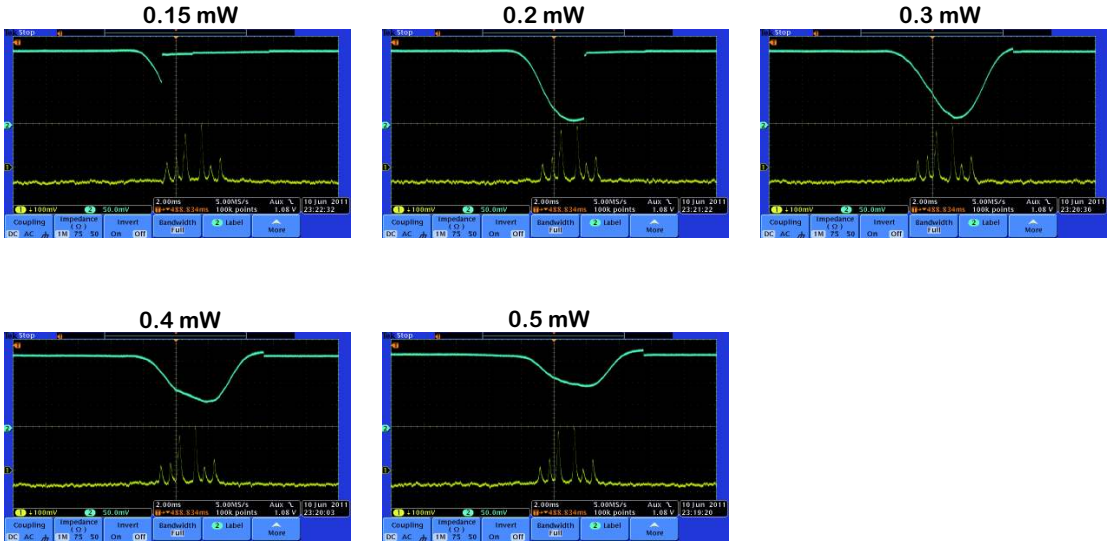

b) Master laser

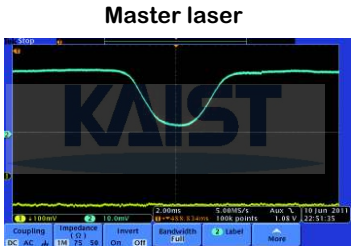

c) Slave laser 2

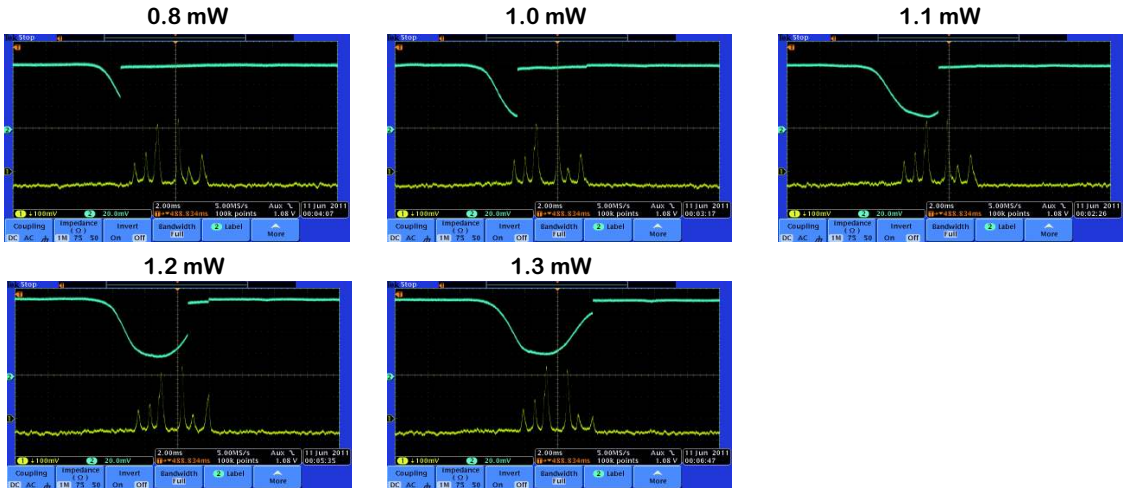

Figure 4.18: a) Doppler absorption signal related to the injection power for the slave laser 1. b) Doppler absorption signal of the master laser. c) Doppler absorption signal related to the injection power for the slave laser 2.

4.2.2 555.8 nm green lasers

Although the $^1S_0$-$^3P_1$ transition is a spin-forbidden transition, the $^1S_0$-$^3P_1$ transition has a small transition amplitude, due to the state mixing between the $^1P_1$ state and the $^3P_1$ state. Thus, the transition linewidth is 182 kHz, which is narrower than the linewidth of a common ECDL (i.e., at 1 MHz). For a successful spectrum analysis of $^1S_0$-$^3P_1$ transition, the laser should have a linewidth that is narrower than the natural linewidth. Moreover, the wavelength of the laser must be tunable. A diode laser system is suitable for a tunable wavelength and for narrow linewidth, as the spectrum of the diode laser follows the external feedback well. To create a laser with a narrow and tunable linewidth, a high-finesse cavity is used, due to the narrow spectrum characteristic. However, a 555.8 nm diode laser does not exist; therefore, we constructed the laser system by doubling frequency of the wavelength of 1111.6 nm.

The laser diode system with the wavelength of 1111.6 nm was a commercial DL100 (Toptica) system. This system contains a scan control system for continuous frequency tuning, a laser current controller, a laser temperature controller and a frequency locking system. It is a Littrow-type ECDL system with single mode emission and an output power of about 70 mW. The laser output is split into two parts. One of the output lasers is sent to the high-finesse cavity (cavity finesse $\sim$ 10000), and the other is sent to an ytterbium-doped fiber amplifier (KPS-CUS-YFA-1111-SLM-10-PM-CO, Keopsys). The amplified laser output passes through the fiber to the second harmonic device.

The laser linewidth is narrowed by means of the high-finesse cavity in conjunction with the PDH(Pound Drever Hall) locking method. The high finesse cavity system is depicted in Fig. 4.21. The high-finesse cavity (Finesse $\sim$ 10000) consists of two concave mirrors (AT-films Co.) placed in a spacer set at a distance of 10 cm. The spacer is made of an ULE(ultra-low expansion) material to diminish the cavity length change due to the temperature variation. A PZT exists on the one of the mirrors to adjust the cavity length and compensate for the temperature variation. After the laser passes through the EOM (electro optic modulator), which modulates the optical phase of the laser to a the frequency of 19 MHz, the laser output propagates to the cavity. The laser beam reflected from the cavity is then detected by a photodiode. The measured signal and the reference signal from the function generator are mixed and filtered by a low-pass filter. The generated error signal is shown in Fig. 4.23. The generated error signal is fed back into injection current of the diode laser by using fast MOSFET current operating devices (Toptica FALC110). Thus, the diode laser is locked, and the current is changed to follow the peak position of the transmission signal. Figure 4.22 shows the transmission signal of the cavity. When the diode laser frequency matches the longitudinal mode of the cavity,

the transmission signal is maximized. The frequency linewidth of the diode laser was reduced to 10 kHz level in this case.

Next, we explain the generation of the 555.8-nm laser. The 555.8-nm laser is generated with a PPLN (periodically-polled lithium niobate) crystal. We used the ridge waveguide, fiber pig-tailed type (NTT). The ridge WG-PPLN(wave-guided PPLN) crystal has advantages compared to a bulk crystal. First, the amplified laser output to the crystal should be aligned to the crystal, whereas the pig-tailed fiber is easy to use. Second, the damage threshold is high. The conversion efficiency of the SHG is related to the temperature of the crystal. Therefore, an embedded TEC is used to control the temperature of the crystal and a thermistor is used to measure its temperature. The temperature of crystal is controlled using a diode laser controller (Thorlabs ITC 510) with a resolution of 0.1 K. The conversion efficiency of crystal as a function of the temperature is shown in Fig. 4.24. The temperature of maximum conversion efficiency values is 39.5°C. The coupling efficiency of the PPLN versus the input laser power is shown in Fig. 4.25. Below an input level of 300 mW, the efficiency is proportional to the input power. As the input power increases, the efficiency nearly saturated. To prevent damage to the crystal, we used a low input power of less than 300 mW.

To stabilize the frequency of the 555.8-nm laser, some part of the laser output is sent to an atom beam machine. The laser output propagates the double pass AOM system to tune the frequency of the laser from the resonance signal. The fluorescence signal of the $^1S_0 - ^3P_1$ transition is obtained from the PMT. The 555.8 nm laser frequency is stabilized by side-locking the fluorescence signal. The error signal of the side lock is fed back to the PZT at the cavity mirror. The PZT adjusts the cavity length, and the frequency of the resonant cavity mode is locked to the fluorescence signal.

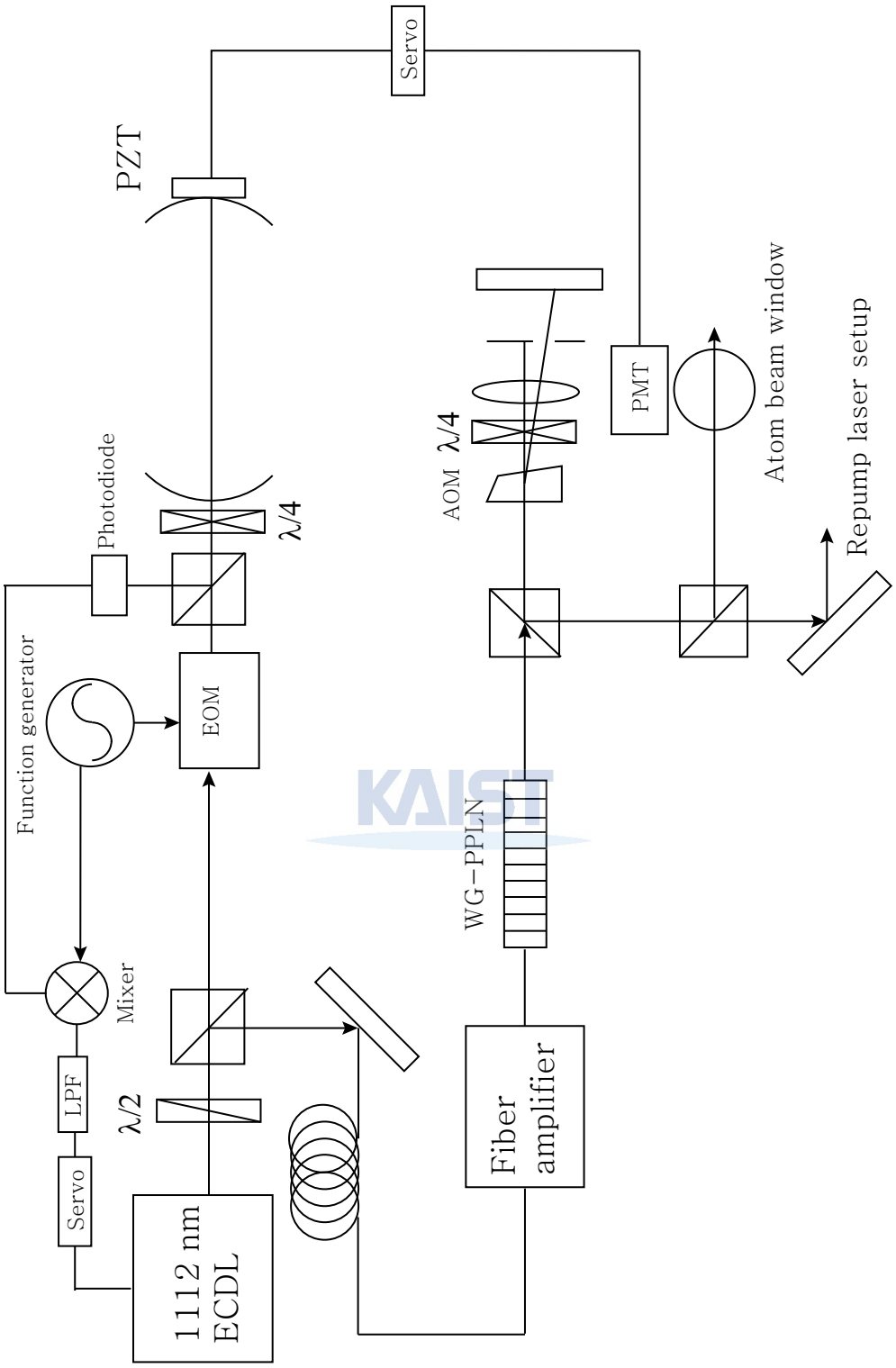

Figure 4.19: A schematic description of 555.8 nm ($^1S_0$-$^3P_1$ transition) laser system. The laser output of 1111.6 nm ECDL is separated into two parts. One of part is used for narrowing the linewidth with PDH setup and the other is used to make second harmonic generation with the ridge waveguide-PPLN. $\lambda/2$: Half-wave plate, $\lambda/4$: Quarter-wave plate, WG-PPLN: Waveguided periodically-polled lithium niobate, EOM: Electro-optic modulator, AOM: Acousto-optic modulator, PZT: Piezo translator.

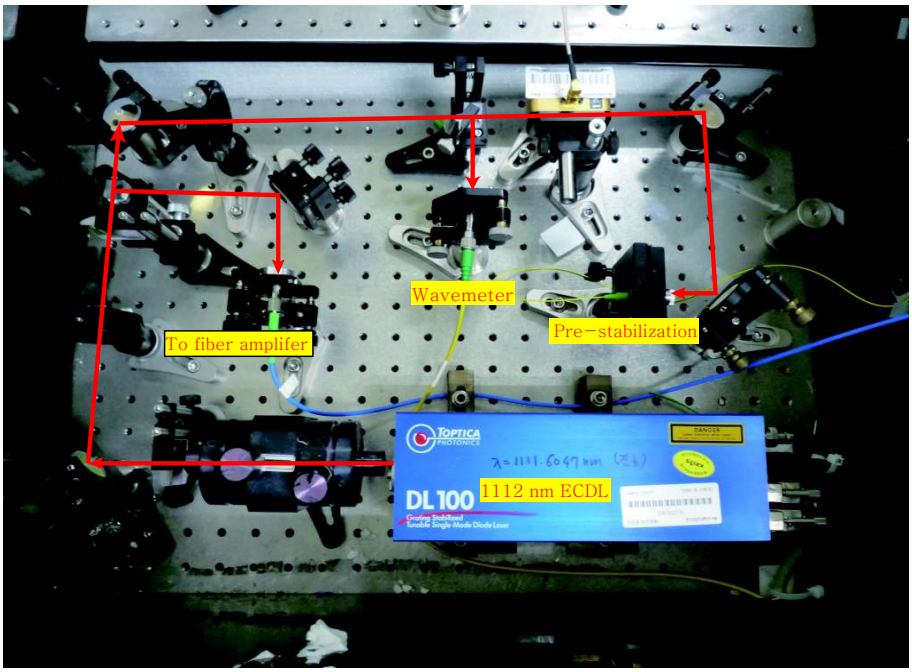

Figure 4.20: A picture for the whole system of 1111.6-nm laser. The output of DL100 (ECDL system of 1111.6-nm laser) is separated two parts : 1) To fiber amplifier, and 2) Pre-stabilization cavity system.

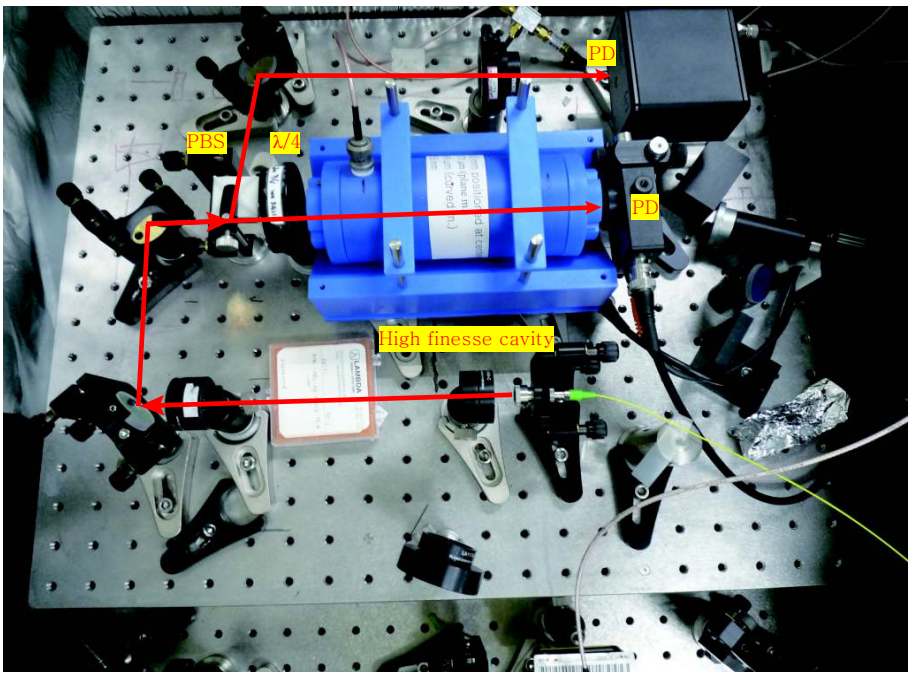

Figure 4.21: The linewidth is narrowed and the frequency of 1111.6-nm diode laser is locked to high finesse cavity mode. The PDH(Pound Drever Hall) locking method is used.

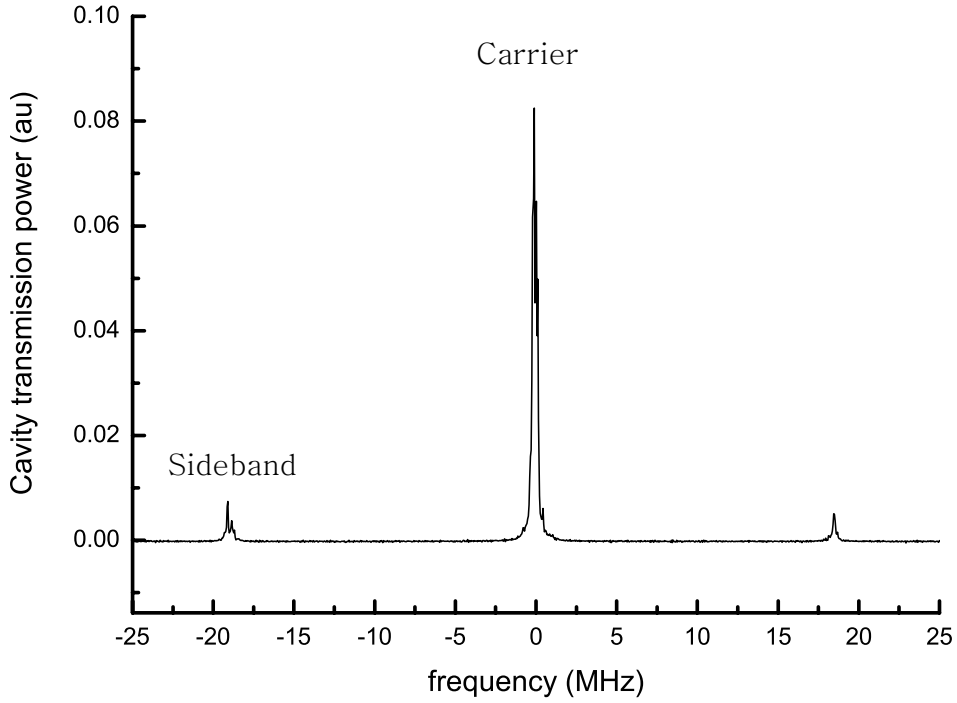

Figure 4.22: The transmission of the high finesses cavity as the PZT of 1111.6-nm laser is scanned. The carrier frequency of 1111.6-nm laser and phase modulated signals at π 19 MHz apart from the carrier frequency are shown.

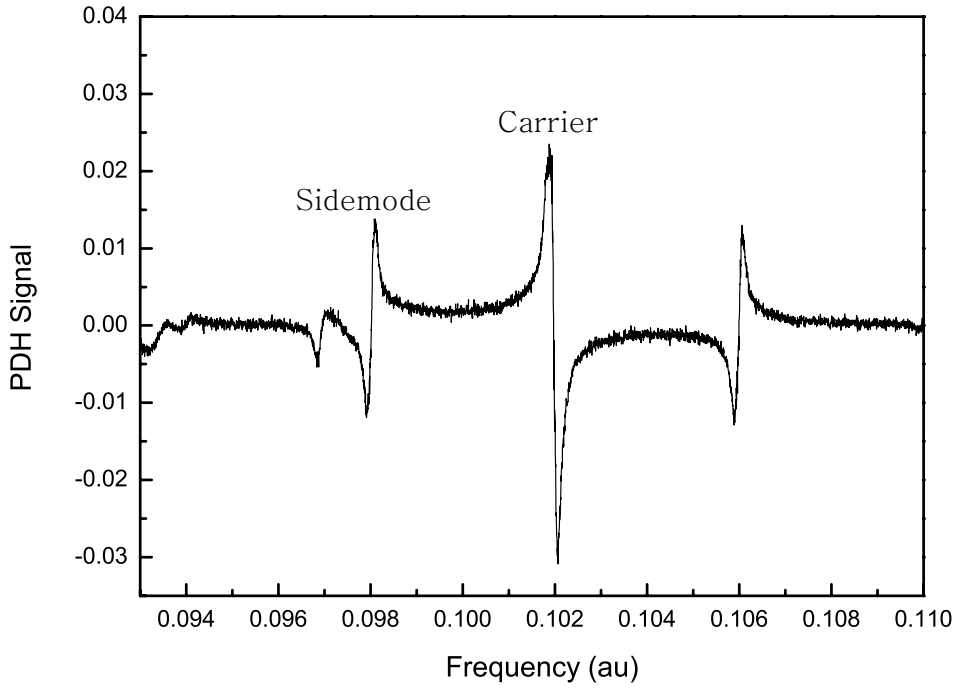

Figure 4.23: The error signal for the PDH locking system.

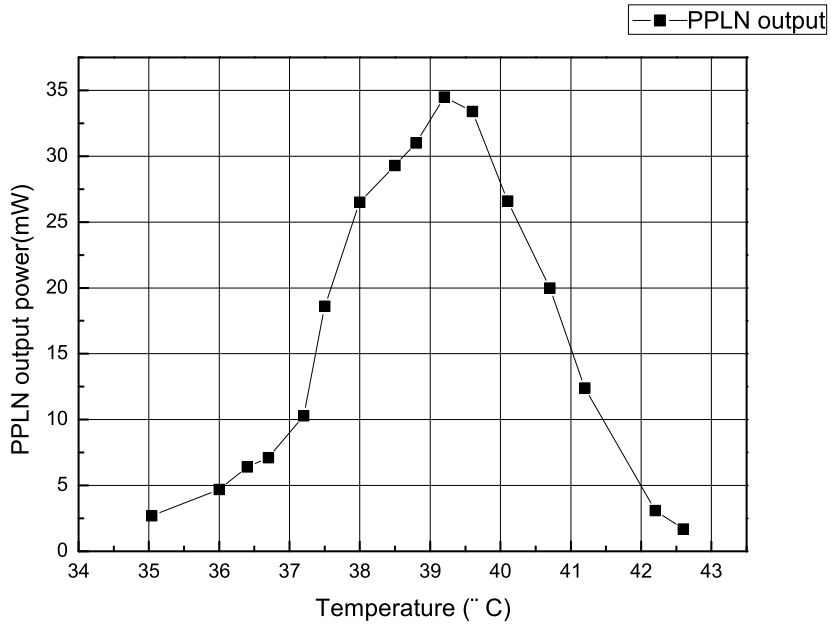

Figure 4.24: The second harmonic conversion efficiency of PPLN as a function of the temperature. The maximum conversion efficiency is at the 39.5°C.

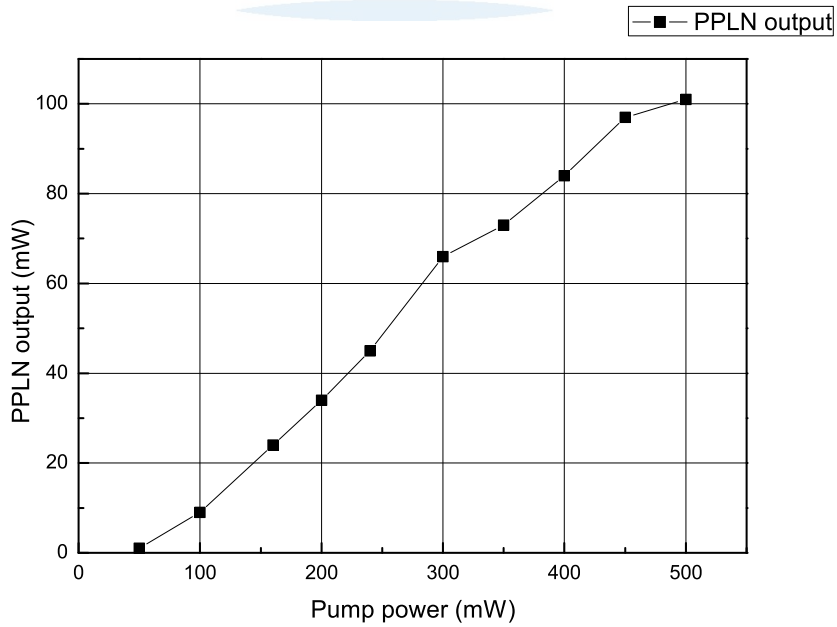

Figure 4.25: Second harmonic generated output power versus the input laser power.

4.2.3 Repumping lasers

The next step was to investigate the population of the metastable state, $^3P_0$, and $^3P_2$. To do this, we introduce a locking method for the repump lasers. Figure 4.26 shows the optical pumping scheme for the repump laser spectroscopy. To lock the laser frequency of repump lasers, we used the generated fluorescence signals of transition between the $^3S_1$ state and the triple P states ($^3P_{0,1,2}$). To generate the fluorescence signal, the atoms should exist in the triplet P state. The atoms in the ground state of $^1S_0$ are excited to the $^3P_1$ state with the 555.8 nm green laser, and the atoms in $^3P_1$ are excited to the $^3S_1$ state with the 680 nm pump laser . The atoms in $^3S_1$ are spontaneously decay to the $^3P_2$, $^3P_1$, and $^3P_0$, after a lifetime of 13.5 ns. Atoms in $^3P_2$ are excited to the $^3S_1$ state by a 770 nm repump laser and spontaneously decay to the triplet P states. The atoms in $^3P_0$ are excited to the $^3S_1$ state by a 649 nm repump laser and spontaneously decay to the triplet P states. The atoms that decay to the state of $^3P_2$ or $^3P_0$ have a relatively long lifetime. Theses are, $^3P_2$ with a lifetime of 14.5 s and $^3P_0$ with a lifetime of 24 s. At this point, atoms exist in all triplet P states, and atomic spectroscopy for repump lasers thus becomes possible. For Doppler-free spectroscopy, we created another atom beam

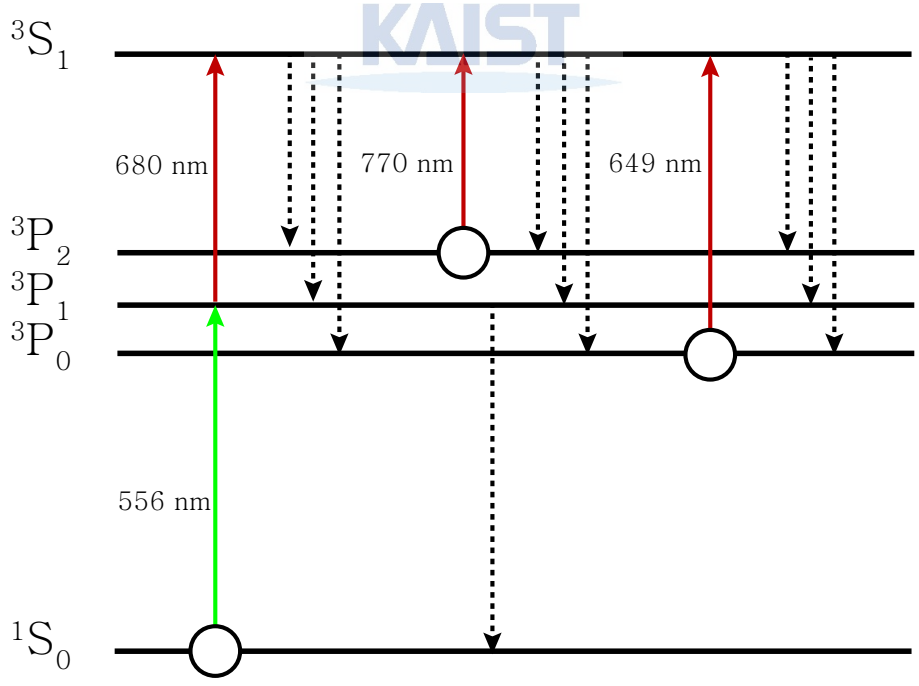

Figure 4.26: A schematic description of the repump laser transition.

system. This atom beam machine includes spectroscopy windows for the laser input and fluorescence signal detection. The atom oven is heated to 540°C and the collimator is heated slightly higher than the oven region.

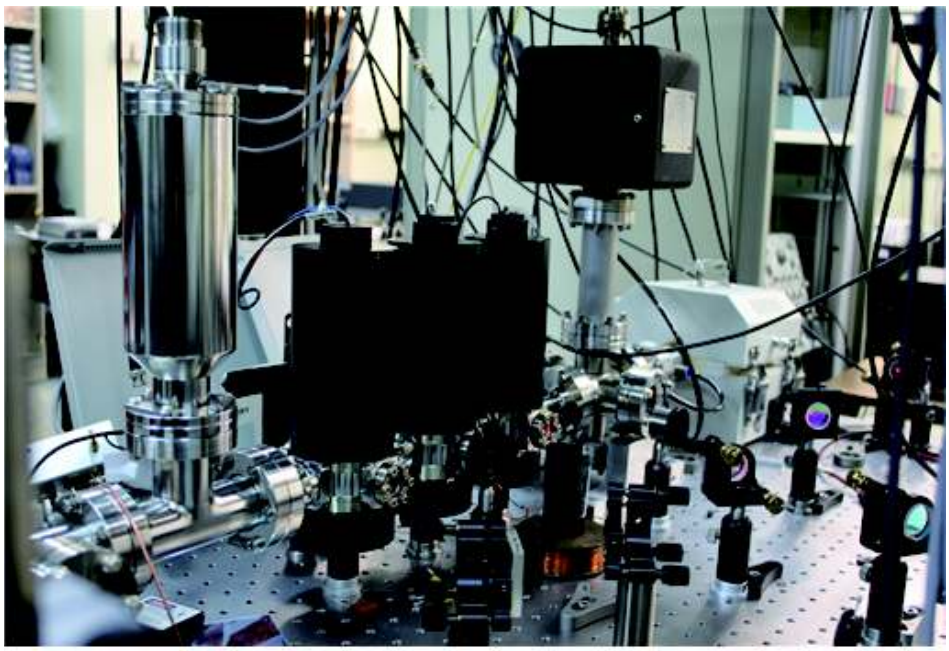

Figure 4.27: The atomic beam machine apparatus for repump laser frequency stabilization.

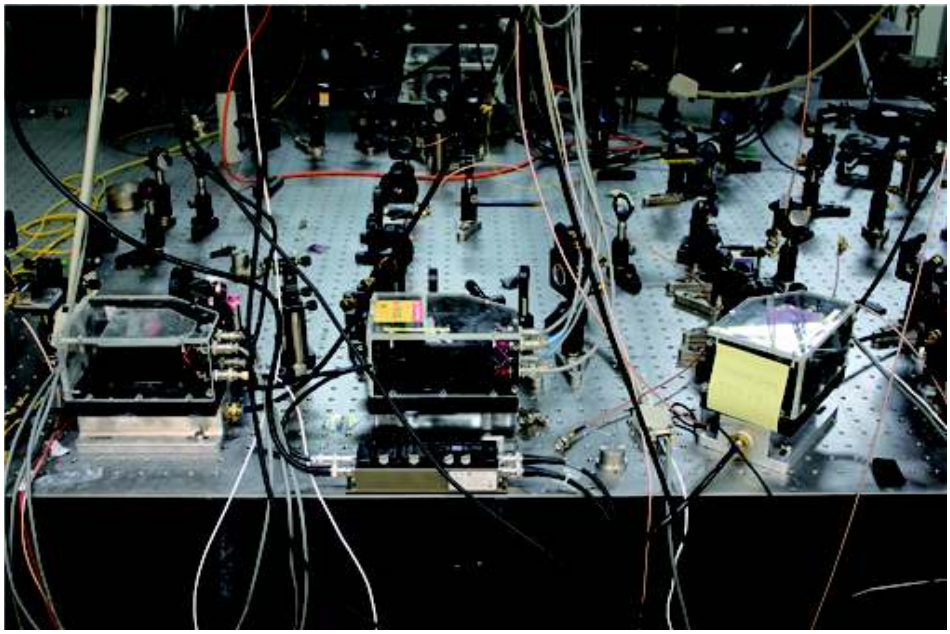

Figure 4.28: A picture of three repump lasers. From left, 650-nm, 770-nm, 680-nm repump lasers are shown.

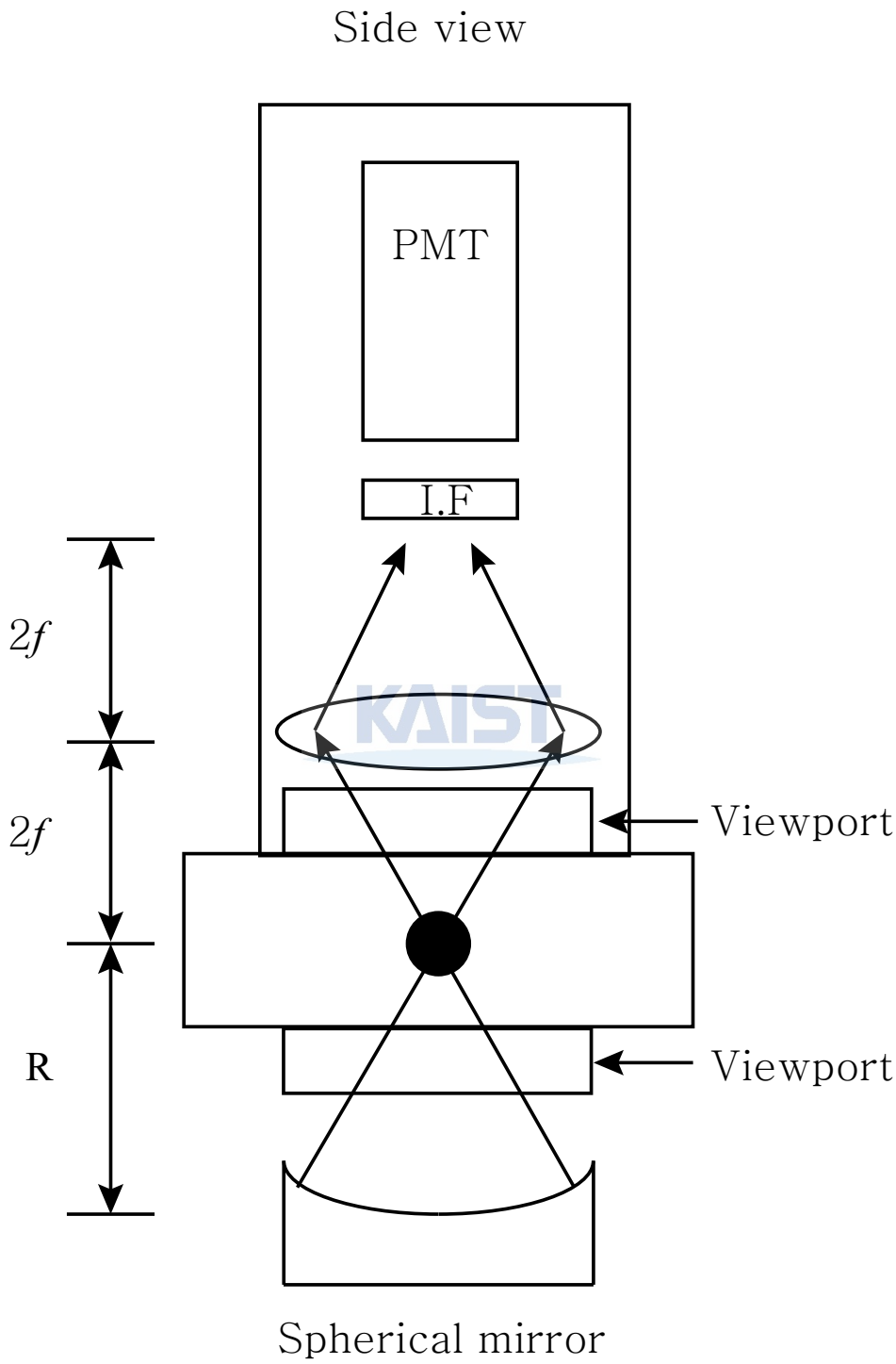

Figure 4.29: A fluorescence signal collector. To collect the signal effectively, the spherical mirror is placed at the bottom atomic beam machine.

The pressure of the atomic beam machine in this case is held below 10^{-7} torr with an ion pump for a sufficiently long mean-free path of the atomic beam output region. A general image of the atomic oven machine is shown in Fig. 4.27. The atomic fluorescence signal is observed through the windows of the vacuum chamber. The fluorescence signal collector includes a PMT module, an interference filter, and a collimation lens. A schematic description of the fluorescence signal collector is shown in Fig. 4.29. The fluorescence signal from the atom beam is collected by lens, and an interference filter reduces the scattering signal inside the vacuum chamber and protects the PMT from high intensity conditions over the saturation intensity. We also use a spherical mirror to collect fluorescence signals at the opposite direction. Thus, we could increase double the value of the fluorescence signal.

Figure 4.30 shows the optical layout of the repump laser setup. The repump lasers for the experiment were constructed with the ECDL systems (Fig. 4.28). In the atomic beam, most of the atoms are in the ground state. The first window close to the atomic oven is used to excite the atoms from the ground state to the $^3S_1$ state with the 555.8-nm laser and the 680-nm laser. The two lasers (555.8 nm, 680 nm) propagate through the atomic beam with same path because they overlap with a dichroic mirror. For this optical pumping scheme, we used the 555.8 nm laser at an intensity of 0.5 mW/cm^2 and the 680-nm laser at an intensity of 1 mW/cm^2. The second and the third windows are used to collecting the fluorescence signals of the 770 nm-laser and the 649-nm laser, respectively. The atomic transition spectrum is measured via the frequency scanning of the ECDL with the PZT. The fluorescence signals are shown in Fig. 4.31, Fig. 4.32, and Fig. 4.33. To lock the laser frequency at the peak point of fluorescence signal, we used a lock-in amplifier (SR 830) and the current modulation of the laser diode controller (Thorlab ITC 502). We added the current modulation signal to the modulation input port of laser diode controller. The modulation frequency was tens of kHz which is limited by the PMT bandwidth. The fluorescence signal from the PMT and the reference signal from the lock-in amplifier were mixed and filtered by a low-pass filter. The error signal is then generated and sent to the PI-servo. The PZT offsets the amount of error from fluorescence peak signal. The error signals for the experiment are shown in Fig. 4.31, Fig. 4.32, and Fig. 4.33. For the experiment with the repump laser, the output of the repump lasers was fiber-coupled. The coupling efficiency is 30%. and the output power is 2.5 mW (770 nm) and 2.0 mW (650 nm). The fiber-coupled output is sent to the main trap chamber.

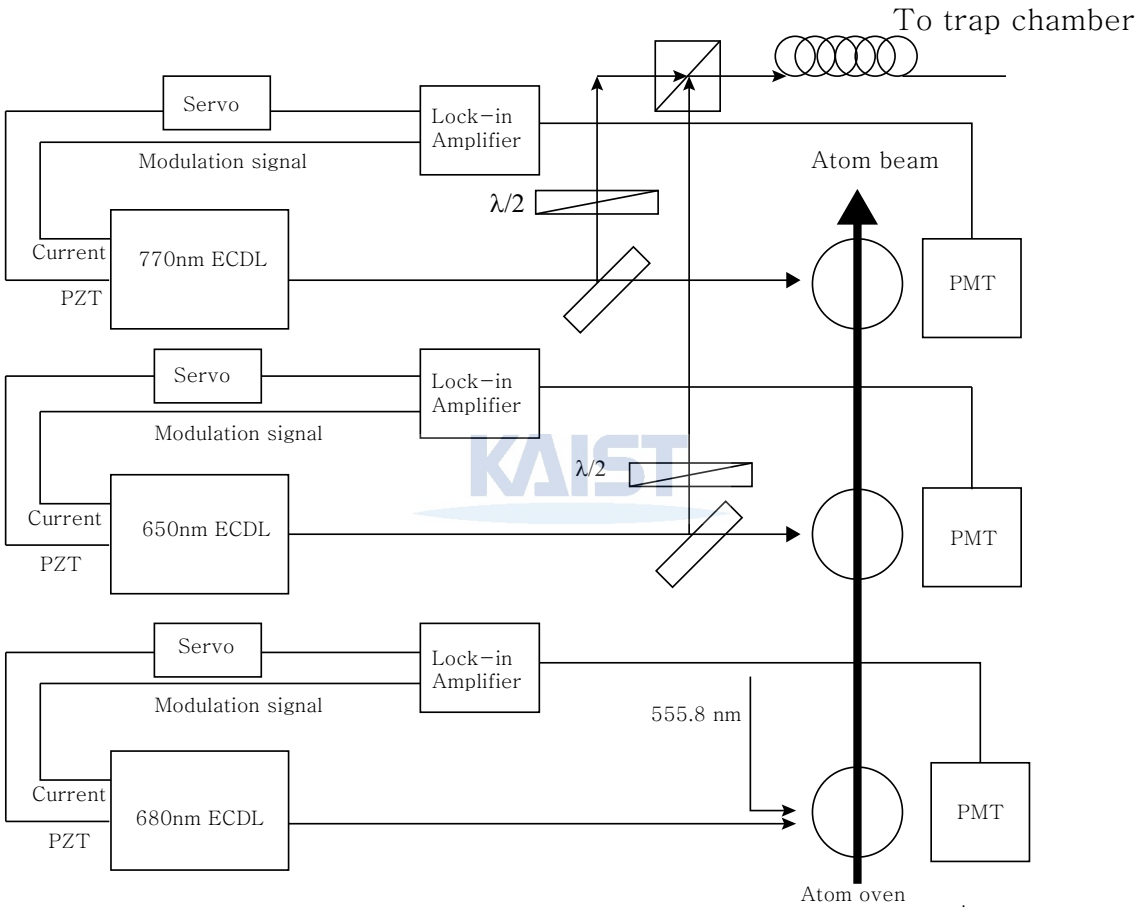

Figure 4.30: A schematic description of repump lasers and atom beam system.

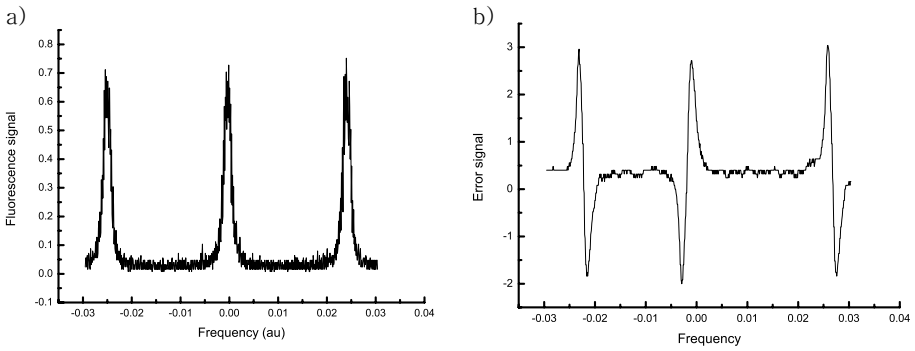

Figure 4.31: a) The fluorescence signal for 680-nm laser. b) The error signal.

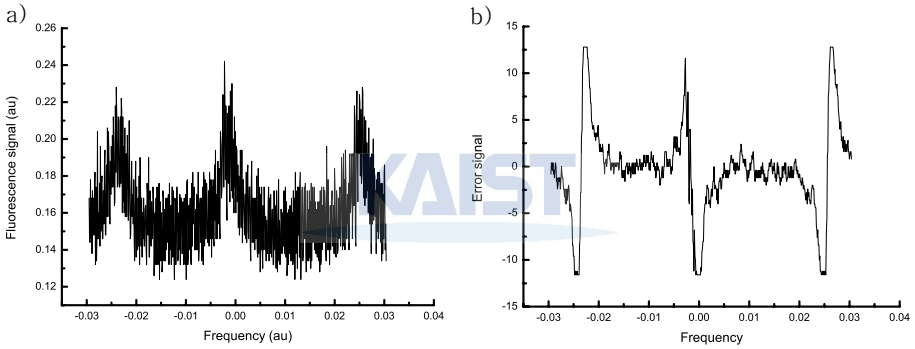

Figure 4.32: a) The fluorescence signal for 770-nm laser. b) The error signal.

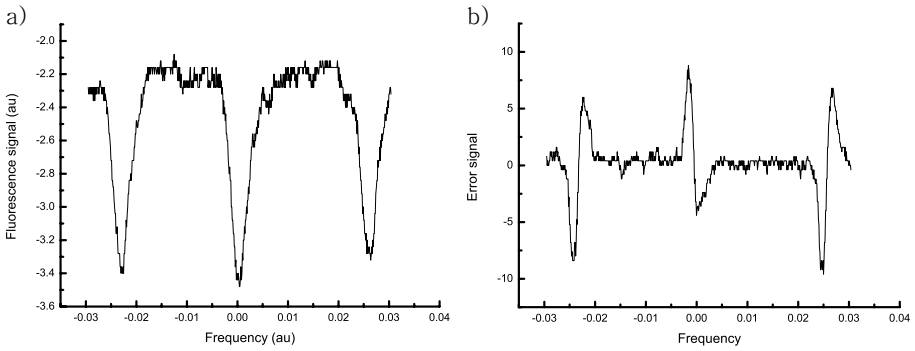

Figure 4.33: a) The fluorescence signal for 650-nm laser. b) The error signal.

4.2.4 Optical layout

Figure 4.34 describes the optical layout for the experiment. To increase the stability of the lasers, all laser systems are placed on another optical table. The output of the Zeeman laser is 30 mW of power, and the spatial profile is expanded to a diameter of 1 cm. The laser passes through the bottom windows of the trap chamber and is reflected in the direction of atomic oven by the mirror inside the vacuum chamber. The mirror inside chamber is placed at the upper position of the vacuum chamber and fixed at an angle of 90° between the bottom window and the atomic beam direction. To control the laser action, a mechanical shutter is used.

The output power of the trap laser is 40 mW and the spatial profile is expanded to a diameter of 1.5 cm. A mechanical shutter is also used here for laser shutting. First, the trap laser output power is split at 2:1 with a polarizing beam splitter. The output power, with a relative intensity of 1, passes parallel to the anti-Helmholtz coil axial direction of the trap chamber; the other output relative intensity of 2 is divided by the beam splitter at 1:1. The lasers pass the chamber at an angle of 45° and 135° in the normal direction to the ground, relatively. The beams that pass the trap chamber are retro-reflected to make a six-beam MOT configuration. The polarization of each six beams is circular because a quarter-wave plate is utilized before the beam is propagate to the chamber.

The fiber-coupled output of the repump lasers (650-nm and 770-nm) is placed in the main chamber with the cage system. The output of the laser crosses the center of the main chamber. When the repump laser passes, the diameter of the laser beam is increased to cover the MOT region at the center of the chamber.

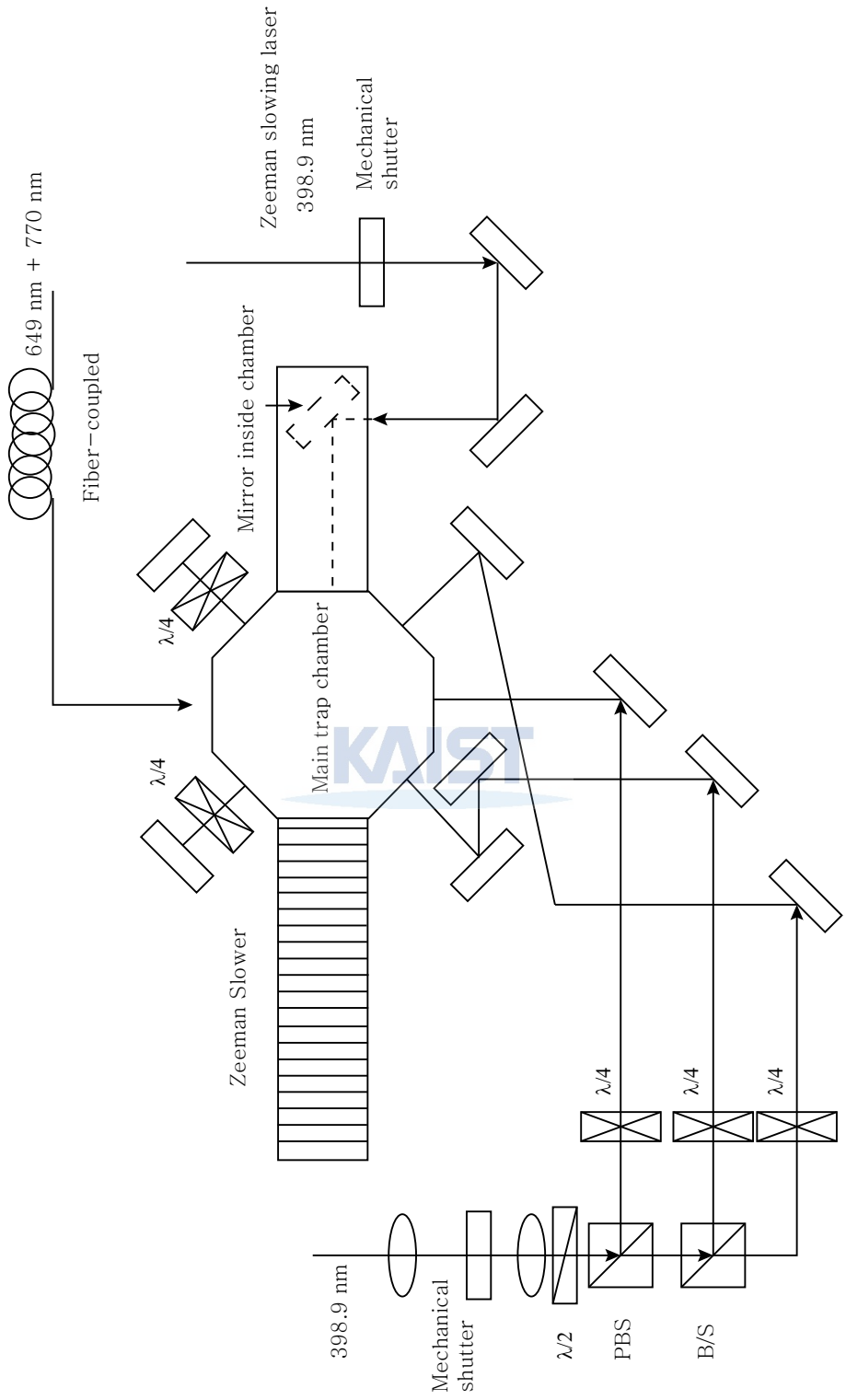

Figure 4.34: Optical layout for cooling and trapping experiment with the 398.9-nm lasers. AOM: Acousto-optic modulator, $\lambda/4$: Quarter-wave plate, $\lambda/2$: Half-wave plate, PBS: Polarizing beam splitter B/S: Beam splitter.

Chapter 5. Experiments and results

5.1 Blue magneto-optical trap

5.1.1 Blue MOT

In this section, we describe how to generate the ytterbium blue MOT. An atomic source was effused from the atomic oven. The atom oven part was heated to 400°C and the collimator part was heated to 415°C. Then the collimated atoms flew into the Zeeman slower region with the flux of 10^{10} atoms/s. In the Zeeman slower, the atomic velocity was slowed down to the capture velocity of MOT with the flux of 10^{9} atoms/s. Trap lasers were also expanded to a diameter of 1.5 cm. The power of trap laser was measured as 6 mW for each x-, y-, and z-axis directions and the magnetic field gradient was 30 G/cm. Figure 5.1 shows the picture of trapped ytterbium. Figure 5.2 shows the trapped number of atoms versus time evolution. The loading time was measured as 0.6 s.

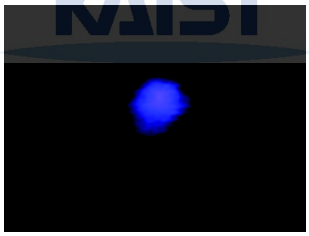

Figure 5.1: A picture of trapped ytterbium atoms.

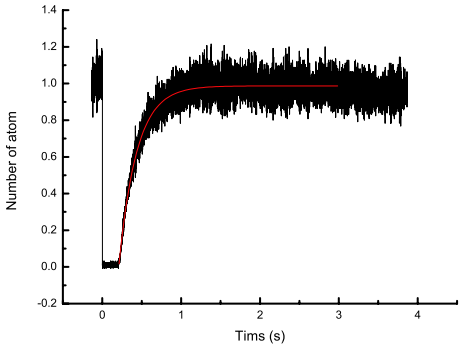

Figure 5.2: Trapping dynamics of ytterbium atoms.

5.1.2 Characteristics for blue MOT

Number of atoms in the trap

We have measured the number of atoms by measuring the fluorescence signal of trapped atoms. Figure 5.3 shows the scheme of measuring the number of atoms. Atoms were trapped in the center of the chamber with 398.9-nm laser. The fluorescence signal from the MOT was collected by an imaging lens. At first, the PMT signal was calibrated with power meter. When the PMT control voltage was 0.3 V, the voltage value of PMT was 5 V which was corresponding to value 0.3 μW for the power meter. From the fluorescence signal, the number of atoms is given by

$$N_{atom} = \frac{P}{\rho_{ee}\Gamma\Omega h\nu}, \tag{5.1}$$

where P is the power of fluorescence signal, ρ_{ee} is the population of atoms in the excited state, Γ is the natural linewidth, Ω is the solid angle, and $h\nu$ is the photon energy. For the trap laser power 6 mW, the excited-state number fraction was 0.76. The number of atom is $N_{atom} = 2.4 \times 10^7$ for the measured optical power(0.3 μW).

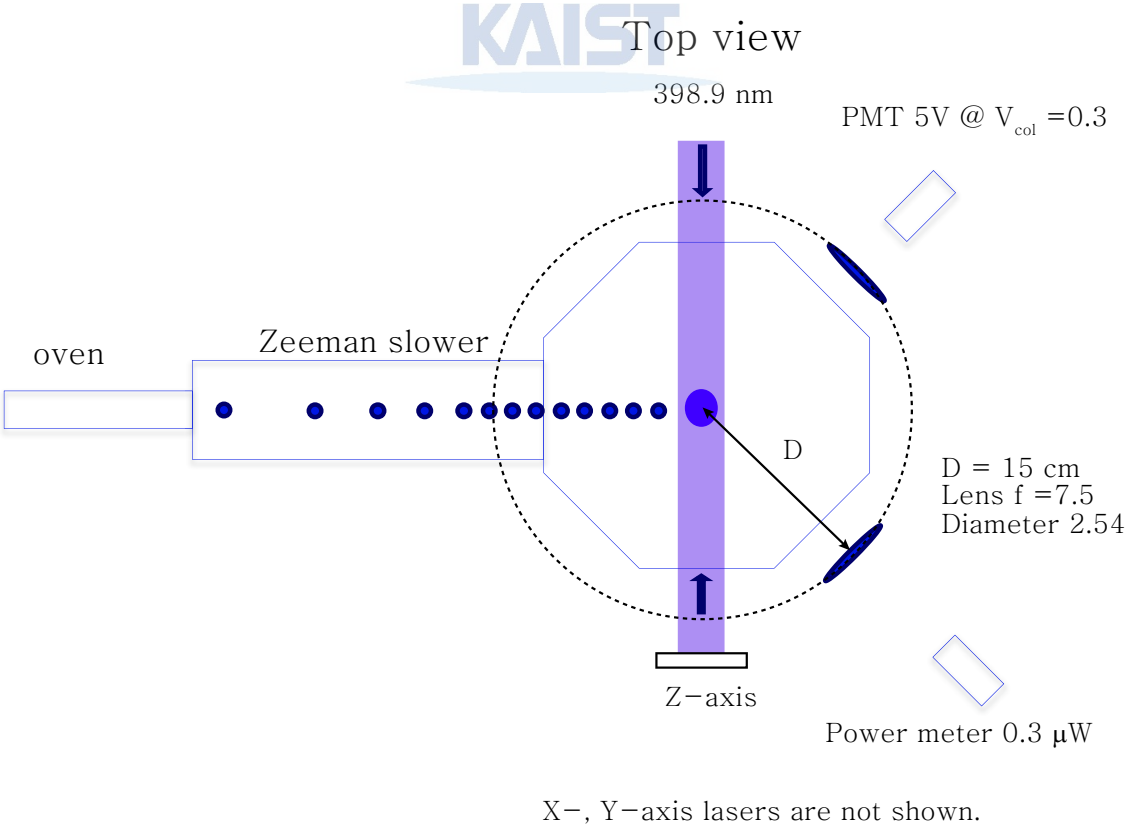

Figure 5.3: Measurement of trapped atom numbers.

Temperature measurement

We have measured the temperature of MOT by using the releasing and recapture method. First, one of the trapping laser was removed for a short time ($\sim$ ms). Second, the trapped atoms were diffused from trap, and third, the trapping laser was on and again trapped the atoms. We have measured the one-dimensional diffusion process by blocking the trap laser parallel to the ground. By doing so, we could ignore the effect of gravitational force on the atom.

Figure 5.4 shows the typical signal of release and recapture. When the shutter was closed, the atoms were diffusing. When the shutter was open, atoms in possible trap region were recaptured and determined the initial values for the loading curve. The trap laser was blocked during the release time T. The recapture ratio was defined by h/H, where h is the fluorescence signal of recapture process and H is the fluorescence signal before the diffusing process.

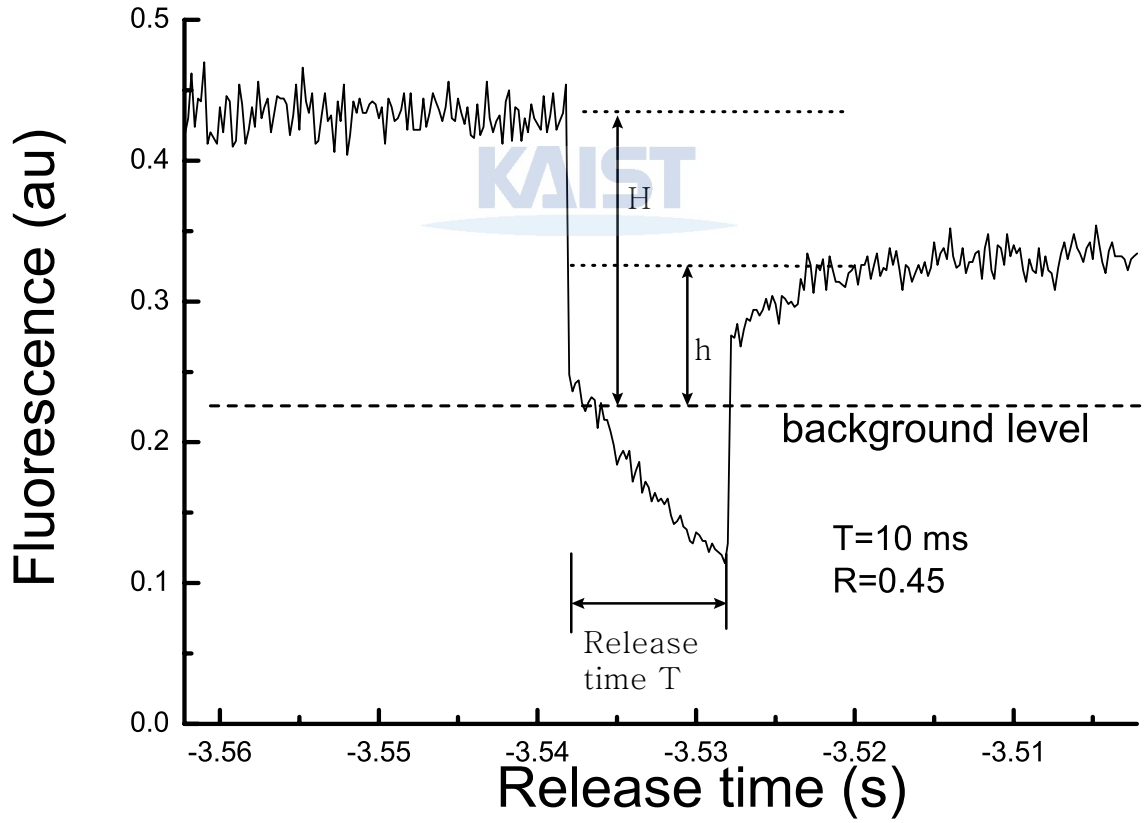

Figure 5.4: Typical release and recapture signals.

At time $t = 0$, When the atoms are accumulated by the trap laser, the spatial profile is given by

$$f(x) = e^{-x^2/\alpha^2}, \tag{5.2}$$

where α is the initial size of the trap. After the trap laser is off, the atoms are diffusing to +x and -x direction with equal probability. Then the atom's distribution is given by

$$f(x, v) = \frac{1}{2} n_0 (e^{-(x+v\times\tau)^2/\alpha^2} + e^{-(x-v\times\tau)^2/\alpha^2}), \tag{5.3}$$

where τ is the evolution time and v is the velocity of atom. To obtain the spatial distribution profile, we integrate the $f(x)$ with Maxwell-Boltzmann distribution :

$$f'(x) = \int M(v) \times f(x, v) dv. \tag{5.4}$$

The the ratio $R = h/H = \frac{\int_0^{x_0} f'(x)dx}{\int_0^{\infty} f'(x)dx}$. Figure 5.5 shows the theoretical recapture ratio as a function of the temperature of the Yb cloud. Figure 5.6 shows the theoretical recapture ratio values as a function of diffusing time at different temperature conditions of 1 mK, 1.5 mK, and 2 mK, respectively.

In Fig. 5.7, we show the measurement of the ratio as a function of the release time. We have measured the fluorescence signal by controlling the trap laser with a mechanical shutter. So the value below the 5 ms is not meaningful due to the slow response of the mechanical shutter. Because the spatial distribution atom affects the theoretical calculation, the simulation result does not follow the measured result. When the Zeeman slower was utilized, the temperature of trapped atoms was decreased. For the ^{174}Yb, temperature of atoms is 1.2 mK. For ^{171}Yb, temperature of atoms was 1.4 mK.

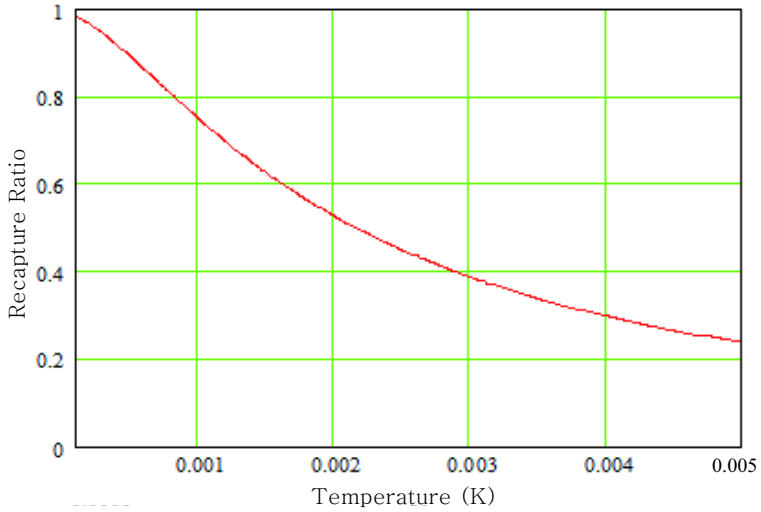

Figure 5.5: Theoretical recapture ratio versus the temperature of the trapped Yb cloud.

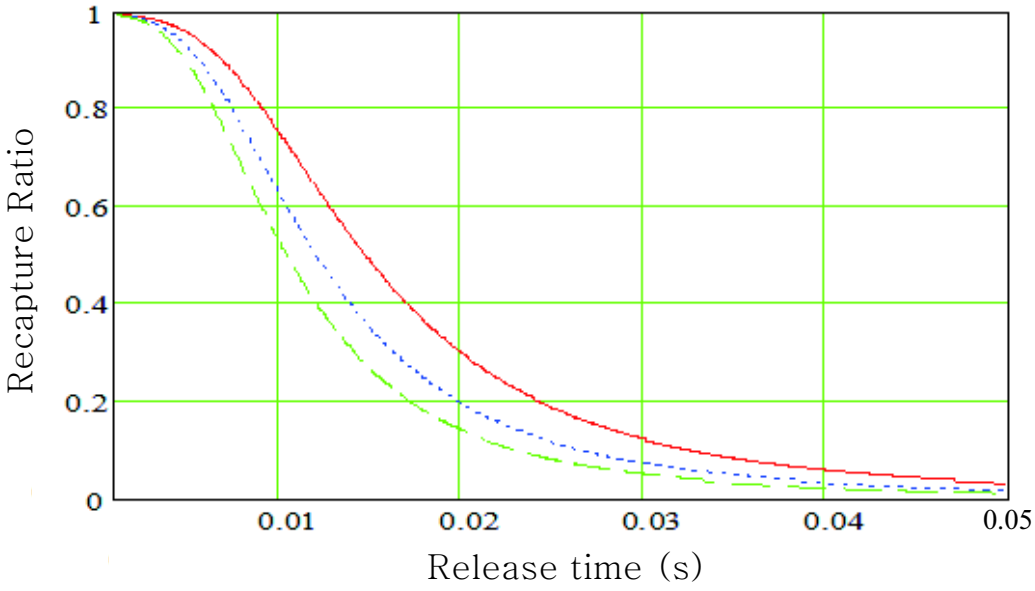

Figure 5.6: Theoretical recapture ratio versus release time. Curves were calculated at three different temperatures, 1 mK(red), 1.5 (blue), and 2 mK (green), respectively.

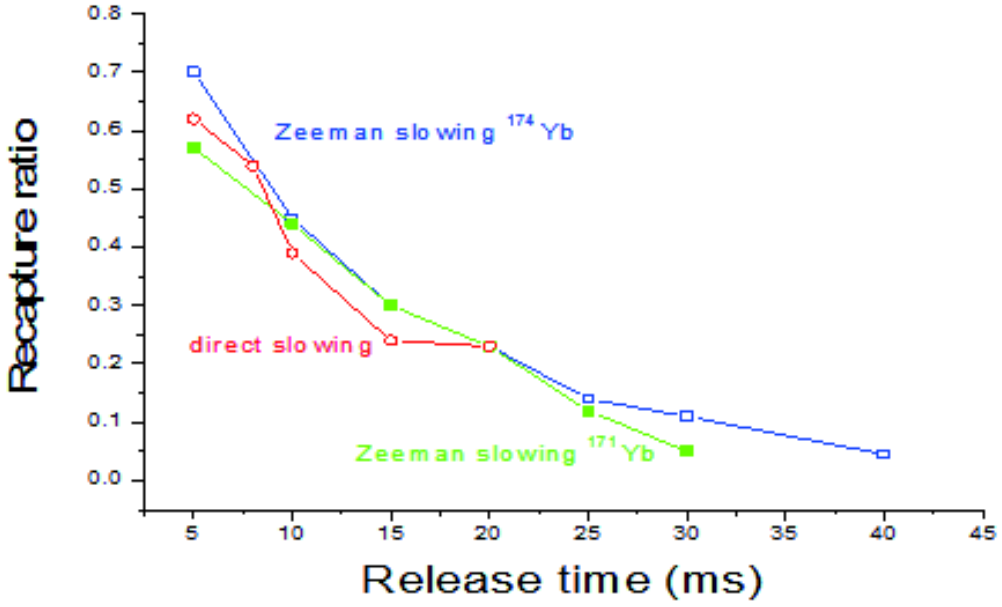

Figure 5.7: Measured recapture ratio versus release time.

5.2 Trap loss investigation of ytterbium MOT

With a 398.9-nm diode laser system for the transition $^1S_0$-$^1P_1$, we have slowed down the velocity of thermal ytterbium atoms and trapped them at the center of the main chamber[33]. As shown in Fig. 5.8, however, the transition between $^1S_0$-$^1P_1$ is not a closed transition. Some of the atoms in $^1P_1$ state decay into the metastable states, $^3P_{2,0}$, and are shelved in a metastable state, which has a relatively long life time on the order of tens of seconds. The lifetime of trap and the number of atoms in the MOT depend on the the $^1P_1$ state number fraction [34]. If the atoms in metastable states are optically pumped into the ground state, the number of atoms is increased and the lifetime of MOT is enhanced. In our experiment, we have measured the number of trapped atoms versus time, by detecting the fluorescence signal of $^1P_1$ state. With optical repump lasers, we can obtain the values of the decay rate of $^1P_1$ state to the metastable state with trap-laser power dependence. As a result, the number of atoms have increased and the lifetime of ytterbium MOT is also increased.

5.2.1 Trapped atom's loss model and rate equations

The rate equations for the loading dynamics for the Yb MOT are given by

$$\begin{aligned}
\frac{d}{dt}(N_g + N_e) &= \eta - (a_0 + a_1 + a_2)N_e \\
&+ \gamma_1 N_1 - \gamma_c(N_g + N_e), && (5.5)\\
\frac{dN_0}{dt} &= a_0 N_e - \gamma_c N_0, && (5.6)\\
\frac{dN_1}{dt} &= a_1 N_e - \gamma_c N_1 - \gamma_1 N_1, && (5.7)\\
\frac{dN_2}{dt} &= a_2 N_e - \gamma_c N_2, && (5.8)
\end{aligned}$$

where η is a loading rate of MOT, N_g is the number of atoms in the ground state ($^1S_0$), N_e is the number of atoms in the excited state ($^1P_1$), $N_{0,1,2}$ are the number of atoms in, respectively, $^3P_{0,1,2}$ states, the decay rates $a_{i(=0,1,2)}$ are from the excited state $^1P_1$ to the ^3P_i states, γ_1 is the spontaneous decay rate of $^3P_1$, and γ_c is the coefficient of the collisional loss, which is the loss due to trapped atoms and background gases. Considering the Yb-Yb collision term(βN^2) which is originated from interaction between ground and excited state depends on the density of the trapped gas. The value $\beta = \beta'/(\sqrt{2\pi}a)^3$, where a is related to the size of the trapped region. The density of the trap is $n = n_0 e^{-(r/a)^2}$, where r is the distance from center and n_0 is the peak density of the atomic cloud.

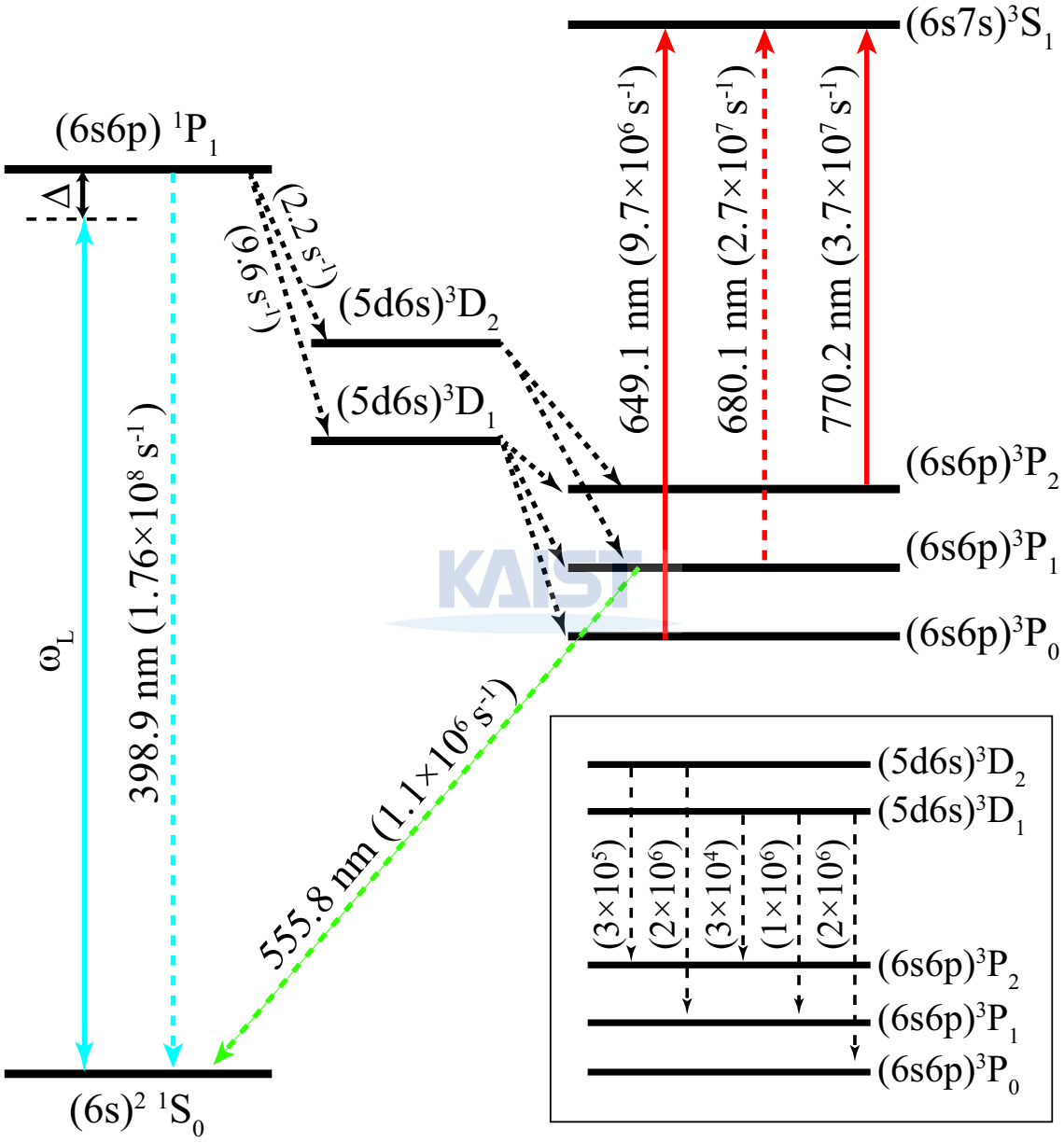

Figure 5.8: Lowest energy level diagram of an Yb atom is shown with the $^1S_0$-$^1P_1$ MOT transition level and decay channels. Because the lifetimes of $^3P_2$,$^3P_0$ are long, they act like loss channels of the MOT.

Then we can summarize the equation for the trapped atoms ($N = N_g + N_e$).

$$\frac{dN}{dt} = \eta - [a_{0,2} f(P_T, \Delta) + \gamma_c]N - \beta(f)N^2 \ . \tag{5.9}$$

In Eq. (5.9), the fraction number f is defined by

$$f = \frac{s/2}{1 + s + (2\Delta/\Gamma)^2}, \tag{5.10}$$

where $\Gamma/2\pi = 28$ MHz is the natural linewidth of ^{1}S$_0$-^{1}P$_1$ transition, and s is the saturation parameter for given laser intensity condition $s = \frac{I}{I_s}$, where I_s is the saturation intensity, 59 mW/cm^2.

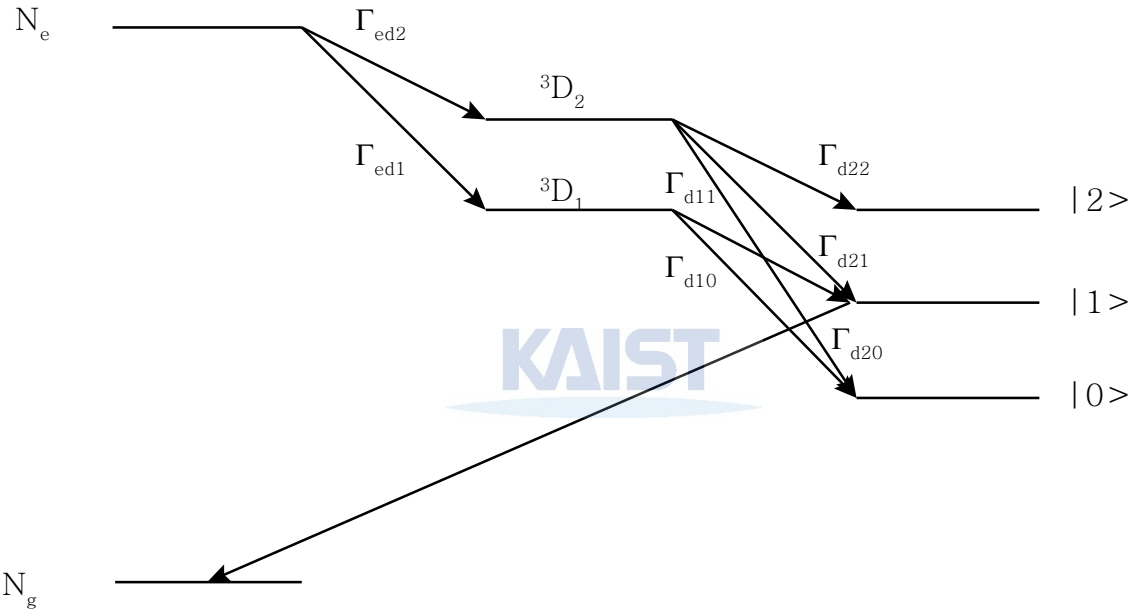

Figure 5.9: Schematic enrgy level diagram of showing the decay channels to triplet-P states of an Yb atom.

In theory, the decay rates of ^{1}P$_1$ state are given by $a_0 = 6.18$ s^{-1}, $a_1 = 5.25$, and $a_2 = 0.37$ [35]. To obtain the values of $a_{0,1,2}$, the decay rate diagram shown in Fig. 5.9,is used as The values for $a_{0,1,2}$ are

$$\begin{aligned} a_0 &= \Gamma_{ed2} \times \frac{\Gamma_{d20}}{\Gamma_{d22} + \Gamma_{d21} + \Gamma_{d20}} + \Gamma_{ed1} \times \frac{\Gamma_{d10}}{\Gamma_{d11} + \Gamma_{d10}}, \\ a_1 &= \Gamma_{ed2} \times \frac{\Gamma_{d21}}{\Gamma_{d22} + \Gamma_{d21} + \Gamma_{d20}} + \Gamma_{ed1} \times \frac{\Gamma_{d11}}{\Gamma_{d11} + \Gamma_{d10}}, \\ a_2 &= \Gamma_{ed2} \times \frac{\Gamma_{d22}}{\Gamma_{d22} + \Gamma_{d21} + \Gamma_{d20}} \end{aligned} \tag{5.11}$$

When the atoms in the either $^3P_0$ or $^3P_2$ are optically repumped to the ^{3}S$_1$ state, they spontaneously decay to the triplet state, ^{3}P$_{0,1,2}$, with the decay rates of $\lambda_{0,1,2}$ respectively

and the atoms in $^3\mathrm{P}_1$ decay immediately to the ground state. And we can consider the following four different repumping cases: (NR) no repumping lasers, (A) repumping $^3P_2$ state only, (B) repumping $^3P_0$ state only, and (A+B) repumping both $^3\mathrm{P}_{0,2}$ states. In the case (NR), the net loss rate of the trapped atom is given as $a_{\mathrm{NR}} = a_0 + a_2 = 6.55\ \mathrm{s}^{-1}$, simply from Eqs 5.6. In the case (A), the atoms in $^3\mathrm{P}_2$ are distributed to $^3\mathrm{P}_0$ and $^3\mathrm{P}_1$ and a_0 in Eq. (5.6) becomes $a_0' = a_0 + \frac{\lambda_1}{\lambda_1+\lambda_0} a_2 = 6.28$, considering the branching ratios, which are given as $\lambda_0 : \lambda_1 : \lambda_2 = 1 : 3 : 5$, from the $^3\mathrm{S}_1$ state to the $^3\mathrm{P}_{0,1,2}$ states. So, the net loss rate of the trapped atoms for the case (A) is $a_{\mathrm{A}} = 6.28\ \mathrm{s}^{-1}$. Likewise, in case (B), a_2 in Eq. (5.8) becomes $a_2' = a_2 + \frac{\lambda_2}{\lambda_2+\lambda 1} a_0 = 3.94$ and, therefore, the total decay rate for the case (B) is obtained as $a_{\mathrm{B}} = 3.94\ \mathrm{s}^{-1}$. In the case (A+B), when the both $^3\mathrm{P}_{0,2}$ are repumped, the net loss rate to the triplet P states becomes zero, (i.e., $a_{\mathrm{A+B}} = 0$).

We simulate the above result : We assume that the decay rate is so slow that the input of atom is zero and that one of metastable state is shelved at the initial time. We ignore the background collisional loss. First the rate equations for the repump laser of 770 nm wavelength are given by

$$\begin{aligned}
\frac{dN_{\mathrm{P}_0}}{dt} &= \Gamma_{sp0} N_{\mathrm{S}_1}, \\
\frac{dN_{\mathrm{P}_1}}{dt} &= \Gamma_{sp1} N_{\mathrm{S}_1} - \Gamma_{p1s} N_{\mathrm{P}_1}, \\
\frac{dN_{\mathrm{P}_2}}{dt} &= -R_{ex} N_{\mathrm{P}_2} + \Gamma_{sp2} N_{\mathrm{S}_1}, \\
\frac{dN_{\mathrm{S}_1}}{dt} &= +R_{ex} N_{\mathrm{P}_2} - (\Gamma_{sp0} + \Gamma_{sp1} + \Gamma_{sp2}) N_{\mathrm{S}_1},
\end{aligned} \tag{5.12}$$

where N_{P_0}, N_{P_1}, N_{P_2}, N_{S_1} are the number of atoms in each state, $\Gamma_{sp2} = 3.7 \times 10^7$, $\Gamma_{sp1} = 2.7 \times 10^7$, $\Gamma_{sp0} = 0.97 \times 10^7$, $\Gamma_{p1s} = 1.1 \times 10^6$ are the decay rate and the optical excitation rate $R_{ex} = 5 \times 10^4$ for the simulation. The simulated result is shown in Fig. 5.10. The atoms in $^3\mathrm{P}_2$ state are removed and some atoms are shelved in $^3\mathrm{P}_0$. The ratio of the shelved atoms is $\frac{\lambda_0(\Gamma_{sp0})}{\lambda_0(\Gamma_{sp0})+\lambda_1(\Gamma_{sp1})} \approx 1/4$.

For optical excitation in the 650-nm laser case, we set

$$\begin{aligned}
\frac{dN_{\mathrm{P}_0}}{dt} &= -R_{ex} N_{\mathrm{P}_0} + \Gamma_{sp0} N_{\mathrm{S}_1}, \\
\frac{dN_{\mathrm{P}_1}}{dt} &= \Gamma_{sp1} N_{\mathrm{S}_1} - \Gamma_{p1s} N_{\mathrm{P}_1}, \\
\frac{dN_{\mathrm{P}_2}}{dt} &= \Gamma_{sp2} N_{\mathrm{S}_1}, \\
\frac{dN_{\mathrm{S}_1}}{dt} &= +R_{ex} N_{\mathrm{P}_0} - (\Gamma_{sp0} + \Gamma_{sp1} + \Gamma_{sp2}) N_{\mathrm{S}_1}.
\end{aligned} \tag{5.13}$$

The simulated result is shown in Fig. 5.11. The atoms in $^3\mathrm{P}_0$ state are removed and some atoms are shelved in $^3\mathrm{P}_2$. The ratio of shelved atom is $\frac{\lambda_2(\Gamma_{sp2})}{\lambda_2(\Gamma_{sp2})+\lambda_1(\Gamma_{sp1})} \approx 5/8$.

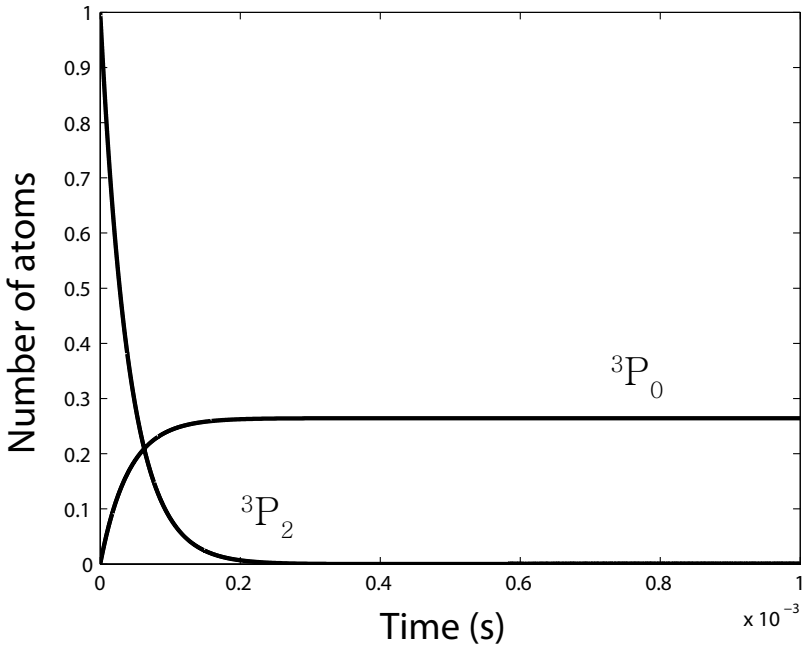

Figure 5.10: Simulated result for the case when optical 770-nm repump laser is on. The atoms in the $^3P_2$ state is removed and some part of atoms shelved in $^3P_0$.

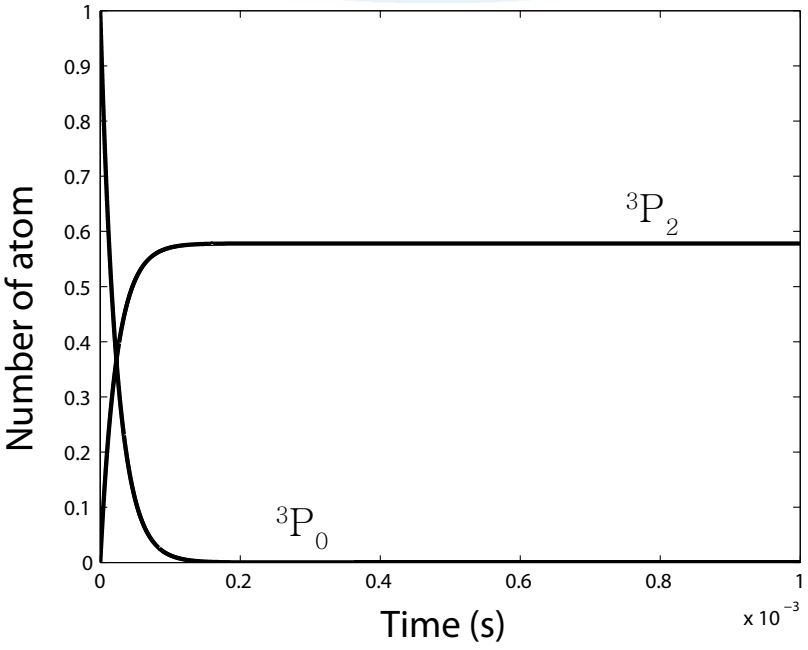

Figure 5.11: Simulated result for the case when optical 649-nm repump laser is on. The atoms in the $^3P_0$ state is removed and some part of atoms shelved in $^3P_2$.

5.2.2 Measurement of the radiative decay rate

We have studied the decay dynamics by closing the atom shutter, which is placed at the Zeeman slower entrance. Generally, the MOT is performed in vapor atomic states. Ytterbium is, however, performed in atomic beam with Zeeman slower. If the atom shutter is closed, the atomic source is not supplied. Then we could measure the decay dynamics of ytterbium MOT and by removing the effect of the atom beam flux. And the loss rate related to shelving of atoms in the metastable state is controlled by repump lasers. As mentioned before, we have measured the four different experiment conditions. If the loading rate ($\eta = 0$) is zero, the solution of the master equation (5.9) for the decay of atoms, is given by

$$N(t) = N(0)e^{-\Gamma t}\left[1 + \frac{\beta N(0)}{\Gamma}\left(1 - e^{-\Gamma t}\right)\right]^{-1}, \tag{5.14}$$

where $N(0)$ is the initial number of atoms in steady states, and Γ is the loss rate of the MOT defined as in Eq. (5.9)

$$\Gamma = a_X f + \gamma_c, \tag{5.15}$$

where the index X in a_X indicates a particular experimental condition among the four repumping cases, i.e. $X \in \{(NR), (A), (B), (A+B)\}$: (NR) No repump laser is on, (A) Only 770 nm laser is on, (B) Only 650 nm laser is on, and (A+B) Both repump lasers are on. Figure 5.12 shows the result of four different experiments. The steady-state number of trapped atoms N(0) and the lifetime τ of the MOT is increased by the repumping of the metastable states. For (A+B) case, the number of atom is increased by 30% and the lifetime τ is increased by 100%. But this result is not consistent with the fact that the change of the number of atoms N(0) is proportional to the change of τ, or $\mathrm{N}(0) = \eta\tau$, as $\tau = 1/\Gamma$. However, the collision loss term γ_c consists of two major parts: (1) collision with the background residual gas and (2) Yb flux from the Zeeman slower. Therefore, the collisional loss term is a function of loading rate η and, as a result, shutting off the atomic beam suddenly reduced the loss rate Γ.

Figure 5.13 shows the logarithmic plot of the fluorescence signal $N(t)$ of, the total number of trap, that is the normalized by $N(0)$, the initial number of atoms. In this graph, the ratio $\beta N(0)/\Gamma$ varies from 0 to 1, so the second term in the parenthesis in Eq. (5.14). β is related with the number density. The Yb-Yb collision loss dominant behavior is significant for the case of (A+B) which is different from the a linear line in the logarithmic plot.

To determine the decay rate, we measured Γ for the four different repumping case with varying the trapping laser power. Figure 5.14 shows the fitted number Γ versus

the fraction number f. Linear regression analysis predict that all the four lines can be extrapolated to converge at 0.43 ± 0.03 as f approaches zero. As a result of linear fitting of graph, the slope of line gives the decay rate value $a_{NR} = 6.48, a_A = 6.27, a_B = 4.14$, and $a_{A+B} \leq 6.3 \times 10^{-3}$.

We can estimate the decay rate $a_0, a_2, a_{0,2}$ from the obtained loss rate, and the result is summarized in Table 5.1. The measured values for the individual decay rate a_0 and a_2 show a good agreement with the theoretical values. The uncertainty of the measured values mainly comes from the uncertainty of the fraction number f. The uncertainty of f comes from the the power fluctuation and spatial beam profile, and the measurement error of the trap laser. And the uncertainty of Δ/Γ is caused by the magnetic field in the trap, laser frequency detuning,etc, and its uncertainty is estimated by 30%. Including the uncertainty in fitting error, the resulting uncertainty of the decay rate is estimated 33%.

	This work	Previous Work	Theory
$a_{2,0}$	6.48 (2.11) s^{-1}	23 (11) s^{-1}	6.6 (4.6) s^{-1}
a_0	5.96 (1.97)		6.18
a_2	0.42(0.14)		0.37
a_1		21.3 (6.9) s^{-1}	5.2 (2.6) s^{-1}

Table 5.1: Summary of the results obtained by fitting of Γ as a funtion of f.

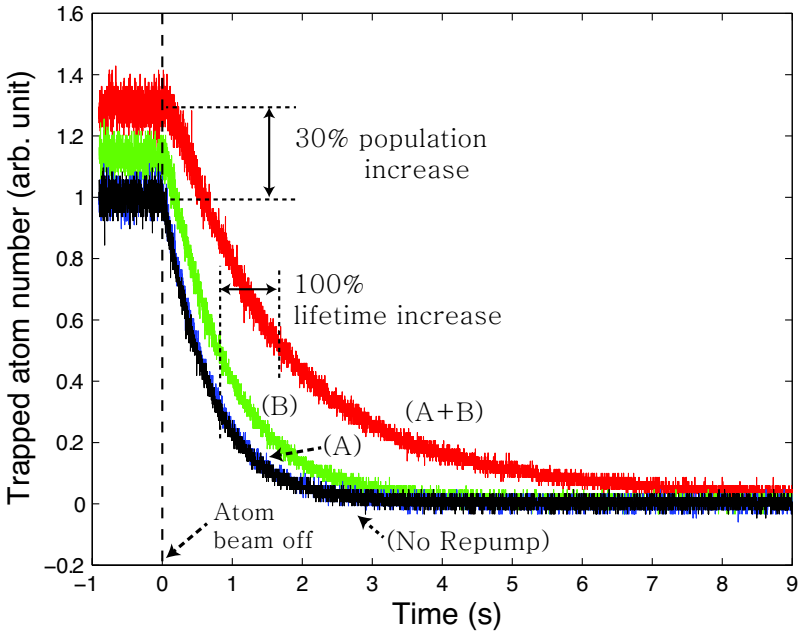

Figure 5.12: Fluorescence signal for $^1S_0$ and $^1P_1$ transition. At t=0, the atomic source is terminated. The decay dynamics of the MOT for the four different repumping cases: (A) The $^3P_2$ state, (B) $^3P_0$, and (A+B) both the states are repumped.

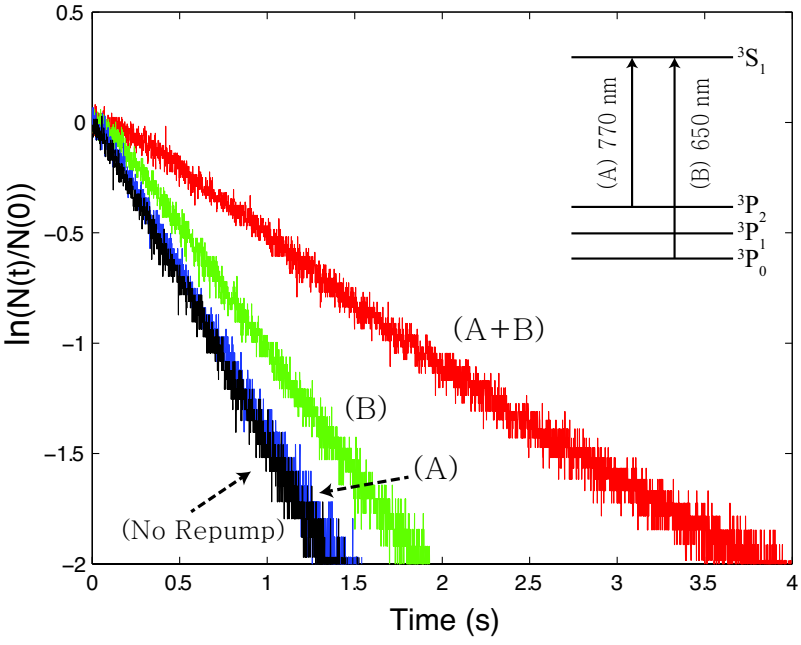

Figure 5.13: Logarithm plot for the decay dynamics versus time evolution

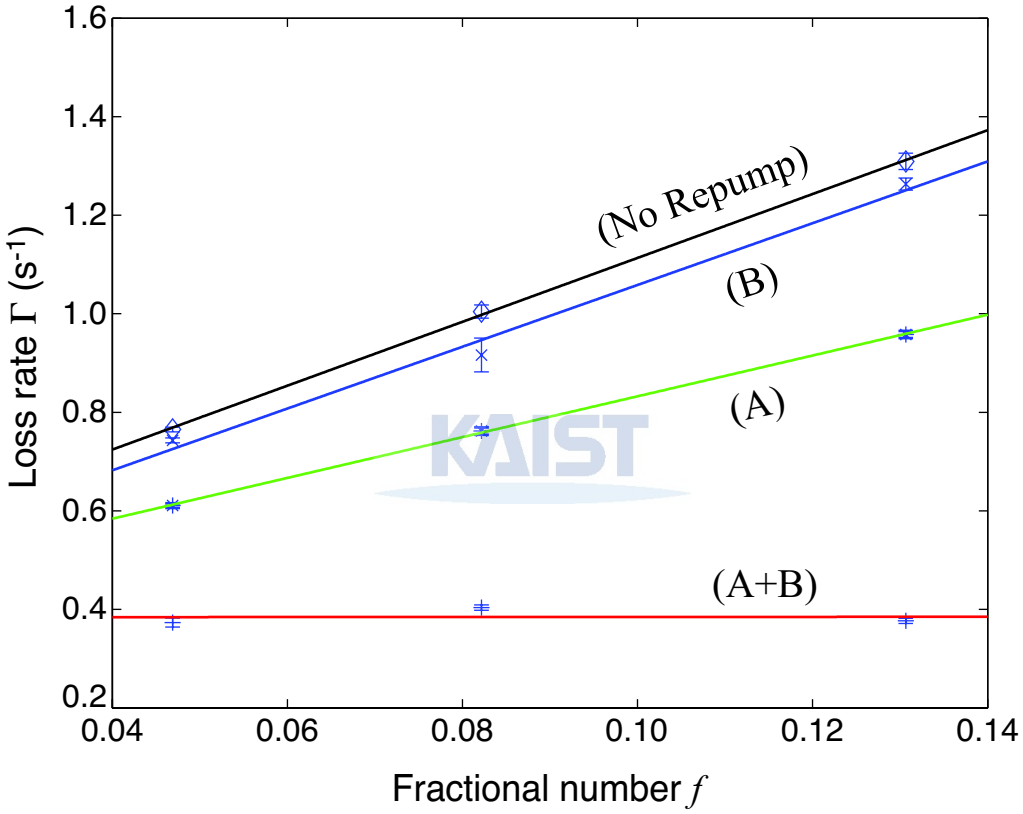

Figure 5.14: Measured loss rate versus the number of atoms in the excited state (f), obtained for the four different repumping cases. The slope of the each graph is 6.48, 6.27, 4.14 and less than 6.3×10^3.

Chapter 6. Conclusion

Optically cooled and trapped ytterbium atoms are useful in basic science research. For example, the narrow linewidth of the spin-forbidden transition due to the state mixing was applied to assess the optical frequency standards. In addition, many types of isotopes of similar natural abundance levels have been researched in terms of the the cold and ultracold collisional properties of their isotope mixtures, such as the Fermion-Boson mixture, and the Boson-Boson mixture. In this dissertation, we trapped ytterbium atoms in a magneto-optical trap with a 398.9 nm diode laser and investigated the properties of the trapped atoms. We trapped atoms on the order of 10^7 in a magneto-optical trap. The trap loading time was 0.6 s, and the temperature of the trapped atoms was 1.2 mK. Next, we investigated the trapped atom loss characteristics in the $^1S_0$-$^1P_1$ transition. We measured the decay dynamics of the MOT by closing an atomic shutter. There are three major causes of trapped atomic loss in an ytterbium MOT: collision loss with background gases, radiative loss due to metastable states, and collisions between trapped ytterbium atoms. Radiative loss occurs in the $^1P_1$ state to the metastable states $^3P_{0,2}$ via the $^3D_{1,2}$ states. We optically repumped the atoms in the metastable states with repump lasers. The atoms in the metastable states decay to the ground states. When the repump lasers are on, the number of trapped atoms increased by more than 30%, and the lifetime of the trap was increased to double the original amount.

By controlling the repump lasers, we determined the loss rates via the fitting of decay curves. We also measured the loss rates while controlling the repump lasers as a function of the power of the trapping laser. Thus, we achieved the decay rate values of the $^1P_1$ state to the metastable states $^3P_{0,2}$. The experimental results are in good agreement with the theoretical values. We obtained decay rates that were different from those of an earlier method.

Chapter A. PI-servo circuit

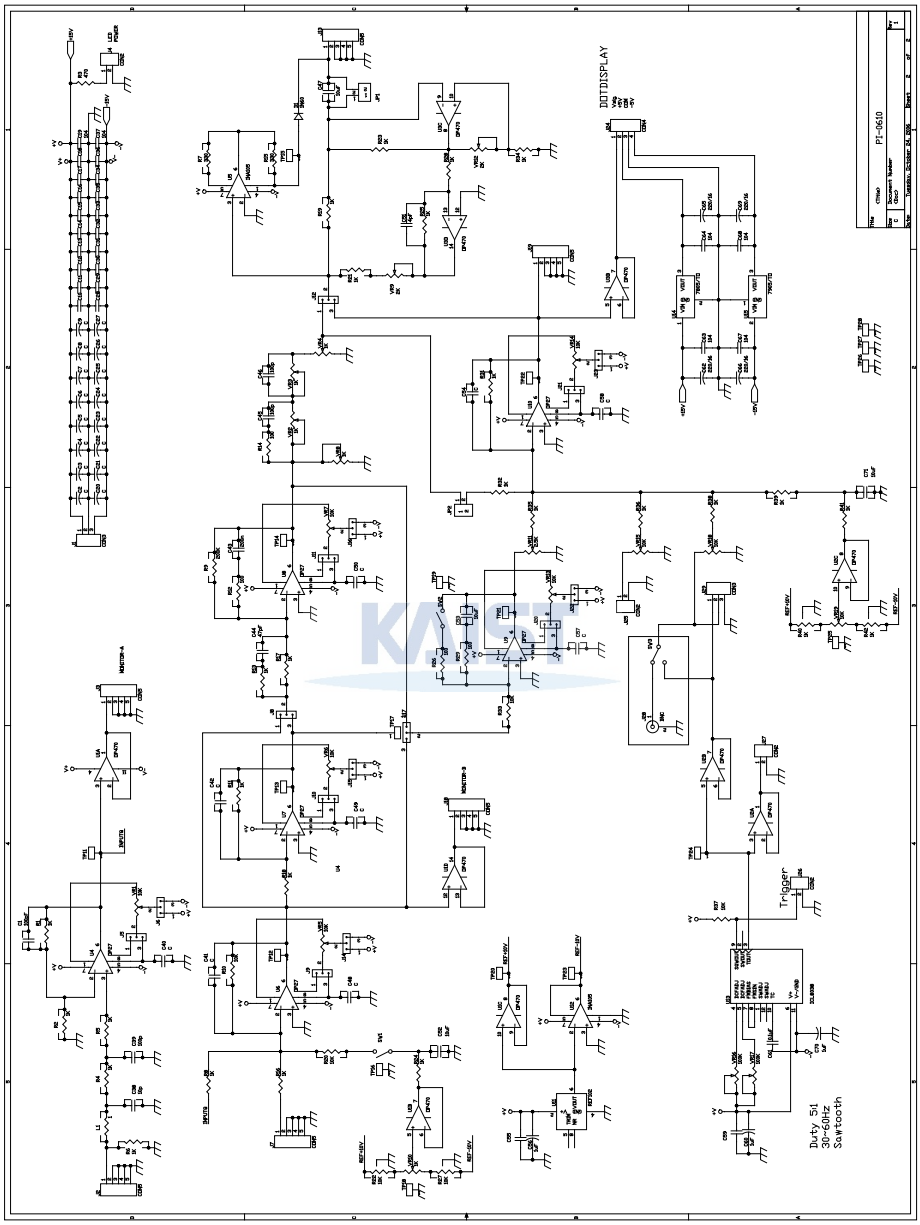

Figure A.1: A PI-servo circuit diagram

Chapter B. PMT signal circuit

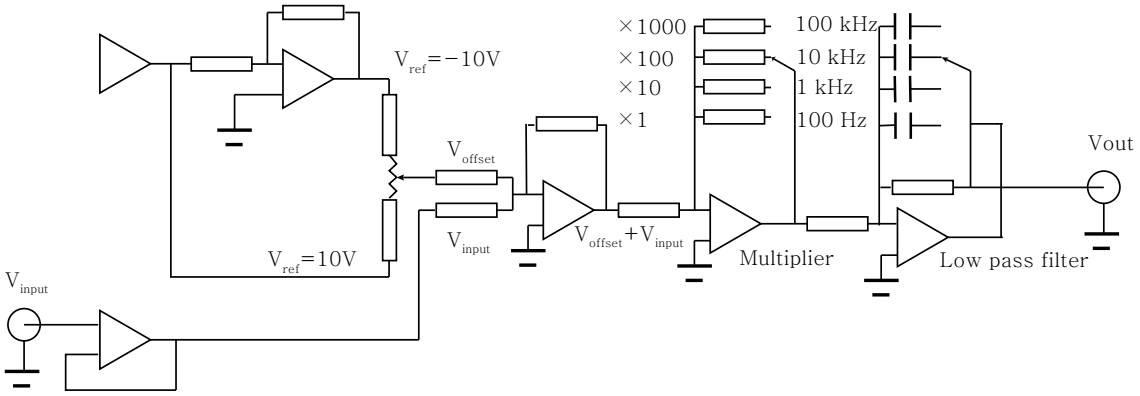

Figure B.1: A circuit for PMT output voltage signal processor. It consists of offset adjuster, low-pass filter adjuster, gain adjuster.

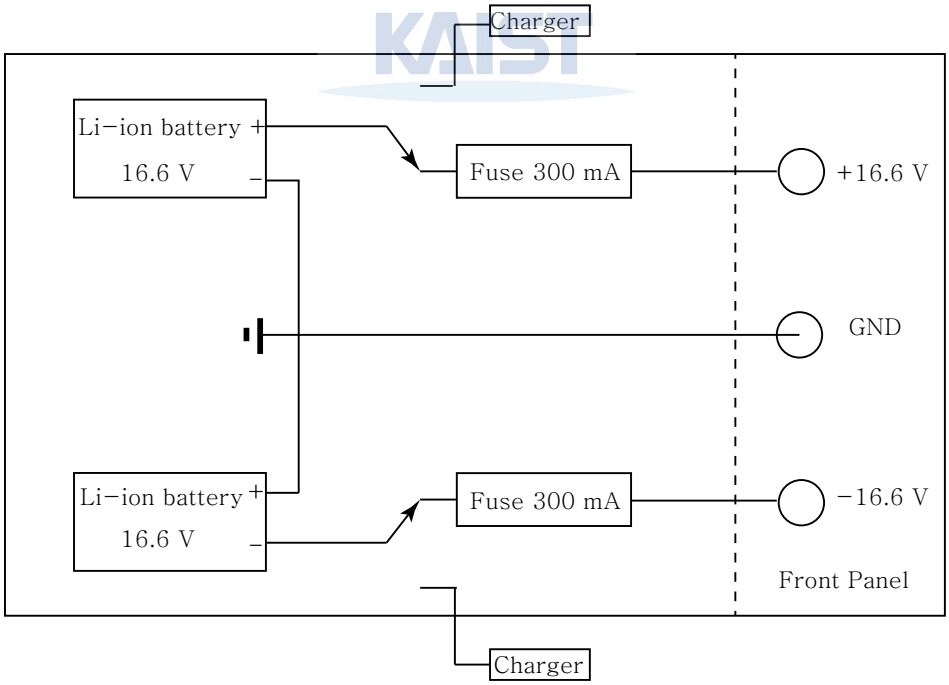

DC power supply for PMT

Figure B.2: Constant-voltage power supply for PMT operation.

References

[1] H. J.Metcalf, P. van der Straten, *Laser Cooling and Trapping* (Springer-Verlag, New York, 1999).

[2] M. H. Anderson, J. R. Ensher, M. R. Matthews, C. E. Wieman, and E. A. Cornell, "Observation of Bose-Einstein condensation in a dilute atomic vapor", Science **269**, 1995.

[3] K. B. Davis, M. O. Mews, M. R. Andrews, N. J. van Druten, D. S. Durfee, D. M. Kurn, and W. Ketterle, "Bose-Einstein condensation in a gas of sodium atoms", Phys. Rev. Lett. **75**, 1995.

[4] T. B.innewies, G. Wilpers, U. Sterr, F. Riehle, J. Helmcke, T. E. Mehlstäubler, E. M. Rasel, and W. Ertmer, "Doppler cooling and trapping on forbidden transitions", Phys. Rev. Lett. **87**, 123002 2001.

[5] X. Xu, T. H. Loftus, J. W. Dunn, C. H. Greene, J. L. Hall, A. Gallangher, and J. Ye, "Single-stage sub-doppler cooling of alkaline earth atoms", Phys. Rev. Lett. **90** 193002, 2003.

[6] F. Ruschewitz, J. L. Peng, H. Hinderthür, N. Schaffrath, K. Sengstock, and W. Ertmer, "Sub-kilohertz optical spectroscopy with a time domain atom interferometer", Phys. Rev. Lett. **80** 3173, 1998.

[7] J. L. Hall, M. Zhu, and P. Buch, "Prospects for using laser-prepared atomic fountains for optical frequency standards applications", JOSA B **6** 2194, 1989.

[8] M. Takamoto and H. Katori, "Spectroscopy of the $^1S_0$-$^3P_0$ Clock Transition of ^{8}7Sr in an Optical Lattice", Phys. Rev. Lett. **91**, 223001, 2003.

[9] Z. Barber. *Ytterbium Optical Lattice Clock*, Ph. D thesis, (University of Colorado, 2003).

[10] A. D. Ludlow, N. D. Lemke, J. A. Sherman, C. W. Oates, G. Quéméner, J. von Stecher, and A. M. Rey, "Cold-collision-shift cancellation and inelastic scattering in a Yb optical lattice clock", Phys. Rev. A **84**, 052724, 2011.

[11] W. M. Itano, L. L. Lewis, and D. J. Wineland, "Shift of $^2S_{1/2}$ hyperfine splittings due to blackbody radiation", Phys. Rev. A **25**, 1233, 1982.

[12] N. D. Lemke, A. D. Ludlow, Z. W. Barber, T. M. Fortier, S. A. Diddams, Y. Jiang, S. R. Jefferts, T. P. Heavner, T. E. Parker, and C. W. Oates, "Spin-1/2 Optical Lattice Clock", Phys. Rev. Lett. **103**, 063001, 2009.

[13] J. R. Gardner, R. A Cline, J. D. Miller, D. J. Heinzen, H. M. J. M. Boesten, and B. J. Verhaar, "Collisions of Doubly Spin-Polarized Ultracold ^{85}Rb Atoms", Phys. Rev. Lett. **74**, 3764, 1995.

[14] W. I. McAlexander, E. R. I. Abraham, N. W. M. Ritchie, C. J. Williams, H. T. C. Stoof, and R. G. Hulet. "Precise atomic radiative lifetime via photoassociative spectroscopy of ultracold lithium", Phy. Rev. A **51**, R871, 1995.

[15] Timothy P. Dinnen, Kurt R. Vogel, Ennio Arimondo, John L. Hall, and Alan Gallangher. "Cold collisions of Sr*-Sr in a magneto-optical trap", Phys. Rev. A **59**, 1999.

[16] G. Zinner, T. Binnewies, and F. Riehle, "Photoassociation of Cold Ca Atoms", Phys. Rev. Lett. **85**, 2292, 2000.

[17] Y. Takasu, K. Komori, K. Honda, M. Kumakura, T. Yabuzaki, and Y. Takahashi, "Photoassociation Spectroscopy of Laser-Cooled Ytterbium Atoms", Phys. Rev. Lett. **93** 123202, 2004.

[18] T. Fukuhara, S. Sugawa, M. Sugimoto, S.Tale, and Y. Takahashi, "Mott insulator of ultracold alkaline-earth-metal-like atoms", Phys. Rev. A **79**, 041604(R), 2009.

[19] Y. Takasu, K. Maki, K. Komori, T. Takano, K. Honda, M. Kumakura, T. Yabuzaki, and Y. Takahashi, "Spin-Singlet Bose-Einstein Condensation of Two-Electron Atoms", Phys. Rev. Lett. **91**, 040404, 2003.

[20] T. Fukuhara, S. Sugawa, and Y. Takahashi, "Bose-Einstein condensation of an ytterbium isotope", Phys. Rev. A **76**, 051604R, 2007.

[21] T. Fukuhara, Y. Takasu, M. Kumarkua, and Y. Takahashi, "Degenerate Fermi Gases of Ytterbium", Phys. Rev. Lett. **98**, 030401, 2007.

[22] S. Tojo, M. Kitagawa, K. Enomoto, Y. Kato, Y. Takasu, M. Kumakura, and Y.Takahashi, "High-Resolution Photoassociation Spectroscopy of Ultracold Ytterbium Atoms by Using the Intercombination Transition", Phys. Rev. Lett. **96**, 153201, 2006.

[23] K. Honda, Y. Takasu, T. Kuwamoto, M. Kumakura, Y. Takahashi, and T. Yabuzaki, "Optical dipole force trapping of a fermion-boson mixture of ytterbium isotopes", Phys. Rev. A **66**, 021401(R), 2002.

[24] T. Kuwamoto, K. Honda, Y. Takahashi, and T. Yabuzaki, "Magneto-optical trapping of Yb atoms using intercombination transition", Phys. Rev. A **60**, R745-R748, 1999.

[25] K.Honda, Y. Takahashi, T. Kuwamoto, M. Fujimoto, and K. Toyoda, "Magneto-optical trapping of Yb atoms and a limit on the branching ratio of the $^1P_1$ state", Phys. Rev. A **59**, R934, 1999.

[26] A. Yamaguchi, S. Uetake, D. Hashimoto, J. M. Doyle, and Y. Takashi, "Inelastic Collisions in Optically Trapped Ultracold Metastable Ytterbium", Phy. Rev. Lett. **101**, 233002, 2008.

[27] K. Deilamian, J. D. Gialspy, and D. E. Kelleher, "Isotope shifts and hyperfine splittings of the 398.8-nm Yb I line", J. Opt. Soc. Am. B **10**, 789, 1993.

[28] W. A. van Wijngaarden and J. Li, "Measurement of isotope shifts and hyperfine splittings of ytterbium by means of acousto-optic modulation", J. Opt. Soc. Am. B **11**, 2163, 1994.

[29] R. Maruyama, *Optical Trapping of Ytterbium Atoms*, Ph. D thesis, University of Washington, 2003.

[30] C. J. Foot, *Atomic Physics* (Oxford University Press, 2005)

[31] P. D. Lett, W. D. Phillips, S. L. Rolston, C. E. Tanner, R. N. Watts, and C. I. Westbrook, "Optical molasses", J. Opt. Soc. Am. B **6**, 157, 1989.

[32] N. Ramsey, *Molecular Beams* (Clarendon Press, Oxford, 1956).

[33] Thomas Howard Loftus. *Laser Cooling and Trapping of Atomic Ytterbium*, Ph.D thesis, University of Oregon, 2001.

[34] T. Loftus, J. R. Bochnski, R. shivitz, and T. W. Mossberg, "Power-dependent loss from an ytterbium magneto-optic trap", Phys. Rev. A **61**, 051401(R), 2000.

[35] S. G. Porsev, Y. G. Rakhlina, and M. G. Kozlov, "Electric-Dipole Amplitudes, Lifetimes, and Polarizabilities of the Low-Lying Levels of Atomic Ytterbium", Phys. Rev. A **60**, 2781, 1999.

Summary

Enhancement of Magneto-Optical Trap of Ytterbium Atom via Optical Repumping of Triplet P-states

저온 상태의 이터븀 (Yb, Z=70) 원자는 많은 기초적인 연구와 응용에 대한 가능성을 가지고 있다. 예를 들어 광 주파수 표준, 패리티 비보존 실험. 초저온 상태의 충돌과 산란에 관한 연구들이 있다. 포획된 이터븀 원자들을 만들기 위해서 두 가지의 자기광포획(MOT)을 이용하고 있다. 첫 번째로 강한 에너지를 가진 398.9-nm 레이저로 자기광포획을 하는 방법, 두 번째로 약한 에너지를 가진 555.8-nm 레이저로 자기광포획을 하는 방법이 있다. 이 학위논문에서는 도플러 냉각, 제만 에너지 차이를 이용한 냉각, 자기광포획에 관한 이론적인 배경에 대한 내용을 설명 하고 실제적으로 이터븀 자기광포획이 어떻게 만들어지고 포획된 원자의 특성을 설명한 후 자기광포획의 효율이 증가됨을 보이고 있다.

^{1}S$_0$-^{1}P$_1$ 전이선을 이용한 자기광포획에서 여기 상태인 ^{1}P$_1$에서 빛을 내면서 준안정 상태로 손실되는 원자는 광포획되는 원자의 갯수를 낮추고 광포획된 원자의 포획 수명을 제한하게 된다. 이 때 $(6s6p)^3$P$_{2,0}$ 로 손실되는 원자를 리펌핑 레이저를 이용하여 제거함으로써 이터븀 자기광포획의 효과가 증대함을 볼 수 있다. 이 때 포획된 원자의 갯수는 ^{1}S$_0$-^{1}P$_1$ 전이에서 발생되는 자발방출된 형광신호를 광수집장치를 통하여 광자의 갯수를 측정하고 이를 통해 포획된 원자의 갯수를 알 수 있게 된다. 포획광의 세기를 변화시키면 여기 상태의 원자 갯수가 변화게 되고 여기 상태의 원자 갯수에 비례하는 준안정 상태로의 손실양을 알 수 있게 된다.

여기서 ^{3}P$_0$-$^3S_1$ 전이선의 리펌핑광인 650-nm 레이저와 ^{3}P$_2$-$^3S_1$ 전이선의 리펌핑광인 770-nm 레이저는 준안정 상태의 원자를 여기시켜 ^{3}S$_1$ 상태로 올라가게 되고 자발방출 과정을 통해 ^{3}P 상태로 이동하게 된다. 이 중 ^{3}P$_1$ 상태의 원자는 다시 자발 광출 과정을 통해 기저 상태인 ^{1}S$_0$ 상태로 이동하게 된다. 이 과정을 이용해서 리펌핑 레이저들의 유무에 따라서 빛을 내면서 준안정상태로 손실되는 양을 조절할 수 있다. 실험결과에서는 레이저의 세기를 포화 여기 상태보다 낮은 영역에서 실험을 하여 포획광의 세기가 여기 상태의 원자의 갯수와 선형적으로 비례하는 조건을 만족하는 영역에서 실험을 수 행하였다.

자기광포획된 원자가 정상 상태에서 리펌핑 레이저 두 개를 모두 사용하여 30% 정도 증가됨을 보이고 원자의 공급을 차단하여 측정한 포획된 원자의 수명은 2배정도 증가됨을 확인하였다. 이는 기존에 잘 알려진 결과인 원자의 포획된 양과 수명이 비례하는 관계와 어긋남이 있고 이는 원자의 포획과정에서 원자빔과 포획된 원자 사이의

충돌에 의한 영향으로 확인된다.

그리고 원자의 손실되는 원리를 원자의 형광신호가 포획된 원자가 손실되면서 발생되는 형광신호를 시간의 변화에 따라서 측정하여 확인하였다. 이 때 손실되는 양은 주변기체와의 충돌, 포획된 원자간의 충돌, 준안정 상태로 전이되어 발생되는 손실로 나눠 볼 수 있다. 이 때 준안정 상태로 떨어지는 원자의 갯수를 포획광의 세기를 통해 조절하고 이를 리펌핑 레이저의 유무를 조절하여 준안정 상태로 떨어지는 비율을 구할 수 있었다.

이런 결과는 리펌핑 레이저를 통해 포획 효율이 증가된 원자는 좀 더 많은 양을 단시간에 포획이 가능하므로 일반적인 원자실험이 밀리초 영역에서 일어나는 현상을 좀 더 효율적으로 관측할 수 있다. 그리고 원자빔을 이용한 자기광포획에 대한 이해를 높일 수 있게 되었다.